Bedrock channel response to tectonic, climatic and eustatic forcings

by
Noah P. Snyder

B.S. Geology
Bates College, 1993

SUBMITTED TO THE DEPARTMENT OF EARTH, ATMOSPHERIC, AND PLANETARY SCIENCES IN PARTIAL FULFILLMENT OF THE REQUIREMENTS FOR THE DEGREE OF

DOCTOR OF PHILOSOPHY
AT THE
MASSACHUSETTS INSTITUTE OF TECHNOLOGY

SEPTEMBER 2001

Signature of Author: _____
Department of Earth, Atmospheric, and Planetary Sciences
June 29, 2001

Certified by: _____
Kelin X Whipple
Thesis Supervisor

Accepted by: _____
Ronald G. Prinn
Department Head

Bedrock channel response to tectonic, climatic and eustatic forcings

Noah P. Snyder

Submitted to the Department of Earth, Atmospheric, and Planetary Sciences on June 29, 2001 in Partial Fulfillment of the Requirements for the Degree of Doctor of Philosophy in Geology.

Abstract

The response of bedrock channels to external forcings is investigated in this thesis. The approach is to test and constrain a theoretical model for bedrock-channel incision based on shear stress using field data. The primary study area is a series of 21 small, coastal drainage basins in northern California, USA with known, varying rates and history of rock uplift. The initial application of a simple form of the model to the stream profiles suggests that (1) the channels are eroding at rates approximately equal to uplift rates (*i.e.* steady-state fluvial incision), and (2) erosion processes are proportionally more effective in the high-uplift-rate zone, with factors in addition to channel gradient responding to tectonic forcing. These results lead to the rest of the study, in which some of the assumptions of the simple model are rejected in order to explain the second observation. A more sophisticated model that includes both a stochastic distribution of floods and a threshold shear stress to initiate bedrock erosion (τ_c) predicts that a greater part of the distribution of flood events will exceed the threshold in steeper channels. Therefore, higher-gradient channels have proportionally higher erosion rates, as is observed in the high-uplift-rate streams of the California field site.

The shear-stress model is tested and constrained through a detailed, field-based analysis of topography, lithology, stream morphology and regional hydrology to isolate those factors that respond to tectonics. The stochastic model is able to incorporate the observed variation in stream discharge due to orographic enhancement of precipitation by high topography associated with high uplift rates. This increase in discharge appears to play a second-order role in setting the erosional effectiveness of the high-uplift zone. Other factors, including channel width, lithologic resistance and sediment flux, do not appear to vary in an important way with uplift rate, although this conclusion is based on analyses that have some limitations. The importance of thresholds is underscored by a direct calculation of critical shear stress during a rare bedrock-incision event in a low-erosion-rate creek in New York state ($\tau_c \approx$100-200 Pa). This event, the only one that caused

significant bedrock plucking at the site in an ~40-year period, is consistent with a low erosion rate, with few events that exceed the threshold. In contrast, similar τ_c values are exceeded during high-frequency flood events in the steep, rapidly eroding California streams. Inclusion of an erosion threshold accounts for the observed relationship between channel gradient and rock-uplift rate in the California site. In summary, by using field examples, the shear-stress bedrock-incision model with a stochastic distribution of flood events and an erosion threshold is demonstrated to be an effective and powerful tool for exploring relationships amongst climatic, tectonic and surficial processes.

In the final section of this thesis, a numerical modeling study couples the shear-stress model for onshore fluvial incision with a simple rule for offshore wave-based erosion of bedrock to explore the response of uplifting streams to eustatic fluctuations. The results highlight the importance of offshore boundary conditions to the onshore response, particularly the position of the edge of the uplifting block and the development of bathymetry. A comparison of model results with the northern California channels suggests that (1) the steady-state hypothesis is consistent with an offshore decrease in rock-uplift rates, and (2) the ubiquitous low-gradient, alluviated mouths of the study-area streams are predicted by the model during uplift of the offshore platform during the late Holocene sea-level stillstand.

Thesis Supervisor: Kelin X Whipple, *Associate Professor of Geology*

Acknowledgments

First, I wish to thank Kelin Whipple, my advisor. His accessibility, enthusiasm and faith made my graduate-school experience fun and enriching. I will always harbor a certain amount of pride for being the first person to start and finish on the Whipple program. All along I have felt that I am playing for Team Whipple, although my perceived role has changed through the years: early on I thought of myself as a utility infielder always ready to put down the sacrifice bunt to help out the team, and now I'm more of a grumpy veteran trying to pad my batting statistics!

I also very much appreciate the help and guidance provided me by Dorothy Merritts and Greg Tucker, who have been collaborators and advisors to this thesis work. I express my gratitude to the other members of my thesis committee, Kip Hodges, John Southard and Rafael Bras for their guidance and suggestions along the way. I also thank professors John Grotzinger, Clark Burchfiel, Wiki Royden and Eric Leonard.

Next, I express my love and thanks to Lydia Bergen who has put up with me for pretty much the whole run at MIT. She deserves as much credit as anyone for making this thesis happen. Her devotion and support have been the greatest source of inspiration and renewal over the past 5 years. We've been through a lot together, and I can't wait to see where we go next!

I want to mention the series of teachers who put me on this path. Dan Flerlage at the Alternative Community School in Ithaca instilled my initial interest in field science. Professors Dyk Eusden and Mike Retelle at Bates College drew me into the geologist fold and laid my geological foundation, as did Ken Fink, John Creasy and Marita Bryant. I also thank Lee Allison, Gary Christensen and Mike Lowe at the Utah Geological Survey. Jon Stock and Tom Dunne told me get in touch with Kelin, and vouched for his (slightly dicey) character.

At MIT, my fellow graduate students made the whole experience fun. I thank the other members of the "gang of four," Eric Kirby, Arthur White, José Hurtado, and all of the other students (as well as postdocs) that I overlapped with, including Simon Brocklehurst, Sinan Akciz, Lindsay Schoenbohm, Mark Behn, Julie Baldwin, Mark Schmitz, Karen Viskupic, Jenny Matzel, Becky Flowers, Kirsten Nicolaysen, Anke Friedrich, Jim VanOrman, Steve Parman, Steve Singletary, Astri Kvassnes, Bill Lyons, Amy Draut, John Thurmond, Steve Dibenedetto, Marin Clark, Matt Dawson, Bridget Berquist, Matt Reuer, Frederik Simons, Eliza Richardson, Peter Dodds, Jeremy Boyce, Chris Studnicki-Gizbert, Blair Schoene, Ben Crosby, Cam Wobus, Jeff Parsons, Mike Kroll, Jahan Ramezani, Stephen Lancaster, Jeff Niemann, Daniel Collins, and Nicole Gasparini. These people taught me most of what I know now, especially about earth-science subjects outside of my primary field. I feel fortunate to have them as colleagues.

Finally, I thank my family, Laurie Snyder, John Wood, Philip Snyder, Pat Paine, Ben Snyder, Norri Paine and Jonathan Paine for their love and support from all corners of the world. Lastly, I want acknowledge the key role of my friends/housemates/ultimate teammates over the past five years, including Matt Bogyo, Becky Allen, Evan Powers, Dave Owen, Lydia, Jessica Parsons, Tom Evans, Greg Hoke, Chris Heppner and Biz Fitzsimons, for providing necessary diversions from the production of this document.

Table of contents

Chapter 1 Introduction 7

Chapter 2 Landscape response to tectonic forcing: Digital elevation analysis of stream profiles in the Mendocino triple junction region, northern California 19

Chapter 3 Channel response to tectonic forcing: Analysis of stream morphology and hydrology in the Mendocino triple junction region, northern California 33

Chapter 4 Stochastic floods and erosion thresholds in bedrock rivers: Implications for landscape relief 85

Chapter 5 Interactions between onshore bedrock-channel incision and nearshore wave-based erosion forced by eustasy and tectonics 105

1. Introduction

This thesis was motivated by growing interest within the earth science community to better understand geomorphic responses to external forcings (*e.g.* Molnar and England, 1990; Bull, 1991; Merritts and Ellis, 1994; Koons, 1995; Tinkler and Wohl, 1998). Bedrock rivers set the relief structure in active mountain belts (Whipple *et al.*, 1999), and their morphology reflects the integrated history of tectonic, climatic and eustatic fluctuations (Howard *et al.*, 1994). At its core, this thesis is concerned with using field settings of known history to test and constrain an incision model of bedrock rivers. The fundamental goal of such work is to advance our knowledge of fluvial response to external forcings so that geomorphologists eventually might unravel tectonic and climatic history from the record preserved in topography.

This project began with the expectation of moving beyond the popular stream-power or shear-stress models for detachment-limited bedrock incision (*e.g.* Howard and Kerby, 1983; Howard, 1994; Whipple and Tucker, 1999). The initial plan was to study aspects of the response of channels to an increase in rock-uplift rate, including: (1) the role of changes in channel morphology (width, bed cover, etc.); (2) the representation of climate and climate differences in erosion models; and (3) the transient form of stream profiles. Analysis of stream longitudinal profiles in the Mendocino triple junction region of northern California, however indicated that (1) the streams were in steady state with rock-uplift rates, and (2) the simple shear-stress model was apparently capable of explaining the observed relationship between topography and uplift rate, provided that some feedback (morphologic, climatic, etc.) existed between uplift and incision rates. These basic observations, contained in Chapter 2, led naturally to the rest of the thesis, in which significant progress is made in understanding and modeling fluvial responses to tectonic and climatic changes. However, the project did not include the opportunity to investigate channels in a transient-response condition.

The basic form of the shear-stress model, with fluvial incision rate given by a power-law function of channel gradient and drainage area modified by a coefficient of erosion (K), comes from a simple, standard set of assumptions. Here, these assumptions are reviewed qualitatively. More complete derivations are available in Chapters 2 and 3, as well as a recent treatise by Whipple and Tucker (1999). The initial postulate of the model is that incision rate is a power-law

function of excess shear stress, or the difference between basal shear stress (τ_b) and a critical (or threshold) shear stress to initiate bedrock incision (τ_c). This approach is similar to models based on stream power (Whipple and Tucker, 1999). In the simplest case, τ_b is assumed to be much greater than τ_c during the floods that do the work, so τ_c can be eliminated from the model. The next step is to place τ_b in terms of easily measured quantities. The assumptions of steady, uniform flow (*i.e.* conservation of momentum) and conservation of water mass yield the classic depth—slope product estimate of τ_b. The addition of a semi-empirical bed-friction relationship (*i.e.* the Manning equation) yields τ_b in terms of stream discharge, channel width, gradient, and a friction factor (*i.e.* Manning's *N*). The final steps are to express discharge and width in terms of drainage area, using empirical power-law relationships (*e.g.* Leopold and Maddock, 1953; Dunne and Leopold, 1978). These steps require the simplifying assumption that incision can be modeled using a representative flood event (*i.e.* bankfull) that occurs during some fraction of the time (Wolman and Miller, 1960). Most applications of the shear-stress model assume implicitly or explicitly that channels respond to tectonic perturbations solely by adjusting bed gradient (Whipple and Tucker, 1999), not other factors such as channel width. This and most of the other assumptions outlined above are explored in this thesis, using both empirical data and theoretical arguments.

The work presented here depicts the evolution of understanding of bedrock incision in the northern California field setting. In a sense, it represents a typical example of the application of a simple model to a complex field setting: the project begins with a set of assumptions that reduce the model to its most basic possible form (described above), and throughout the thesis assumptions that prove unacceptable are rejected. The final product is a richer, more robust, more complicated model, which can fully explain the *observed* topographic—tectonic—climatic relationships. The next few pages introduce the four chapters that follow, with emphasis on critical evaluation of the application of the shear-stress model to field settings. The chapters are presented in the order in which they were originally written, which is appropriate. Chapters 2 through 4 represent a direct progression of the model predictions for response to tectonics and climate, and they lead naturally from one to the next. Chapter 5, on modeling response to eustatic forcing, is most directly an offshoot of Chapter 2, but it has important implications for the thesis as a whole.

Outline of Chapters 2-5

Chapter 2 is an analysis of the longitudinal profiles of 21 small, coastal drainage basins in the tectonically active Mendocino triple junction region of northern California. This is the primary field area of the thesis. It was chosen because the uplift rates and history are known from studies of emergent Pleistocene and Holocene marine terraces (Merritts and Bull, 1989; Merritts and Vincent, 1989; Merritts, 1996). Rock-uplift rates (U) vary from ~0.5 mm/yr in the southern part of the study area (low-uplift zone; LUZ) to ~4 mm/yr in the King Range to the north (high-uplift zone, HUZ). Merritts and co-workers found that uplift rates accelerated in the HUZ at ~100 ka. This observation led to the initial interest in the region, for it affords the opportunity to study the response of streams to a change in uplift rate, perhaps even capturing the topography in a transient state. In addition to the known uplift-rate history, the field area was well suited for this study because (1) the lithology was approximately uniform spatially, and (2) climate was constant spatially (except known orographic effects) and temporally, although these assumptions are evaluated carefully in Chapter 3.

The stream profiles were extracted from digital elevation models (DEMs). An initial goal of the study was to compare topography from DEMs with data derived from topographic maps and field surveys, and further to develop techniques for stream-profile analysis using DEMs. The profiles themselves exhibit smooth, concave-up shapes, even in the HUZ, suggesting that the streams may be in steady state with current uplift rates. The steady-state channel hypothesis is evaluated in Chapter 2, and it is central to the rest of the study, for it permits the use of topography to estimate shear-stress model parameters. The resulting analysis indicates that the linear version of the model can explain the observed relationship between channel slope and rock-uplift rate only if the coefficient of erosion (K) varies significantly in concert with U, with higher values in the HUZ (addressed in Chapter 3, see below). Also, the channel concavity (θ) is constant throughout the study area, consistent with shear-stress model predictions for steady-state channels and with a preliminary channel-width dataset. The chapter closes with a calculation of theoretical response time for the HUZ channels, which matches the field evidence from Merritts and Bull (1989) reasonably well.

Chapter 3 delves deeper into the observation from Chapter 2 that erosion processes are apparently more effective (higher K) in the HUZ. Here the central question is: what aspects of the environment and morphology are responding to uplift rate or otherwise changing between the LUZ and HUZ? The search for an answer began with a list of four possible factors that could explain the observed variability in K: (1) discharge—increase in the HUZ due to orographic enhancement of precipitation; (2) channel width—decrease in the HUZ as the channels entrench to more efficiently incise; (3) lithology—more resistant in the HUZ; and (4) sediment flux—higher in the HUZ and more effective as an erosive agent. These four hypothesized responses motivated a fieldwork-based effort to explore differences in each factor between the uplift-rate zones and therefore carefully constrain and evaluate the shear-stress model.

For the field-based study, the morphology and lithology of 7 streams was analyzed, as well as discharge data from 15 gauging stations throughout the region. Orographic enhancement of precipitation appears to cause an approximately twofold increase in discharge in the HUZ, which can explain part (but not all) of the apparent variation in K. Measurements of high-flow channel width indicate that streams of the LUZ are actually narrower (at a given drainage area) than those in the HUZ, counter to the hypothesized response. However, this decrease in width is likely the result of a recent (last 100 yr) land-use difference between the zones, not a long-term response. Valley width does not appear to vary significantly between the HUZ and LUZ, and it is not sensitive to land use. Measurements of rock strength and qualitative joint-spacing surveys (Selby, 1993) suggest that lithologic resistance to erosion is reasonably constant throughout the study area. Finally, observations of bed sediment are hampered by the land-use difference, so definitive statements about the influence of sediment flux on erosion rates cannot be made from the field data. Thus, of the responses hypothesized above, the first (discharge) was confirmed but too weak to explain the variability fully, the second and third (width and lithology) were invalidated, and the fourth (sediment flux) was untestable in this landscape. However, a careful review of the model assumptions indicated that a fifth factor—the threshold for erosion of bedrock—that is usually neglected could play an important role. This chapter closes by showing that inclusion of a nonzero value for threshold shear stress (τ_c) in the model changes the theoretical relationship between steady-state channel gradient and rock-uplift rate, suggesting that this term should not be omitted from the model.

In Chapter 4 the role of thresholds and stochastic processes in driving bedrock incision by rivers is examined. As mentioned above, τ_c is usually omitted from modeling efforts because of the simplifying assumption that bedrock erosion occurs only during major floods that far exceed this threshold. Essentially, this omission is directly coupled to the assumption of a dominant discharge event that does all the geomorphic work. The threshold term gains importance only if some part of a distribution of floods is able to exceed it in a given field area. This was demonstrated by Tucker and Bras (2000), who used a model forced by a stochastic distribution of storms to show that omission of τ_c leads to the counterintuitive prediction that the least-variable climate yields the most rapid incision rates. Therefore, models will be most effective if they include both thresholds and a realistic distribution of the magnitude and frequency of flood events.

In the first part of Chapter 4, basal shear stress during a 1981 flood event on a New York river was calculated. This flood was the only event in the past ~40 years that caused significant plucking of in-place bedrock on the river bed, therefore the shear stress yields a maximum estimate of the threshold shear stress ($\tau_c \approx$100-200 Pa) for this setting, a difficult quantity to measure from field data. This result highlights the importance of erosion driven by discrete, rare (in low erosion-rate settings) flood events that generate shear stresses in excess of thresholds.

In the second part of Chapter 4, the more sophisticated Tucker and Bras version of the shear-stress model that includes a threshold shear stress for bedrock incision and stochastic distribution of storm events (Tucker and Bras, 2000; Tucker, 2001) is applied to the northern California streams. To do this, Poisson pulse rainfall model parameters (Eagleson, 1978) were calculated for two weather-data stations to represent the climate in the LUZ and HUZ. This model indicates that a reasonable, low value of threshold shear stress ($\tau_c \approx$100 Pa) is capable of explaining the observed relationship between channel gradient and uplift rate without need to appeal to unexplained and untestable influences, such as sediment flux. Because of the relatively high channel gradients of the California streams, this value of τ_c is exceeded during high-frequency events in the study area, particularly in the HUZ. Therefore, erosive events occur more often, consistent with the overall high erosion rates and the observed increase in erosional efficiency in the HUZ. This approach yields a satisfying, fully explained picture of the channel response in the northern California field site. Moreover, it underscores the importance of modeling climate with

a stochastic distribution of events (some capable of exceeding thresholds), not with a single "representative" flood event (*i.e.* Chapters 2 and 3).

Chapter 5 couples the shear-stress model to a simple rule for offshore wave-based erosion (Anderson *et al.*, 1999), to investigate how eustatic fluctuations in sea level affect onshore fluvial profiles. This work is partially motivated by a question raised in Chapter 2: can channels exhibit steady-state topography if the base level is constantly fluctuating? Two sets of experiments with the coupled erosion model were done, the first using a constant rate of sea-level rise or fall, and the second forced by a realistic Late Quaternary sea-level curve. Systematic variations in offshore bathymetry and uplift-rate boundary conditions were used in the various runs. The model explores the interplay of four rates: sea-level change, rock-uplift, fluvial incision, and wave-based erosion. The results highlight the importance of boundary conditions in setting model response. The development of approximately constant onshore channel topography depends on the existence of a relatively stable shoreline position, for which a decrease in rock-uplift rate from onshore to offshore is generally necessary. The onshore response to sea-level regression depends critically on the bathymetry, which is developed by wave-based erosion and uplift. Further advances in this kind of modeling will require a more sophisticated model to describe wave-based erosion of bedrock. In the final analysis, the model results are compared to topographic and bathymetric profiles from the Mendocino triple junction area. Several aspects of the longitudinal profiles are consistent with model results, including the common, relatively flat, alluviated channel mouths, and the observed scatter in channel-gradient data. The model indicates that the steady-state hypothesis for the California streams is reasonable, if the rock-uplift rates derived from onshore marine terraces decrease seaward in the nearshore.

To summarize, the structure of this thesis is to begin with a basic model (Chapter 2), test simplifying assumptions and constrain empirical internal relationships (Chapters 3 and 5), and add complexity as necessary (Chapters 4 and 5). The final picture of the Mendocino triple junction study area is a well-developed picture of channel response to tectonic, climatic and eustatic forcings, fully informed by field and hydrologic data, and modeled using a minimum number of unconstrained parameters. Bedrock-incision modeling efforts will be most effective for rigorously testing climate—tectonic hypotheses if they are driven by a realistic suite of flood magnitude and frequency, modified by physically based erosion thresholds.

The following four chapters have been written for publication in journals, with coauthors Kelin Whipple, Gregory Tucker, and Dorothy Merritts. Chapter 2 was published in the August 2000 issue of the *Geological Society of America Bulletin*. Chapter 3 was submitted to *Geomorphology* on January 25, 2001. Chapter 4 was submitted to *Nature* on May 16, 2001. Chapters 3 and 4 are presently in review. Chapter 5 is intended for submission to the *Journal of Geology*.

Future work

Further advances in bedrock-incision modeling will depend primarily on studies in other well-chosen field sites and on laboratory experiments. Bedrock incision, unlike for instance sediment transport or mass wasting, is difficult to monitor in the field because the rates are usually slow compared to human timescales. Field-based advances generally require well-preserved strath terraces (*e.g.* Merritts *et al.*, 1994; Wegmann and Pazzaglia, 1998) or other natural experiments (*e.g.* chapters 2-4; Stock and Montgomery, 1999; Whipple *et al.*, 2000b). Here several avenues for further work on bedrock incision are suggested. As in this thesis, the focus is on detachment-limited incision processes, but recent studies also indicate that transport-limited incision (as well as transitions between these states) is also an important area for continued work (Willgoose *et al.*, 1991; Howard, 1998; Sklar and Dietrich, 1998; Whipple and Tucker, 2001).

The work presented in this thesis argues strongly for a stochastically based approach to geomorphic modeling, with inclusion of erosion thresholds. To understand this better, more field settings where bedrock erosion has occurred during discrete, historical events need to be found (*e.g.* Whipple *et al.*, 2000b). Such field studies will be most successful if the events are captured by a monitored suite of precipitation and discharge data (*e.g.* Chapter 4). Also, the influence of variations in orographic precipitation (Barros and Lettenmaier, 1993) on stream discharge, both within a field area (*e.g.* Chapter 3), and within a drainage basin (*e.g.* Roe *et al.*, 2001) must be monitored and quantified, so that this feedback can be better included in stochastic models.

A second kind of natural experiment requires areas with a demonstrable transient condition (*e.g.* Stock and Montgomery, 1999; Whipple *et al.*, 2000b), where the river profile is clearly in the process of responding to a perturbation. The best such experiment would be at a place where a sudden base-level drop or change in tectonic forcing can be seen clearly and the timing of this

change can be constrained using precise geochronologic techniques (Noller *et al.*, 2000). Initially, this was thought to be the case in the King Range of northern California, but analysis showed that the most likely scenario was that the streams have responded to the uplift-rate acceleration. Field settings with such transient conditions must be found (*e.g.* Spotila *et al.*, 1998) and studied from the standpoint of physics-based fluvial incision modeling. A well-dated transient condition might yield a unique opportunity to (1) constrain all of the unknown model parameters and (2) test differing bedrock erosion models against each other.

Finally, a richer understanding of the physics of bedrock erosion is critical (*e.g.* Foley, 1980; Slingerland, 1997; Hancock *et al.*, 1998; Sklar and Dietrich, 1998; Whipple *et al.*, 2000a). This thesis concludes that a shear-stress-based model can describe the observed response, but it does little to test or constrain the fundamental relationship between fluvial fluid flow (*i.e.* shear stress, stream power) and bedrock erosion. As seen by the example of sediment-transport processes, the details of the physics will be best understood through well-designed laboratory experiments. Recent work by Sklar and Dietrich (Sklar and Dietrich, 1999) on bedrock erosion by impact abrasion shows great promise for understanding the critical role of sediment flux in bedrock incision (Sklar and Dietrich, 1998). Flume work by Parker and colleagues (*e.g.* Parker and Izumi, 2000) on knickpoint-driven incision demonstrates the importance of this process. Large-scale flume experiments on plucking of bedrock blocks may be a parallel avenue for advancement. Recent experiments of deposition in a tank where subsidence rates can be systematically varied (*e.g.* Hasbargen and Paola, 2000) hold immense promise for using controlled studies to unravel responses and interactions among base level, tectonics and thresholds. Of course, detailed monitoring of bedrock-erosion processes in natural channels must also be done (*e.g.* Hancock *et al.*, 1998; Whipple *et al.*, 2000a), including reoccupation of field surveys (*e.g.* Whipple *et al.*, 2000b). Until geomorphologists can develop a more complete theoretical understanding of both the fluid processes that drive bedrock incision and how these processes are affected and changed by factors such as lithologic resistance and sediment flux, modeling efforts will be hampered by the presence of several difficult-to-constrain parameters.

References cited

Anderson, R.S., Densmore, A.L., and Ellis, M.A., 1999, The generation and degradation of marine terraces: Basin Research, v. 11, p. 7-19.

Barros, A., and Lettenmaier, D., 1993, Dynamic modeling of orographically induced precipitation: Reviews of Geophysics, v. 32, p. 265-284.

Bull, W.B., 1991, Geomorphic Responses to Climatic Change, Oxford, Oxford University Press, 326 p.

Dunne, T., and Leopold, L.B., 1978, Water in Environmental Planning, New York, W.H. Freeman and Company, 818 p.

Eagleson, P.S., 1978, Climate, soil, and vegetation 2. The distribution of annual precipitation derived from observed storm frequencies: Water Resources Research, v. 14, p. 713-721.

Foley, M.G., 1980, Bed-rock incision by streams: Geological Society of America Bulletin, Part II, v. 91, p. 2189-2213.

Hancock, G.S., Anderson, R.S., and Whipple, K.X., 1998, Beyond Power: Bedrock Incision Process and Form, *in* Tinkler, K.J., and Wohl, E.E., eds., Rivers Over Rock: Fluvial Processes in Bedrock Channels: Geophysical Monograph 107: Washington, American Geophysical Union, p. 35-60.

Hasbargen, L.E., and Paola, C., 2000, Landscape instability in an experimental drainage basin: Geology (Boulder), v. 28, p. 1067-1070.

Howard, A.D., and Kerby, G., 1983, Channel changes in badlands: Geological Society of America Bulletin, v. 94, p. 739-752.

Howard, A.D., 1994, A detachment-limited model of drainage basin evolution: Water Resources Research, v. 30, p. 2261-2285.

Howard, A.D., Seidl, M.A., and Dietrich, W.E., 1994, Modeling fluvial erosion on regional to continental scales: Journal of Geophysical Research, v. 99, p. 13,971-13,986.

Howard, A.D., 1998, Long profile development of bedrock channels: interaction of weathering, mass wasting, bed erosion, and sediment transport, *in* Tinkler, K.J., and Wohl, E.E., eds., Rivers Over Rock: Fluvial Processes in Bedrock Channels: Geophysical Monograph 107: Washington, American Geophysical Union, p. 297-320.

Koons, P.O., 1995, Modeling the topographic evolution of collisional belts: Annual Reviews in Earth and Planetary Science, v. 23, p. 375-408.

Leopold, L.B., and Maddock, T., Jr., 1953, The hydraulic geometry of stream channels and some physiographic implications: U.S. Geological Survey Professional Paper 252.

Merritts, D., and Bull, W.B., 1989, Interpreting Quaternary uplift rates at the Mendocino triple junction, northern California, from uplifted marine terraces: Geology, v. 17, p. 1020-1024.

Merritts, D., and Vincent, K.R., 1989, Geomorphic response of coastal streams to low, intermediate, and high rates of uplift, Mendocino junction region, northern California: Geological Society of America Bulletin, v. 101, p. 1373-1388.

Merritts, D., and Ellis, M., 1994, Introduction to special section on tectonics and topography: Journal of Geophysical Research, v. 99, p. 12,135-12,141.

Merritts, D.J., Vincent, K.R., and Wohl, E.E., 1994, Long river profiles, tectonism, and eustasy: A guide to interpreting fluvial terraces: Journal of Geophysical Research, v. 99, p. 14031-14050.

Merritts, D.J., 1996, The Mendocino triple junction: Active faults, episodic coastal emergence, and rapid uplift: Journal of Geophysical Research, v. 101, p. 6051-6070.

Molnar, P., and England, P., 1990, Late Cenozoic uplift of mountain ranges and global climate change: chicken or egg?: Nature, v. 346, p. 29-34.

Noller, J.S., Sowers, J.M., and Lettis, W.R., 2000, Quaternary geochronology: methods and applications: AGU Reference Shelf 4, Washington, American Geophysical Union, 582 p.

Parker, G., and Izumi, N., 2000, Purely erosional cyclic and solitary steps created by flow over a cohesive bed: Journal of Fluid Mechanics, v. 419, p. 203-238.

Roe, G.H., Montgomery, D.R., and Hallet, B., 2001, Effects of orographic precipitation variations on steady-state river profiles and relief: in preparation.

Selby, M.J., 1993, Hillslope Materials and Processes, Oxford, Oxford University Press, 451 p.

Sklar, L., and Dietrich, W.E., 1998, River longitudinal profiles and bedrock incision models: stream power and the influence of sediment supply, *in* Tinkler, K.J., and Wohl, E.E., eds., Rivers Over Rock: Fluvial Processes in Bedrock Channels: Geophysical Monograph 107: Washington, DC, American Geophysical Union, p. 237-260.

—, 1999, Relating rates of fluvial bedrock erosion to rock strength: an experimental study (abstract): EOS, Transactions, AGU, v. 80, p. F448.

Slingerland, R., 1997, A new fluvial bedrock erosion model based on the work-energy principle: EOS, Transactions, AGU, v. 78, p. F299-F300.

Spotila, J.A., Farley, K.A., and Sieh, K., 1998, Uplift and erosion of the San Bernardino Mountains associated with transpression along the San Andreas fault, California, as constrained by radiogenic helium thermochronometry: Tectonics, v. 17, p. 360-378.

Stock, J.D., and Montgomery, D.R., 1999, Geologic constraints on bedrock river incision using the stream power law: Journal of Geophysical Research, v. 104, p. 4983-4993.

Tinkler, K.J., and Wohl, E.E., 1998, Rivers over rock: Fluvial processes in bedrock channels: Geophysical Monograph 107, Washington, American Geophysical Union, 323 p.

Tucker, G.E., and Bras, R.L., 2000, A stochastic approach to modeling the role of rainfall variability in drainage basin evolution: Water Resources Research, v. 36, p. 1953-1964.

Tucker, G.E., 2001, Long-term average river erosion and transport rates: Analytical solution for finite-threshold cases: Water Resources Research, v. in preparation.

Wegmann, K., and Pazzaglia, F.J., 1998, Rock uplift and deformation of the Olympic subduction complex determined by fluvial terraces in the Clearwater River basin, Northwest Washington State: Abstracts with Programs - Geological Society of America, v. 30, p. 329.

Whipple, K.X., Kirby, E., and Brocklehurst, S.H., 1999, Geomorphic limits to climate-induced increases in topographic relief: Nature, v. 401, p. 39-43.

Whipple, K.X., and Tucker, G.E., 1999, Dynamics of the stream-power river incision model: Implications for the height limits of mountain ranges, landscape response timescales, and research needs: Journal of Geophysical Research, v. 104, p. 17661-17674.

Whipple, K.X., Anderson, R.A., and Hancock, G.S., 2000a, River incision into bedrock: Mechanics and relative efficacy of plucking, abrasion, and cavitation: Geological Society of America Bulletin, v. 112, p. 490-503.

Whipple, K.X., Snyder, N.P., and Dollenmayer, K., 2000b, Rates and processes of bedrock incision by the Upper Ukak River since the 1912 Novarupta ash flow in the Valley of Ten Thousand Smokes, Alaska: Geology, v. 28, p. 835-838.

Whipple, K.X., and Tucker, G.E., 2001, Transitions between detachment-limited and transport-limited river incision: Implications for the form, occurrence, and dynamics of "mixed-bedrock-alluvial" channel systems: Journal of Geophysical Research, v. in review.

Willgoose, G., Bras, R.L., and Rodriguez-Iturbe, I., 1991, A coupled channel network growth and hillslope evolution model,1 theory: Water Resources Research, v. 27, p. 1671-1684.
Wolman, M.G., and Miller, J.P., 1960, Magnitude and frequency of forces in geomorphic processes: Journal of Geology, v. 68, p. 54-74.

Landscape response to tectonic forcing: Digital elevation model analysis of stream profiles in the Mendocino triple junction region, northern California

Noah P. Snyder* **Kelin X. Whipple** *Department of Earth, Atmospheric, and Planetary Sciences, Massachusetts Institute of Technology, Cambridge, Massachusetts 02139-4307, USA*

Gregory E. Tucker *Department of Civil and Environmental Engineering, Massachusetts Institute of Technology, Cambridge, Massachusetts 02139-4307, USA*

Dorothy J. Merritts *Department of Geosciences, Franklin and Marshall College, Lancaster, Pennsylvania 17604-3003, USA*

ABSTRACT

The topographic evolution of orogens is fundamentally dictated by rates and patterns of bedrock-channel incision. Quantitative field assessments of process-based laws are needed to accurately describe landscape uplift and denudation in response to tectonics and climate. We evaluate and calibrate the shear stress (or similar unit stream-power) bedrock-incision model by studying stream profiles in a tectonically active mountain range. Previous work on emergent marine terraces in the Mendocino triple junction region of northern California provides spatial and temporal control on rock-uplift rates. Digital elevation models and field data are used to quantify differences in landscape morphology associated with along-strike northwest to southeast changes in tectonic and climatic conditions. Analysis of longitudinal profiles supports the hypothesis that the study-area channels are in equilibrium with current uplift and climatic conditions, consistent with theoretical calculations of system response time based on the shear-stress model. Within uncertainty, the profile concavity (θ) of the trunk streams is constant throughout the study area ($\theta \approx 0.43$), as predicted by the model. Channel steepness correlates with uplift rate. These data help constrain the two key unknown model parameters, the coefficient of erosion (K) and the exponent associated with channel gradient (n). This analysis shows that K cannot be treated as a constant throughout the study area, despite generally homogeneous substrate properties. For a reasonable range of slope-exponent values (n), best-fit values of K are positively correlated with uplift rate. This correlation has important implications for landscape-evolution models and likely reflects dynamic adjustment of K to tectonic changes, due to variations in orographic precipitation, and perhaps channel width, sediment load, and frequency of debris flows. The apparent variation in K makes a unique value of n impossible to constrain with present data.

Keywords: channel geometry, digital elevation models, erosion rates, fluvial erosion, geomorphology, landscape evolution.

INTRODUCTION

The potential for dynamic interactions among surficial processes, crustal processes, and climate has received broad interdisciplinary attention in recent years (e.g., Molnar and England, 1990; Beaumont et al., 1992; Raymo and Ruddiman, 1992; Hoffman and Grotzinger, 1993; Koons, 1995). This interest has helped spur numerical modeling attempts to analyze the interplay of these large-scale processes on topographic evolution of mountain ranges (e.g., Anderson, 1994; Tucker and Slingerland, 1994; Kooi and Beaumont, 1996). While considerable progress has been made, these modeling efforts have been hampered by the lack of data on fluvial bedrock-erosion rates and processes, as noted by Merritts and Ellis (1994). In particular, many aspects of the dynamic response of bedrock channels to tectonic forcing are not known quantitatively (Whipple and Tucker, 1999).

Bedrock channels play a key role in landscape evolution. The ability of streams to incise through bedrock ultimately sets the rate of lowering of a landscape, and therefore mass removal, in actively rising mountainous regions. Several recent studies of bedrock channels have focused on erosion processes and morphology (e.g., Foley, 1980; Howard and Kerby, 1983; Hancock et al., 1998; Pazzaglia et al., 1998; Sklar and Dietrich, 1998; Wohl, 1998; Whipple et al., 2000). We build on this research in an area of known, spatially variable tectonic rock-uplift rates, where dynamic stream response can be quantified (Merritts and Vincent, 1989). The nature and timing of channel response are crucial unknowns in our ability to describe quantitatively many aspects of landscape evolution and the geologic record, including hillslope response, sediment flux, and transmission of base-level signals through a watershed. In this paper we evaluate and calibrate a model for channel longitudinal-profile evolution in a tectonically active mountain range. The effort combines testing of certain model predictions with field constraints on key model parameters.

Various models based on the postulate that bedrock-channel incision rate is proportional to shear stress or unit stream power have been proposed (e.g., Howard and Kerby, 1983). Although these models have been applied to field data (Howard and Kerby, 1983; Seidl and Dietrich, 1992; Rosenbloom and Anderson, 1994; Pazzaglia et al., 1998; Sklar and Dietrich, 1998; Talling and Sowter, 1998; Weissel and Seidl, 1998; Stock and Montgomery, 1999), they remain relatively untested and their parameters poorly constrained. More quantitative field tests of these models are required, particularly in active tectonic settings. Even in the simplest form, the dynamics of landscape evolution

*E-mail: noahp@mit.edu.

GSA Bulletin; August 2000; v. 112; no. 8; p. 1250–1263; 10 figures; 3 Tables.

driven by the shear-stress model depend on at least two key unknown parameters: the coefficient of erosion and the exponent associated with channel gradient (Whipple and Tucker, 1999). In field areas where substrate properties are invariant, and climate and uplift histories are known, these parameters may be estimated from field and map data.

We study 21 small coastal streams in the Mendocino triple junction region of northern California, where the lithologic, climatic, and tectonic conditions can be constrained both spatially and temporally. Highly fractured mudstone and sandstone underlie the area (McLaughlin et al., 1994); variations in lithologic resistance are only on a local scale. Late Quaternary climate fluctuations were subdued in the maritime region (Johnson, 1977), although the orographic effect of topography causes important, quantifiable precipitation differences. The previous work of Merritts and collaborators on flights of emergent marine terraces in the Mendocino triple junction region shows that along the coast, late Pleistocene and Holocene rock-uplift rates vary over nearly an order of magnitude, from 0.5 mm yr^{-1} to 4 mm yr^{-1} (Merritts and Bull, 1989; Merritts and Vincent, 1989; Merritts, 1996). In addition, high rock-uplift rates only began ca. 100 ka (Merritts and Bull, 1989), affording the opportunity to investigate channel response to a change in tectonic forcing.

We use data from digital elevation models (DEMs), field surveys, and topographic maps. DEMs have been used by numerous workers to analyze fluvial channels (e.g., Tarboton et al., 1991; Dietrich et al., 1993; Montgomery and Foufoula-Georgiou, 1993; Willgoose, 1994, Moglen and Bras, 1995; Tucker, 1996; Sklar and Dietrich, 1998; Weissel and Seidl, 1998) Comparisons among various digital topographic analysis techniques are provided, and these methods are tested using topographic maps and field surveys for a few basins. The goal of this analysis is to critically evaluate the applicability of DEMs to study of bedrock channels in the context of the shear-stress incision model. DEMs are used to quantify channel longitudinal profile form, drainage area, and local slope, focusing on the bedrock-channel dominated part of the system. Field measurements and observations are used to constrain the relationship between bedrock-channel width and drainage area, and to characterize local channel morphology.

This paper is an attempt to evaluate and constrain the shear-stress model, using DEMs and field data, in a field site where the tectonic history is known. Specifically, we present data quantifying. (1) the concavity and steepness of trunk streams in study-area drainages and their dependence on uplift rate; (2) variations in the coefficient of erosion in concert with differences in uplift rate; (3) the degree of nonlinearity in the relation between channel slope and incision rate; and (4) the time scale of channel response to a change in tectonic conditions.

These analyses yield a picture of landscape evolution in a bedrock-channel–dominated, young mountain range. We begin by developing the theoretical basis of the shear-stress model, with reference to the possibilities for constraining model parameters with field and DEM data. Second, the tectonic history, lithology, climate, and channel morphology of the Mendocino triple junction study area are described. Third, the applicability of the theory to the field area is carefully evaluated. Next, the methods and results of the longitudinal-profile analysis are reviewed and presented. Finally, the implications of the results are discussed in terms of channel-response processes and time scale.

THEORETICAL FRAMEWORK

Many workers have modeled detachment-limited bedrock-channel incision using a form of the shear-stress (or similar unit stream-power) model, in which incision rate is given by a power function of drainage area and channel slope (e.g., Howard and Kerby, 1983; Seidl and Dietrich, 1992; Anderson, 1994; Howard, 1994; Moglen and Bras, 1995; Tucker, 1996; Stock and Montgomery, 1999; Whipple and Tucker, 1999). Here we provide a brief synopsis of the derivation of this law. The shear-stress model is used to describe the evolution of bedrock-channel longitudinal profiles. The objective of this section is to establish how measurements of topography and channel form in real landscapes can be used to constrain model parameters.

Shear-Stress Incision Model

The shear-stress incision model is predicated on the hypothesis that bedrock-channel-erosion rate (E), in volume per unit channel area per time, is a power-law function of basal shear stress (τ_b):

$$E = k_b \tau_b^a, \tag{1}$$

where k_b is a dimensional coefficient dependent on dominant erosion process, rock resistance, and possibly sediment load, and a is a positive, process-dependent constant. Theoretical predictions for the value of a vary from 1 for a linear-erosion process in easily eroded material (Howard and Kerby, 1983) to ~5/2 for impact abrasion (Foley, 1980; Hancock et al., 1998; Whipple et al., 2000). Combining the assumptions of conservation of mass (water), and steady, uniform flow, the following expression for basal shear stress (τ_b) is obtained:

$$\tau_b = \rho C_f^{1/3} \left[\frac{gSQ}{W} \right]^{2/3}, \tag{2}$$

where ρ is density of water, C_f is a dimensionless friction factor, g is gravitational acceleration, S is local channel slope (dz/dx), Q is a characteristic stream discharge (Wolman and Miller, 1960), and W is a characteristic channel width. Next, a relationship for basin hydrology is assumed:

$$Q = k_q A^c, \tag{3}$$

where A is upstream drainage area, k_q is a dimensional coefficient, and c is a positive constant, the value of which is approximately unity or slightly less (Dunne and Leopold, 1978; Pazzaglia et al., 1998), particularly for small, steep drainages, such as those studied here. Then, a relationship for downstream increase in channel width with discharge is assumed, and combined with equation 3:

$$W = k_w Q^b = k_w k_q^b A^{bc}, \tag{4}$$

where k_w is a dimensional coefficient and b is a positive constant, empirically observed to be ~0.5 in alluvial rivers (Leopold and Miller, 1956). The products $k_w k_q^b$ and bc may be found from drainage-area data and field measurements of channel width. Finally, equations 1–4 are combined to obtain the well-known shear-stress incision law,

$$E = KA^m S^n, \tag{5}$$

with the relations

$$K = k_b k_w^{-2a/3} k_q^{2a(1-b)/3} \rho^a g^{2a/3}; \tag{6}$$

$$m = (2ac/3)(1 - b); \tag{7}$$

$$n = 2a/3; \tag{8}$$

and

$$m/n = c(1 - b). \tag{9}$$

Equations 5–9 highlight the key unconstrained parameters in the shear-stress model. Equation 9 indicates that the ratio m/n is expected to be constant for a broad set of shear-stress–driven fluvial incision processes (Whipple and Tucker, 1999), an important, testable model prediction. For the typical, empirically determined values of b and c (equations 3 and 4), the value of m/n is ~0.5. However, the exponent b is only known well for alluvial channels, and further means of constraining this ratio by measuring channel width as a function of drainage area (equation 4) are discussed in the following. This relation reduces the modeling problem to two key unknowns: K and n. The slope exponent (n) depends on the mechanics of erosion processes (a), as discussed here. Whipple and Tucker (1999) show that the value of n exerts strong control on equilibrium channel slope, equilibrium topographic relief, transient profile form, and response time scale. We now briefly investigate the factors that control the value of K.

Erosion Coefficient

The erosion coefficient (K) is not well calibrated, but one study (Stock and Montgomery, 1999) has presented evidence that K varies over orders of magnitude among different study areas. K is a dimensional coefficient with units of meters^{1-2m} yr^{-1}. A wide variety of factors probably influence K, including rock strength, channel bed material, channel width, runoff, and debris-flow frequency. Although the frequency of debris flows in a fluvially dominated channel may influence K, the shear-stress incision model is likely to be inadequate in debris-flow–dominated channels (Howard, 1998; Stock and Dietrich, 1998). In addition, K, or specifically k_b (equation 1), may be a function of sediment load, with large sediment concentrations protecting the bed, as argued by Sklar and Dietrich (1998). We revisit this issue later in this paper. Within an area of relatively uniform lithology, K (or an analogous erodibility parameter) has often been modeled as constant in both space and time (e.g., Seidl and Dietrich, 1992; Anderson, 1994; Kooi and Beaumont, 1996). Holding K constant in a model of landscape response to tectonic forcing includes the implicit assumption that channel gradient is the only variable that is free to adjust to changes in rock-uplift rate. However, many of the factors that control K are likely to adjust during the evolution of a mountain range. For example, higher uplift rates are likely to lead to higher topography, which leads to increased orographic precipitation, presumably increasing k_q and therefore K (equation 6). In addition, channels may narrow in response to an increase in the rate of relative base-level fall (decreasing k_w and increasing K), or may become more alluviated in response to changes in sediment flux (perhaps decreasing k_b and K; equation 6). We present evidence here that the coefficient of erosion (K) may indeed vary in response to tectonic forcing. We also place some preliminary constraints on the relative importance of adjustments in channel width, bed configurations, and orographic precipitation.

Steady-State Longitudinal Profiles

The shear-stress incision model can be combined with a statement of conservation of mass to analyze the rate of change of river-bed elevation (dz/dt), given by a competition between uplift and erosion (e.g., Howard, 1994):

$$dz/dt = U - E = U - KA^m S^n, \quad (10)$$

where U is the rock uplift rate relative to base level. In the case of a steady-state landscape ($dz/dt = 0$), equation 10 can be solved for equilibrium slope (S_e):

$$S_e = (U/K)^{1/n} A^{-m/n}, \quad (11)$$

where, for cases of uniform U and K, m/n dictates the concavity of the equilibrium profile, and likewise the coefficient $(U/K)^{1/n}$ dictates equilibrium profile steepness. The power-function relation implied by equation 11 has been observed empirically in many different geologic settings, with stream gradient described by

$$S = k_s A^{-\theta}. \quad (12)$$

The exponent, θ (the concavity index), and coefficient, k_s (the steepness index), can be measured directly by regression of slope and area data. The concavity index (θ) is generally found to be between 0.3 and 0.6 (Hack, 1957; Flint, 1974; Willgoose et al., 1990; Tarboton et al., 1991; Moglen and Bras, 1995; Slingerland et al., 1998), but values to 1.1 have been measured in some channels (Sklar and Dietrich, 1998). The coefficient k_s is similar in principle to the stream-gradient index developed by Hack (1973), but more general. In any analysis of stream longitudinal profiles, the relationships implied by equations 11 and 12:

$$\theta = m/n, \quad (13)$$

and

$$k_s = (U/K)^{1/n}, \quad (14)$$

hold true if and only if (1) the river profile is in steady state with respect to current climatic and uplift conditions; and (2) both uplift rate (U) and coefficient of erosion (K) are uniform through the channel reach. Where these conditions are met, the parameters $(U/K)^{1/n}$ and m/n can be estimated directly through regressions of channel-gradient and drainage-area data. In such cases, the degree of correlation between channel steepness and rock-uplift rate can be used to place important constraints on shear-stress model parameters. If K is constant throughout the study area, a unique value of n may be determined directly. In addition, the model prediction that the m/n ratio is a constant, largely dictated by the relationship between channel width and drainage area (equation 4), can be tested directly. Whipple and Tucker (1999) derived an expression for channel response time to changes in rock-uplift rate. Predicted response times can be tested where information on the rock-uplift history is available, such as in the Mendocino triple junction region. In the discussion section of this paper, we modify the channel response-time equation give by Whipple and Tucker to account for possible changes in K in concert with increased uplift rate and compare predicted response times to uplift history (Merritts and Bull, 1989).

FIELD AREA

The King Range is an area of rugged relief at the northern terminus of the San Andreas fault in northern California (Fig. 1). The study area consists of a subparallel series of 21 small coastal drainage basins from Cape Mendocino in the north, through the King Range to Fort Bragg in the south (Fig. 2; Table 1), previously studied by Merritts and Vincent (1989). Late Pleistocene and Holocene rock-uplift rates vary nearly an order of magnitude along this 120 km transect, from ~3 mm yr^{-1} near the Bear River, to 4 mm yr^{-1} in the King Range, to ~0.5 mm yr^{-1} at Fort Bragg (Fig. 3) (McLaughlin et al., 1983; Merritts and Bull, 1989; Merritts, 1996). These uplift rates are obtained from radiocarbon dating of fossil shells sampled either from in-place growth positions on emergent marine platforms or from within intertidal marine sediments overlying marine platforms (Merritts and Bull, 1989; Merritts, 1996). Marine platforms and cover-bed sediments are numerous throughout the study area, forming flights of uplifted late Pleistocene and Holocene marine terraces that are correlated with a eustatic sea-level curve

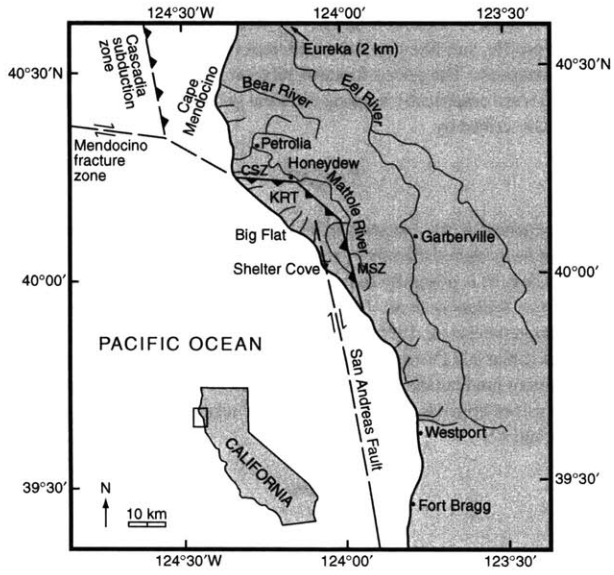

Figure 1. The Mendocino triple junction region study area, including the King Range terrane (KRT). Eastern and northern boundaries of the terrane are the Mattole and Cooskie shear zones (MSZ and CSZ), respectively (McLaughlin et al., 1994). Modified from Merritts and Vincent (1989), Merritts (1996), and Prentice et al. (1999).

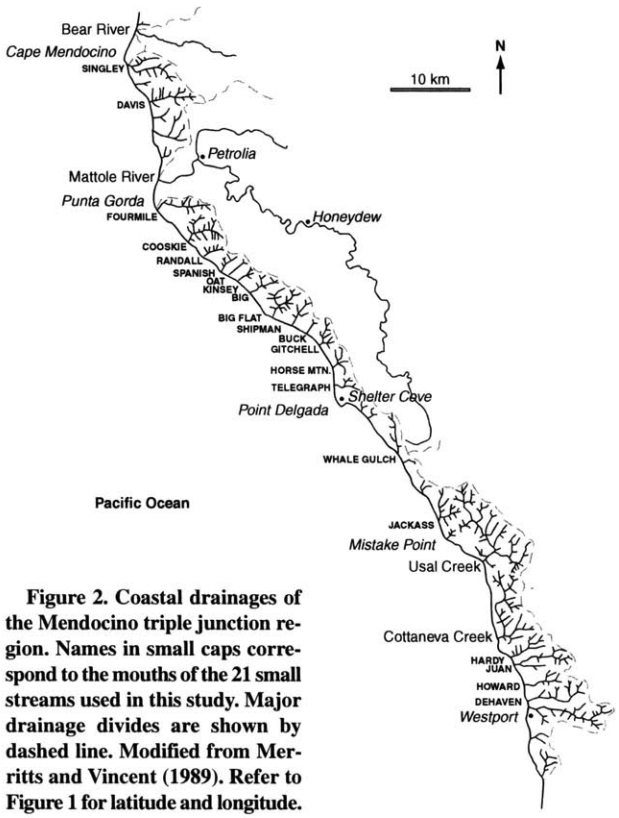

Figure 2. Coastal drainages of the Mendocino triple junction region. Names in small caps correspond to the mouths of the 21 small streams used in this study. Major drainage divides are shown by dashed line. Modified from Merritts and Vincent (1989). Refer to Figure 1 for latitude and longitude.

in order to extend the uplift-rate record back to 330 ka, beyond the range of radiocarbon dating (Merritts and Bull, 1989). The terraces do not show any signs of significant coast-perpendicular tilting, indicating that the uplift rates are approximately uniform within each study-area basin. Much of our analysis hinges upon these uplift-rate data, which are an important potential source of uncertainty (Merritts and Bull, 1989; Merritts, 1996). The extremely high uplift rate of the King Range terrane, between the Cooskie and Mattole shear zones, is related to plate boundary interactions around the northward-propagating Mendocino triple junction (McLaughlin et al., 1994; Merritts, 1996; Prentice et al., 1999).

The uplift-rate data and local structural geology provide a rough means of dividing the study area into four distinct zones, from north to south, the northern transition zone (Singley Creek to Cooskie Creek), the King Range high-uplift zone (Randall Creek to Gitchell Creek), the intermediate-uplift zone (Horse Mountain Creek to Whale Gulch), and the low-uplift zone (Jackass Creek to Dehaven Creek; Fig. 3). The northern and high-uplift zones underwent an acceleration in uplift rates after 96 ka from low-uplift-zone conditions (<1 mm yr^{-1}) to 3–4 mm yr^{-1} (Merritts and Bull, 1989). Uplift rates in the southern part of the study area have been constant for at least the past 330 k.y. (Merritts and Bull, 1989). The transition in tectonic setting from low- to high-uplift rates provides the opportunity to isolate the effects of this change by comparison of topographic data between two otherwise generally similar regions.

Bedrock lithology in the study area consists of Tertiary and Cretaceous marine sandstones and mudstones of the Franciscan assemblage (Beutner et al., 1980; McLaughlin et al., 1994). In general, the rocks are jointed on the submeter scale and easily eroded, although local variations in resistance provide some areas of small-scale lithologic control on channel characteristics. In addition, the large shear zones that surround the King Range terrane produce differences in the level of deformation and jointing of the rocks (Figs. 1 and 3; Beutner et al., 1980; McLaughlin et al., 1994). Although heterogeneous at the small scale, the rocks of the study area show no clear large-scale variations in lithologic resistance between catchments (S. Ellen, unpublished data; Merritts and Vincent, 1989) although this possibility cannot entirely be ruled out.

The 21 study-area drainage basins are variable-bed-gradient bedrock streams (morphologic terminology of Wohl, 1998). The basins range from 3.1 to 20.8 km^2 in area. The streams are steep and narrow. Generally, the local stream-bed morphology varies from cobble to sand plane bed near the mouths of the larger drainages to a locally variable mix of step-pool, boulder-cascade, bedrock, and colluvial conditions in the higher parts of the basins (classification scheme of Montgomery and Buffington, 1997). Strath and fill terraces are common in many of the drainages.

In the higher, steeper channel reaches (bed slope > 1°–2°) away from channel mouths, the bed composition of the streams is a mix of exposed bedrock and scattered alluvial and colluvial deposits (Fig. 4A). In heavily jointed areas, plucking along joint planes appears to be the dominant erosion process, evidenced by numerous unweathered and only slightly abraded exposed joint surfaces. Streambed exposures of massive bedrock (joint spacing > 0.3 m) generally are polished, and probably sculpted by bedload abrasion (Fig. 4B). Discontinuous coarse-grained alluvial deposits are common throughout the basins. Occasional debris-flow deposits are found locally, particularly higher in the basins. Debris flows probably contribute to channel incision, but the significance of this contribution is unknown at present. Landslide deposits are common at sites of recent mass-wasting activity on steep side slopes throughout the study drainages. These colluvial deposits appear to be reworked rapidly and retransported by flu-

TABLE 1. TOPOGRAPHIC DATA FOR THE 21 STUDY-AREA CHANNELS

No	Basin name	Distance* (km)	Uplift rate, U (m yr^{-1})	Drainage area A (km^2)	Basin length L (m)	Critical distance† x_c (m)	± 2σ§	k_s, for θ = 0.43§	K, for n = 1 (m$^{0.14}$ yr^{-1})§
1	Singley	6 2	0 003	20 8	8939	367	0 37 ± 0.14	60	5.0 × 10^{-5}
2	Davis	12 0	0 003	17.7	8851	544	0.29 ± 0 16	64	4.7 × 10^{-5}
3	Fourmile	24 7	0 0035	13 5	9568	440	0.58 ± 0.11	56	6.3 × 10^{-5}
4	Cooskie	30 6	0 0035	18 1	7398	342	0.43 ± 0.12	48	7 3 × 10^{-5}
5	Randall	33 5	0 004	4 8	3743	350	0.45 ± 0 11	74	5 4 × 10^{-5}
6	Spanish	36 3	0 004	4 8	4304	472	0 44 ± 0 15	75	5.3 × 10^{-5}
7	Oat	37 4	0 004	4 1	3680	342	0 41 ± 0.11	77	5.2 × 10^{-5}
8	Kinsey	38 6	0 004	3.9	3300	357	0 40 ± 0 09	83	4.8 × 10^{-5}
9	Big	41 0	0 004	9 4	5513	399	0 58 ± 0.10	88	4.6 × 10^{-5}
10	Big Flat	45.3	0 004	16 1	6804	422	0 25 ± 0 14	121	3 3 × 10^{-5}
11	Shipman	47 5	0.004	8.7	5742	475	0.36 ± 0.09	108	3 7 × 10^{-5}
12	Buck	49 2	0 0033	3 1	3044	492	0.39 ± 0.08	109	3.0 × 10^{-5}
13	Gitchell	51 7	0 0033	8.4	5127	342	0 31 ± 0.10	90	3 7 × 10^{-5}
14	Horse Mtn	55 0	0 0023	6 9	4520	567	0.47 ± 0 15	62	3.7 × 10^{-5}
15	Telegraph	56 9	0 001	7.6	4954	404	0 42 ± 0.14	60	1 7 × 10^{-5}
16	Whale	69 5	0 001	9 7	6735	440	0 37 ± 0.13	56	1 8 × 10^{-5}
17	Jackass	79 8	0 0005	13 8	4635	427	0 52 ± 0.13	45	1 1 × 10^{-5}
18	Hardy	100 7	0 0005	13 0	7202	470	0 48 ± 0.11	52	9 6 × 10^{-4}
19	Juan	101 7	0 0005	19 4	9810	397	0.46 ± 0 10	58	8 6 × 10^{-4}
20	Howard	104 8	0 0005	11 3	7038	482	0 59 ± 0 11	58	8.6 × 10^{-4}
21	Dehaven	106 5	0 0005	20.8	10454	312	0 36 ± 0 14	50	1 0 × 10^{-5}
	MEAN		0 0012	11.2	6255	421	0 43 ± 0 22	71	3 5 × 10^{-5}

*Distance from Cape Mendocino, south along N30°W (coast-parallel) transect.

†Distance downstream from divide where drainage area is 0 1 km^2, corresponds to the observed scaling break between colluvial and fluvial channels (see Fig 7).

§Main-trunk channel, 10 m contour method data (Table 3, run 1, equation 14)

vial processes. The most extensive sedimentary deposits are found behind woody-debris dams and are generally up to 50 m long and 3 m thick.

The climate of the study area is maritime and humid, with a mean annual temperature of ~13 °C. Floral evidence indicates that the temperate climate extended into the Pleistocene, without large fluctuations, such as ice-age glaciations (Johnson, 1977). Wet winters characterize the area, with 90% of the annual precipitation during the period from October to April. The orographic effect of the rugged topography of the central part of the region causes a significant variation in annual precipitation, from ~1 m north and south of the study area, to between 1.5 and 3 m in the King Range (National Weather Service data; Rantz, 1968).

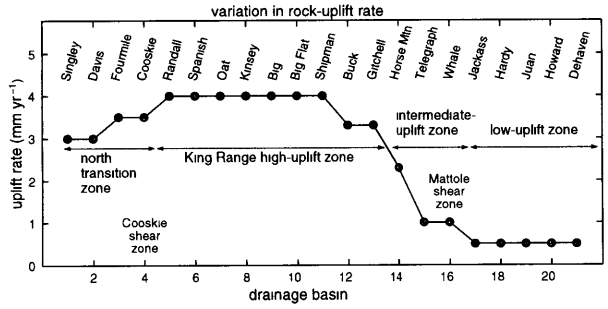

Figure 3. Comparison of latest-Pleistocene to Holocene rock-uplift rates for the 21 study area drainage basins, from north to south. Data are from Merritts and Bull (1989).

EQUILIBRIUM CHANNEL HYPOTHESIS

As shown in the theoretical framework section, only longitudinal profiles of streams in equilibrium with rock uplift and prevailing climate can be interpreted directly in terms of critical model parameters (equations 13 and 14). Therefore, we need to carefully assess whether the bedrock channels in the study area are reasonably close to an equilibrium state. The question of equilibrium is most important in the high-uplift zone where channels have had only ~100 k.y. to respond to the imposed rock-uplift rate.

We expect near steady-state conditions in the low-uplift zone for two reasons. First, uplift rates in the region have been approximately constant for a long period of time, at least 330 k.y. (Merritts and Bull, 1989). Second, late Quaternary climate fluctuations have been subdued in the region (Johnson, 1977). However, our analysis implicitly concerns the time-integrated effects of climatic changes. Sea-level fluctuations likely affect sedimentation in lower reaches of the channel, but probably not the bedrock-channel reaches upstream. We make this assertion because the offshore low-gradient, wide marine bench simply would extend the length of the lower parts of the channels during sea-level lowstands, rather than dramatically affect the rate of rock uplift relative to base level. Finally, the smooth, concave longitudinal profiles, without knick zones or large-scale convexities, seen in each channel are consistent with the steady-state hypothesis. To conclude, all available indicators suggest that the low-uplift-rate streams are in or near equilibrium.

Disequilibrium conditions are more likely in the high-uplift zone because uplift rates increased only 100 k.y. ago. The shear-stress incision model predicts longitudinal profiles with a large convexity migrating upstream as a wave, and a steepened lower reach during transient response to an acceleration in uplift rate (Fig. 5). However, high-uplift-zone streams consistently exhibit smooth concave profiles without large-scale convexities. Furthermore, Merritts and Vincent (1989) showed that the high-uplift signal has already reached the first-order streams. For these reasons, we cannot disprove

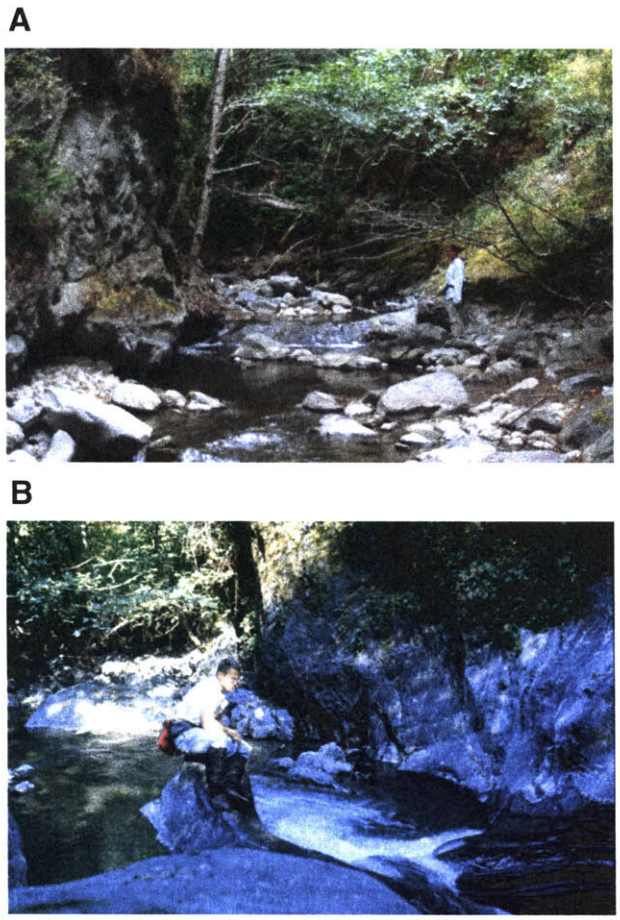

Figure 4. Photographs of study area channel morphology. (A) A view upstream at a mixed bedrock and alluvium reach in Davis Creek; note the prominent bedrock rib across the channel. (B) Sculpted and polished bedrock in a section of relatively unjointed rocks along Shipman Creek.

the equilibrium channel hypothesis in any of the study-area channels. Later calculations herein of response time indicate that the steady-state hypothesis is reasonable, given 100 k.y. of high-uplift-rate conditions. Our analysis proceeds by accepting the hypothesis that these channels are close to their equilibrium form.

For the observed topography to match the theory (and for the relationships of equations 13 and 14 to be valid), two criteria, in addition to steady-state erosion, must be met: both U and K must be spatially constant within each drainage basin. The following analysis of slope-area data assumes that these conditions exist. The observation that late Pleistocene and Holocene emergent marine terraces are not significantly tilted away from the original coastward dip supports the assumption of spatially constant uplift rate (U). Similarly, preliminary field observations that indicate no systematic downstream variations in either rock mass quality or the degree of sediment cover in the modeled channel reaches (defined in the following) support the assumption of spatially constant erosion coefficient (K). Moreover, analysis of slope-area data should detect significant downstream changes in K if they occur (Slingerland et al., 1998). We proceed with the reasonable assumption that longitudinal profile analysis of the study-area channels provides direct measurements of theoretical parameters (equations 13 and 14).

LONGITUDINAL PROFILE SLOPE-AREA ANALYSIS

Methods

Data were acquired in three stages. First, channel longitudinal profiles (streamwise distance, elevation, and drainage area) were generated from DEMs, topographic maps, and field surveys, and the results of these methods were compared. Second, power-law regressions of channel slope as a function of drainage area were used to derive estimates of channel concavity and steepness (equation 12). This analysis was limited to include only the part of the drainage network dominated by bedrock erosion (defined in the following). Slope-area data can be generated in a variety of ways, and several methods were critically evaluated. Third, channel widths were measured in the field as a function of drainage area for two basins in the high-uplift zone.

Channel Longitudinal Profiles. Our analysis began with measurements of elevation and drainage area at points along the length of each study-area channel. We compared three methods of measuring channel longitudinal profiles (elevation and stream distance). The first method, field surveying (using either hand levels or inclinometers), is time consuming but accurate on a fine (<10 m) horizontal scale. Field surveys for Kinsey and Shipman Creeks were conducted (Fig. 2). The second method, digitizing elevations from topographic maps, is also laborious, with accuracy limited by the counter interval (12 m for U.S. Geological Survey [USGS] 7.5′ maps in the study area). Profiles from several channels were digitized. The third technique, extraction of channel profiles from DEMs, is highly efficient, but accuracy is limited by the resolution and quality of the DEM. In this study, USGS 30 m pixel DEMs, generated from 7.5′ topographic maps, were used. The rasterization process used to produce DEMs introduces inaccuracies on the pixel scale, and the resulting longitudinal profiles are not as smooth as those produced from the other techniques. Therefore, DEM-derived stream profiles require the implementation of some smoothing algorithm prior to computation of local slopes. DEMs are the simplest and most accurate method of generating basin-wide drainage-area data sets, and the only method used in this study for this purpose. Comparison of these three methods for several channels indicated that for the topographic analysis used in this study, the differences between the three techniques are not significant on a basin scale (Fig. 6). Therefore, the DEM-generated longitudinal profiles of all 21 channels were used for their ease in extraction and direct comparison to drainage area data (Fig. 7).

Slope-Area Analysis. Linear regression of the logarithms of local channel gradient and drainage area data was used to find values for the concavity index (θ) and the steepness index (k_s) (equation 12; Fig. 7). In this section we discuss some of the complications of this type of analysis. The considerable scatter in local-slope data leads to large uncertainties in best-fit regression parameters. Much of the observed scatter in slopes can be attributed to the resolution of USGS 30 m DEMs. The results of several smoothing methods are compared.

The slope-area relations in equations 11 and 12 only have meaning in the context of detachment-limited bedrock channels, so the parts of the drainage basin where these equations are an appropriate model were isolated on the basis of inspection of the slope-area data and field observations. Regressions of slope-area data that cross process transitions do not provide useful information. The scaling break or transition between colluvial and fluvial channels has been identified from DEM data by many workers (e.g., Dietrich et al., 1993; Montgomery and Foufoula-Georgiou, 1993). For all of the

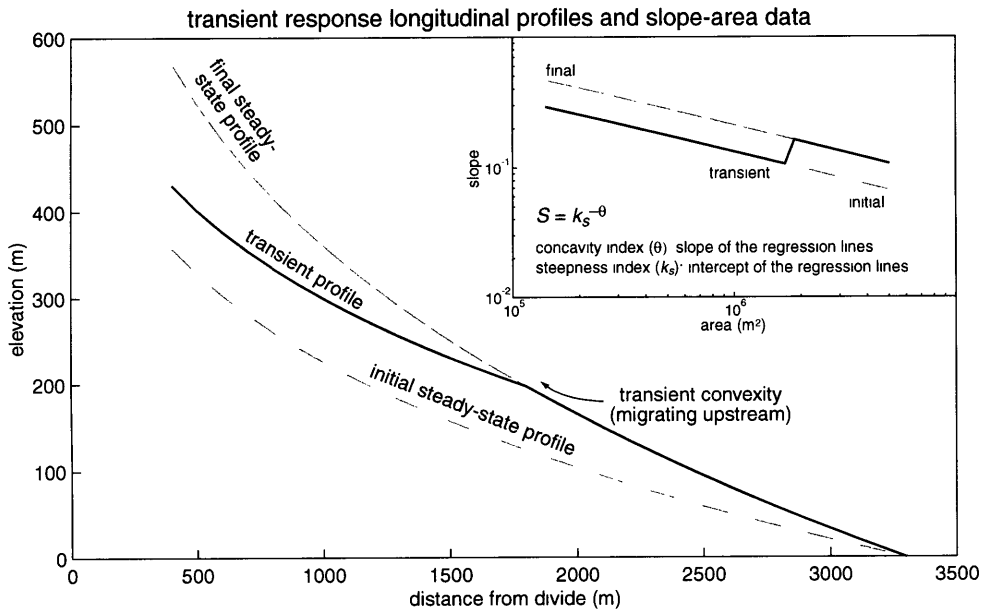

Figure 5. Example of a simulated transient-state profile between initial low-uplift and final high-uplift zone conditions. Note the prominent convexity at the midprofile position. This knick zone migrates upstream as the channel responds to the uplift-rate change. Inset shows the slope-drainage area data for the three longitudinal profiles. Note that the channel concavity (θ, the slope of the slope-area regression line) is the same for both the initial and final profiles, while the steepness (k_s, the intercept) is considerably higher for the final (high uplift rate) profile.

basins in the study area, this break is well defined and occurs at drainage areas between 10^4 m^2 and 10^5 m^2 (Fig. 7). Conservatively, all data points with areas $<10^5$ m^2 were omitted from the regression analysis. Field mapping of channel-bed characteristics indicates that the lower reaches of channels in the larger study-area basins are alluviated. The transition from bedrock to alluvial channels typically occurs at drainage areas above about 10^7 m^2 and appears to be associated with a decrease in channel slope (Fig. 7). A critical drainage area of 5×10^6 m^2 was chosen as a conservative upper bound on bedrock channels in the regression analysis provided in the following. Limiting the data series to a defined range of drainage areas allowed for unbiased comparison between bedrock-erosion dominated channel reaches of similar size. The 10^5 to 5×10^6 m^2 range in area corresponds to 3000–4000 m in horizontal channel length.

Two different sets of slope-area data were compared: those for main-trunk streams and those for entire drainage basins. First, the domain was limited to just the main channel This technique avoided complications due to errors in computing flow paths across gently sloping terrain on ridges and valley bottoms, and reduced scatter due to interbasin variations. In addition, this method required no assumptions about tributary-channel erosion rates. Second, we used points from the entire basin (within the specified range of areas). This includes the trunk stream, as well as tributaries, and is the domain used by most previous workers (Tarboton et al., 1991; Montgomery and Foufoula-Georgiou, 1993; Tucker, 1996).

The stair-step nature of USGS 30 m DEM-derived longitudinal profiles produces considerable scatter in slope-area data, including many channel segments with zero slopes (nonphysical artifacts of DEM resolution and pit-filling routines). Therefore, some smoothing of the data was required. In order to test the sensitivity of the results to the choice of smoothing algorithm, two methods were compared. For both the basin-wide and main-channel slope-area data sets, the technique of averaging the slopes in logarithmic bins of drainage area was used, similar to other studies (Tarboton et al., 1991; Montgomery and Foufoula-Georgiou, 1993; Willgoose, 1994; Tucker and Bras, 1998). For the main-channel data sets, slopes were also calculated on interpolated 10 m contour intervals. This technique is directly analogous to measuring longitudinal profiles from topographic maps We show the results of this comparison of methods in the next section.

Channel-Width Measurements. Downstream variations in channel width were measured in an attempt to constrain the *m/n* ratio (equations 4 and 9). Width data were collected for most of Kinsey Creek and the lower part of Shipman Creek. Because effective channel width is not always easy to define in rugged bedrock channels, three different width measurements were made: (1) low-flow (late summer) channel width; (2) high-flow channel width, largely defined by channel banks and vegetation patterns (roughly analogous to the bankfull condition for alluvial channels); and (3) valley-bottom width, measured from one steep side-wall to the other, commonly equal to the high-flow width in steep, narrow canyons. In general, we anticipate that the high-flow width most likely represents the geomorphically significant flow condition (Wolman and Miller, 1960). However, the valley-bottom width is also important because it is a measure of the longer term width over which the channel must operate (Pazzaglia et al., 1998). Each of these three width measurements varied considerably on the 10 m scale along the channel. Therefore, a large number of measurements were made to characterize the overall increase in channel width with drainage area. Measurements were taken at regular intervals, spaced ~50 m apart along the stream profile.

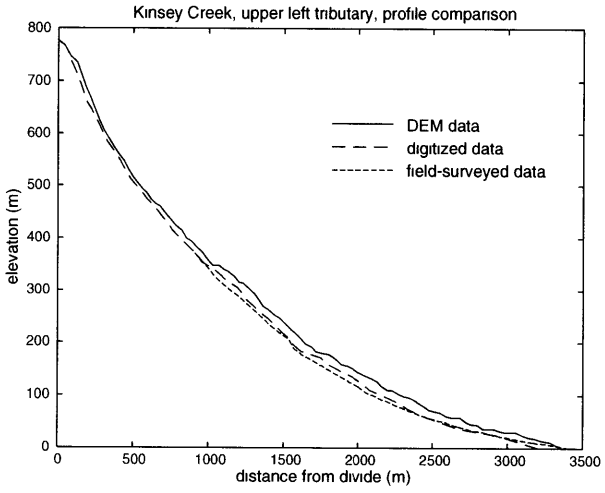

Figure 6. Comparison of longitudinal profiles for Kinsey Creek, upper left tributary. An ~4× vertical exaggeration is used to highlight differences. Outlet of each profile is arbitrary, and no effort has been made to match this point. The surveyed profile did not reach the divide, and was done using both hand level and hand inclinometer. Slope-area regressions of the two complete profiles (digital elevation model [DEM] and digitized) yield values of θ and k_s (equation 12) that are indistinguishable from each other.

Results

Comparison of Slope-Area Techniques. In general, the three different slope-area methods produce similar values of θ, and similar correlations between k_s and U, from regression analyses of equation 12 (Table 2). The two calculations that use only the main channel data points produce nearly identical results (methods 1 and 2). The calculation using the basin-wide data set produces a slightly higher mean value for θ. We use the method 1 data (main-trunk channel, elevation-contoured slopes) for subsequent discussion and calculations This technique is the simplest and least subject to error or unintended bias, for four reasons: (1) by using only the main-channel data, we need not make any assumptions about the response of small, steep sideslope tributaries; (2) by averaging slopes on 10 m contours we give each elevation interval within the profile equal weight in the regression; (3) the 10 m contouring method averages out much of the noise introduced by the poor vertical resolution of USGS 30 m DEMs (particularly in steep, narrow basins); and (4) the contour method is directly comparable to profiles digitized from topographic maps.

Channel Width to Drainage-Area Relation. Our preliminary measurements of the power-law relationship between channel width and drainage area, based on equation 4, are presented in Table 3. The data for Kinsey Creek span a full order of magnitude in drainage area, and therefore are constrained much better than for Shipman Creek. As noted earlier, empirical data for small basins with alluvial channels ($b \sim 0.5$, $c \sim 1$) predicts that channel width will increase with the square root of drainage area. In Kinsey Creek, the high-flow and valley-bottom widths increase with drainage area to the 0.6–0.7 power (bc, equation 4; Table 4), higher than the expected relation for alluvial channels. Assuming that discharge increases approximately linearly with drainage area ($c = 1$), then b is likely to be greater than 0.5. For the purposes of calculations in the rest of this paper we use $b = 0.6$ and $c = 1$. Using these estimates, the shear-stress incision model predicts that the m/n ratio for these streams should be 0.4 (equation 9).

Measurements of Channel Concavity. The values of the concavity index (θ) for 17 of the 21 channels agree within 2σ errors (equations 11 and 12, Fig. 8 and Table 1). The individual measurements of θ range from 0.25 to 0 59, and produce an error-weighted mean value of 0.43 ± 0.22 (2σ). This mean value (and range of values) is similar to other slope-area analyses (Hack, 1957; Flint, 1974; Tarboton et al., 1991; Moglen and Bras, 1995; Slingerland et al., 1998). The scatter in the slope-area data is considerable, as are the uncertainties on estimated θ values. However, the mean value is consistent with both the theoretical prediction that m/n should depend only on the exponents b and c (equations 9 and 13) (Whipple and Tucker, 1999) and the equilibrium channel hypothesis. The approximately constant concavity index (θ) of 0.43 throughout the study area agrees well with the expected value of 0.4 (equation 9). We consider the mean value of θ a good representation of the study-area channel concavity, to be used in subsequent calculations, because the data reveal no systematic, statistically significant deviations from the mean as a function of rock-uplift rate. The good agreement between the concavity results from all three slope-area methods further supports this assertion and indicates that the mean value is not dependent on technique (Table 2).

Measurements of Channel Steepness. To facilitate direct comparison among the drainage basins, we calculate the steepness index (k_s) for the mean value of θ = 0.43 for all 21 channels (equations 11 and 12; Fig. 8 and Table 1). This is necessary because small changes in θ produce large apparent changes in k_s. Given that few of the regressions produce statistically significant differences in θ away from the mean value of 0.43, such apparent variations in k_s likely reflect only the inherent scatter in slope-area data. Fixing the profile concavity to standardize the calculation of profile steepness is directly analogous to measuring deviations from an assumed logarithmic profile form in the stream-gradient index technique (Hack, 1973; Merritts and Vincent, 1989; Goldrick and Bishop, 1995) and the normalization technique described by Sklar and Dietrich (1998).

The steepness values thus derived broadly correlate to the uplift-rate data, with above-average values in the high-uplift zone (drainage basins 5–13) and below-average values in the low-uplift zone (drainage basins 17–21; Fig. 8). The relation between uplift and steepness is expected, because steepness is essentially a measure of the ratio of basin relief and basin length, which is much higher in the rugged high-uplift zone. This relationship was also observed in the channel-reach-slope analysis by Merritts and Vincent (1989). The two populations can be averaged to produce representative steepness indices of 92 in the high-uplift zone and 53 in the low-uplift zone (Table 2). Via the equilibrium channel hypothesis (equations 13 and 14), these rough values allow for some simple calculations to constrain the coefficient of erosion (K), the slope exponent (n), and basin-response time scale.

DISCUSSION

Implications of Constant Channel Concavity

This study shows that concavity is generally constant within measurement error among the 21 drainage basins. This observation is consistent with a prediction of the shear-stress incision model (equations 9 and 13; Whipple and Tucker, 1999), and has important implications for possible downstream variation of the erosion coefficient, and the style of channel response to changes in uplift rate.

As mentioned previously, if K significantly changes downstream within a basin as a function of sediment load (Sklar and Dietrich, 1998), we would expect to see differences in channel concavity within a profile from that expected for the simple shear-stress model. Because the profiles exhibit

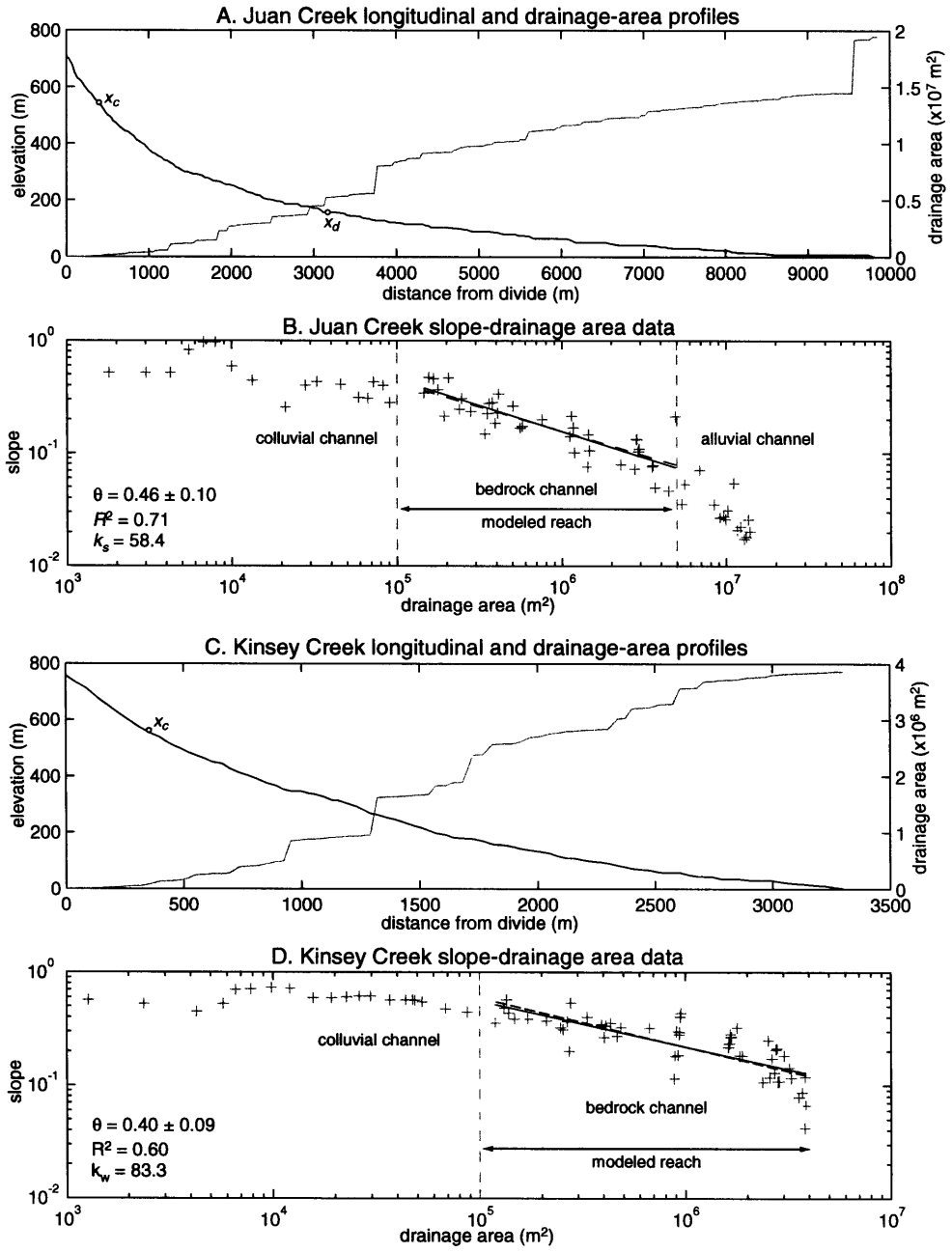

Figure 7. Examples of digital elevation model–derived channel topographic data from Juan Creek, in the low-uplift-rate zone, and Kinsey Creek, in the King Range high-uplift-rate zone. Note that the scales are different for the two streams. (A, C) Longitudinal profile (black line) and drainage area profile (gray line); steps correspond to tributary junctions. For Juan Creek, the bedrock-channel study domain is between x_c (drainage area, $A = 10^5$ m^2) and x_d ($A = 5 \times 10^6$ m^2). Kinsey Creek is smaller than the $A = 5 \times 10^6$ m^2 threshold, so the entire channel below x_c is within the study domain. (B, D) Slope and drainage-area data with regression lines. Data domain in these examples only includes the main channel, with slopes calculated for 10 m elevation intervals. From equation 12, the slope of these lines is θ and the y-axis intercept is k_s. Solid line is the least-squares best fit, used to calculate θ. Dashed line is the best fit with θ = 0.43 used to calculate k_s. If the regression domain for Juan Creek includes drainage areas greater than 5×10^6 m^2, then θ = 0.60 ± 0.07. This greater concavity is seen in all of the low-uplift drainages if the lower, alluvial part of the channel is included in the regression domain.

TABLE 2 COMPARISON OF SLOPE-AREA METHODS

No	Slope domain	Slope calculation method	θ mean ± 1σ	k_s mean ± 1σ*	k_s mean ± 1σ*	
					High-uplift	Low-uplift
1	Main-trunk channel	10 m elevation contours	0 43 ± 0 11	71 ± 22	92 ± 17	53 ± 6
2	Main-trunk channel	log-bin average	0 44 ± 0 14	73 ± 21	93 ± 17	55 ± 6
3	Entire basin	log-bin average	0 46 ± 0 09	98 ± 30	129 ± 17	66 ± 4

*Calculated with θ = θ mean

smooth, uniform concavities consistent with those expected from theory and preliminary width-area data, we see no evidence for downstream changes in K over the modeled reaches (10^5 m$^2 \le A \le 5 \times 10^6$ m^2). This observation is congruent with the finding of Slingerland et al. (1998) that channel-profile concavities in the Central Range of Taiwan are more consistent with a shear-stress or unit-stream-power incision rule than with a sediment-flux–dependent erosion rule. However, the relatively short length of channels studied here may prevent detection of the effects of a gradual downstream increase in K. Further research of this issue is warranted.

Channel Response to Tectonic Forcing

We now explore constraints on two key unknowns (K and n) in the shear-stress incision model (equation 5) by comparing stream-profile data of the high- and low-uplift zones. Under the equilibrium channel hypothesis, equation 14 is valid, and since U is known, some broad constraints can be placed on both the slope exponent (n) and possible dynamic adjustment of the coefficient of erosion (K) in response to changes in uplift rate. Naturally, the analysis that follows depends on both the accuracy of the uplift-rate data and the estimated steepness index (k_s) values (Table 2). The effects of the variation in tectonic conditions within the study area are shown by solving equation 14 for K and dividing the high-uplift-rate case (subscript 2) by the low-uplift-rate case (subscript 1):

$$K_2/K_1 = (U_2/U_1)(k_{s1}/k_{s2})^n \quad (15)$$

This equation allows us to analyze the magnitude of possible changes in the value of K between the different uplift-rate zones, given broad theoretical constraints on the plausible range of the slope exponent (n) (Foley, 1980; Howard and Kerby, 1983, Howard et al., 1994; Hancock et al., 1998; Whipple et al., 2000). Implicit in this approach is the assumption that erosion process (and therefore n) does not change with uplift rate.

In landscape-evolution models that consider zones of similar climate and lithology, K often is assumed to be a constant throughout the model domain. This assumption is testable by setting K constant throughout the study area ($K_2/K_1 = 1$), and solving equation 15 for n. A simple calculation using $k_{s1} = 53$ and $k_{s2} = 92$ (the low- and high-uplift zone mean values, respectively) indicates that for K to be constant throughout the study area, n must be 3.8 (Fig. 9A) If we set $k_{s2} = 74$ and 121 (the minimum and maximum high-uplift zone values, respectively) then n must be 6.2 and 2.5, respectively. These values are considerably higher than any suggested by theoretical arguments (Foley, 1980; Howard and Kerby, 1983; Howard et al., 1994; Hancock et al., 1998; Whipple et al., 2000), suggesting that K is probably greater in the high-uplift zone than the low-uplift zone (Fig. 9A). Given the likely range of n values, K must increase two to six fold between the low- and high-uplift zones. For example, with n equal to 1 (a commonly cited value, with $a = 3/2$), equation 15 indicates at least a four- to five-fold variation in K (Fig. 9A), with mean values for the low- and high-uplift zones of 9.6×10^{-6} and 4.4×10^{-5} m$^{0.14}$ yr^{-1} (units calculated with $m = n\,\theta$, from equation 13), respectively (Fig 8; Table 1). This change in erosion coefficient corresponds to an eight-fold variation in uplift rate; high K values are associated with the high-uplift zone. We now have two end-member cases: either n is quite large and K is constant throughout the study area, or $n \sim 1$ and K varies significantly between the high- and low-uplift zones. Such dynamic adjustment of K is not unexpected given present knowledge of the geomorphic controls on bedrock-incision rates.

Variations in lithology will directly affect the value of the erosion-rate coefficient. The rocks of the study area range from mudstones to sandstones. The King Range terrane is mapped as more argillaceous than sandstone rich, while in the low-uplift zone sandstone predominates over finer grained sedimentary rocks (McLaughlin et al., 1994). However, preliminary field measurements of intact rock strength (using a Schmidt Hammer), joint spacing, and weathering characteristics by the authors, and detailed aerial-photograph analysis of hillslope morphology by S. Ellen (unpublished data) do not reveal any systematic large-scale variations in lithologic resistance. More work is necessary before a lithologic explanation can be ruled out with certainty, but at present north to south changes in lithology appear unimportant. The data for Cooskie Creek provide an important exception (Fig. 8, drainage 4). This basin is oriented along a shear zone and was previously identified as a zone of weaker lithology (Beutner et al., 1980; McLaughlin et al., 1994). It is interesting that this drainage has the highest value of K in the study area, indicating that this methodology can indeed detect differences in bedrock resistance

Increased orographic precipitation in the King Range high-uplift zone, where a maximum three-fold increase in annual precipitation is observed (Rantz, 1968), is one known source of variation in K. This change in precipitation will most likely directly affect the value of k_q, the coefficient as-

TABLE 3 CHANNEL WIDTH AND DRAINAGE AREA RELATIONSHIP

Drainage basin	Width measurement	Drainage area range (m^2)	bc (± 2σ)*	$k_w k_q^b$	Number of data points
Kinsey Creek	Low flow	$3 \times 10^5 - 3\,9 \times 10^6$	0 43 ± 0 13	$6\,9 \times 10^{-3}$	50
	High flow	$3 \times 10^5 - 3\,9 \times 10^6$	0 65 ± 0 19	$6\,9 \times 10^{-4}$	48
	Valley bottom	$3 \times 10^5 - 3\,9 \times 10^6$	0 67 ± 0 23	$5\,5 \times 10^{-4}$	39
Shipman Creek	Low flow	$3 \times 10^6 - 8\,7 \times 10^6$	0 61 ± 0 33	$5\,5 \times 10^{-4}$	50
	High flow	$3 \times 10^6 - 8\,7 \times 10^6$	0 46 ± 0 32	$9\,4 \times 10^{-3}$	49
	Valley bottom	$3 \times 10^6 - 8\,7 \times 10^6$	0 50 ± 0 47	$6\,6 \times 10^{-3}$	49

*Power-law model based equation 4 $W = (k_w k_q^b) A^{bc}$

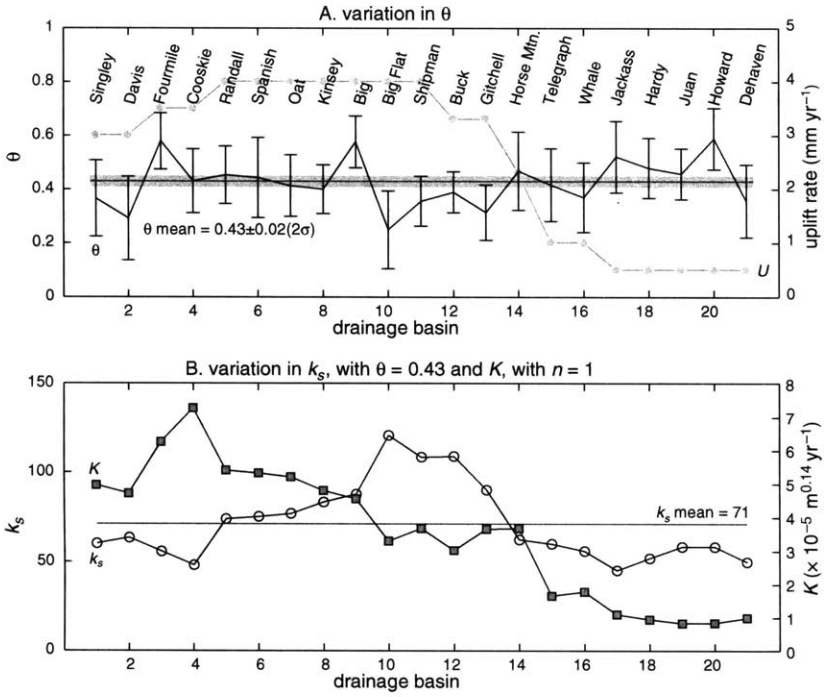

Figure 8. Comparisons among the 21 study-area channels, from north to south. (A) Concavity index (θ, with error bars) calculated from slope-area data using the equation 12 relation. Error bars show 2σ uncertainty on each regression. Shaded area represents the mean value with 2σ error on its calculation, as opposed to the error-weighted mean value cited in the text. Also included is the uplift-rate graph from Figure 3. (B) Steepness index (k_s, circles) calculated from equation 12 with θ = 0.43 and erosion coefficient (K, squares) calculated from equation 14 with $n = 1$.

sociated with the discharge-area relation (equation 3). Because we have no specific information about the change in flood magnitudes and frequencies, we make the simplifying assumption that the dominant discharge is proportional to mean-annual precipitation. To explore this aspect of the erosion coefficient, we isolate contribution of enhanced runoff on the value of K by using equations 6 and 8:

$$K = K' k_q^{n(1-b)}, \tag{16}$$

where K' is controlled by substrate lithology, sediment flux, and channel width. Substituting equation 16 into equation 15 and solving for the remaining variation in the coefficient of erosion (K_2'/K_1') yields

$$\frac{K_2'}{K_1'} = \left(\frac{U_2}{U_1}\right)\left[\left(\frac{k_{s1}}{k_{s2}}\right)\left(\frac{k_{q1}}{k_{q2}}\right)^{(1-b)}\right]^n, \tag{17}$$

where the ratio $k_{q1}/k_{q2} \sim 1/3$ (Rantz, 1968). With $b = 0.6$ and the same k_{s1} and k_{s2} values as above, the $n = 1$ case yields a two- to four-fold variation in K' between the high- and low-uplift zones (Fig. 9B). Alternatively, we can make the simplifying (but probably incorrect) assumption that K varies solely and directly in response to this precipitation difference ($K_2'/K_1' = 1$), and solve equation 17 for n. This calculation gives an average value for n of 2.1, with a range of 1.6 to 2.7. These values of n just overlap with the range of those suggested by theoretical considerations ($n \sim 2/3$ to 5/3; Fig. 9B). Therefore, precipitation differences can explain some, and perhaps all, of the variation in K. However, as shown in Figure 9B, for most of the range of plausible n values, K must increase by a factor of 1.5 to 4.5 beyond that attributable to orographic precipitation. Moreover, several other factors that influence K are likely to change in response to increased rates of rock uplift.

As mentioned earlier, holding K constant carries with it the implicit assumption that only channel slope is free to adjust to changes in boundary conditions. At least four other channel attributes that influence K may adjust in concert with channel slope: channel width, amount of alluvial cover, sediment flux, and frequency of debris flows. First, channels are likely to narrow in response to the steepening caused by increased uplift rates. Second, the degree of alluvial cover may also be an important control on K. Sediment can protect the bed, reducing or stopping erosion (Sklar and Dietrich, 1998). Third, increased sediment flux may increase the erosivity of floods. Fourth, the increased steepness and orographic precipitation associated with higher uplift rates may produce an increase in the frequency of debris-flow events. This might result in more erosive conditions and a higher effective value for K, although a complete transition to debris-flow dominated conditions might be expected to invalidate the assumptions of the shear-stress model (Stock and Dietrich, 1998).

Although we cannot at present solve for a unique combination of K and n for this field area, our analysis does place some constraints on these parameters. The most likely case, based on our present knowledge, is that K varies systematically between the high- and low-uplift zones and that n is less than 2. The finding that K (and perhaps n) changes significantly depending on boundary conditions implies that a fully generalized shear-stress model will require similar studies in a variety of geologic, tectonic, and lithologic conditions in order to quantify these effects.

Time Scale of Response Calculations

The King Range provides an excellent setting to explore the time scale of basin response to a change in tectonic conditions. Around 100 ka, uplift rates in the high-uplift zone accelerated from 0.5–1.2 mm yr^{-1} to 4 mm yr^{-1} (Merritts and Bull, 1989). We have proposed that the trunk streams have achieved steady state in response to this change, and we test whether this hy-

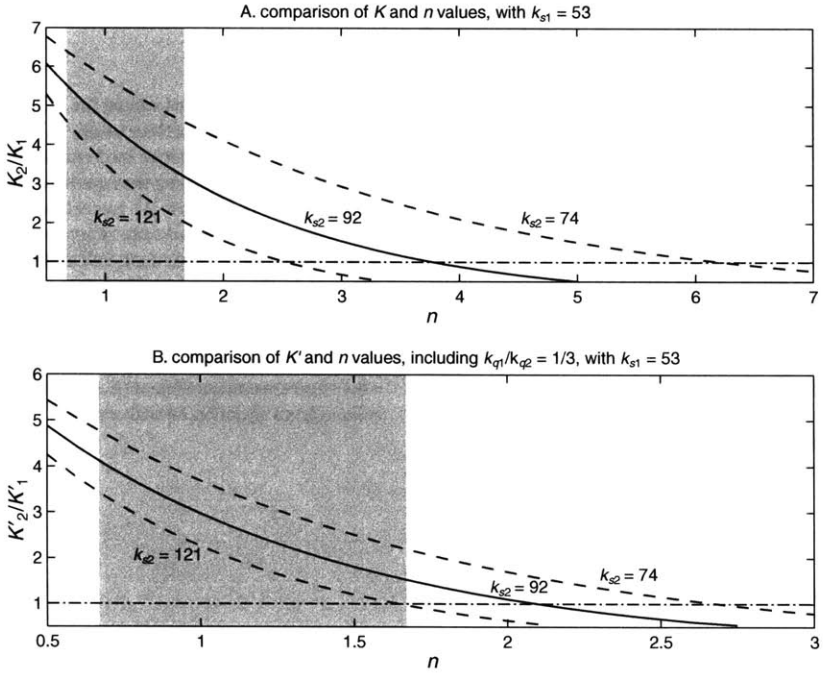

Figure 9. Calculations of erosion coefficient (K) and slope exponent (n). (A) The ratio of high-uplift-rate to low-uplift-rate erosion coefficients (K_2/K_1) calculated for values of n from 0.5 to 7, using equation 15, with uplift rates, U_1 = 0.0005 m yr^{-1} and U_2 = 0.004 m yr^{-1}, and steepness index, k_{s1} = 53. Shaded region indicates region of theoretically predicted values of n. Solid line is the mean value of k_{s2}, dashed lines are for the minimum and maximum. This calculation indicates that n must be greater than 2.5 for K to be constant throughout the study area, or that K varies widely. (B) The same calculation as in A, but now taking into account the observed variation in orographic precipitation, using equation 17, with the U and k_s values as above, and b = 0.6. This calculation suggests that if and only if $n \sim 2$, K varies directly and solely with discharge (or precipitation) differences. For most of the expected range of n values these data suggest that K increased by a factor of 1.5 to 4.5 beyond that expected from orographic effects in response to the eight-fold increase in uplift rate.

pothesis is internally consistent with the shear-stress model via the following analysis. Whipple and Tucker (1999) derived the response time (defined as the time required to attain a new steady-state condition) for a change in uplift rate (T_U). Their analysis explicitly assumed that K remains constant during landscape response. Here we generalize their result by writing their equation 34 in dimensional form and allowing for the possibility that K adjusts in concert with incision rate:

$$T_U = \frac{k_a^{\frac{m}{n}}\left(1-\frac{hm}{n}\right)^{-1} K_f^{-\frac{1}{n}} U_f^{\frac{1}{n}-1}\left(L^{1-\frac{hm}{n}} - x_c^{1-\frac{hm}{n}}\right)\left[-\left(\frac{K_i}{K_f}\right)^{-\frac{1}{n}}\left(\frac{U_i}{U_f}\right)^{\frac{1}{n}}\right]}{\left(1-\frac{U_i}{U_f}\right)}, \quad (18)$$

where x_c is the critical distance downslope from the divide to the top of the fluvial channel network ($A = 10^5$ m^2), L is the basin length (Table 1), k_a and h relate drainage area to channel distance ($A = k_a x^h$, where x denotes horizontal channel distance; Hack, 1957), and the subscripts i and f refer to initial and final conditions, respectively. The derivation of equation 18 assumes that K only changes below the upstream propagating wave of incision (i.e., downstream of the convexity in Fig. 5). We use equation 14 to rewrite equation 18 in a simpler form in terms of k_{si} and k_{sf}:

$$T_U = \frac{k_a^{\frac{m}{n}}\left(1-\frac{hm}{n}\right)^{-1} \frac{k_{sf}}{U_f}\left(L^{1-\frac{hm}{n}} - x_c^{1-\frac{hm}{n}}\right)\left[-\frac{k_{si}}{k_{sf}}\right]}{\left(1-\frac{U_i}{U_f}\right)} \quad (19)$$

showing that, in this case, the response time scale can be evaluated without knowledge of n. Equation 19 is implemented by assembling 3 pieces of data for each of the 9 high-uplift drainage basins: (1) the channel characteristics from Table 1; (2) an empirical drainage-area to stream-distance relationship (Hack, 1957); and (3) an assumed initial low-uplift condition (U_i = 0.5 mm yr^{-1}, $k_{si} = k_{s1}$ = 53) with the present-day drainage-network structure (drainage area and distance along trunk streams). With these parameters, we generate modeled initial and final steady-state profiles and solve for the time scale of response between them (Fig. 10). This calculation yields response times from 47.4 k.y. to 196 k.y., with a mean of 102 k.y. Five of the nine channels have calculated response times of ~100 k.y. or less, indicating that the steady-state assumption is reasonable. This analysis suggests that bedrock channels, at least in small basins with weak lithology, have a remarkable ability to respond rapidly to changes in tectonic forcing. Equation 18 indicates explicitly that an increase in K resulting from channel morphologic adjustments to an increase in uplift rate ($K_i/K_f < 1$) accelerates response time, underscoring the importance of the dynamic adjustment of the coefficient of erosion to the tectonic response of the landscape.

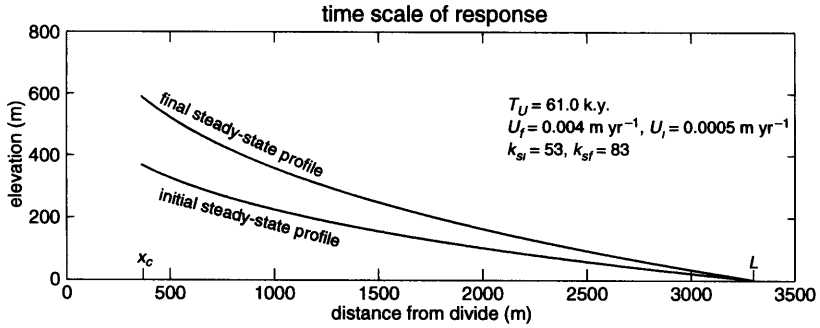

Figure 10. An example of a time scale of response (T_U) calculation using equation 19. Model stream-profile parameters are from Kinsey Creek, in the high-uplift zone.

CONCLUSIONS

This study of field and DEM data from streams in the variable rock-uplift-rate Mendocino triple junction region produces three important outcomes with implications for the shear-stress model of bedrock-channel incision, and landscape evolution in general. (1) The main channels have uniform concavity regardless of uplift rate; (2) the erosion coefficient is not a constant, but varies in concert with rock-uplift rate; and (3) the streams appear to respond rapidly to tectonic forcing, at a rate that appears to be internally consistent with the model.

The DEM slope-area analysis of longitudinal profiles yields the important result that within uncertainty, the concavity index (θ or m/n via the equilibrium hypothesis, equation 13) does not vary throughout the study area (Fig. 8). This observation is consistent with shear-stress incision model predictions (Whipple and Tucker, 1999), and the mean value ($\theta = 0.43 \approx m/n$) is broadly consistent with preliminary observations of channel width (equations 4 and 9). In addition, channel steepness correlates (k_s) well with uplift rate, supporting the method.

The parameters from the slope-area analysis place constraints on possible values of the key unknowns in the shear-stress model, the erosion coefficient (K) and the slope exponent (n, equations 13 and 14). In particular, K appears to have adjusted to tectonic conditions. Since the problem involves one equation with two unknowns, values between two end-member cases, either a constant K or $n = 1$, are explored. These two cases yield the result that either: (1) K is constant and n is greater than 2.5, or (2) K varies with uplift rate, exhibiting a five-fold increase if n is assumed to be unity (Fig. 9A). If K is allowed to vary directly with orographic precipitation, then models with $n \sim 2$ satisfactorily explain observed channel steepness (k_s) values (Fig. 9B). While theoretical formulations allow values of the slope exponent (n) up to ~2 (Foley, 1980; Hancock et al., 1998; Whipple et al., 2000), changes in channel width, sediment load, and debris-flow frequency are likely to influence K. These calculations strongly support the hypothesis that the erosivity of bedrock channels dynamically adjusts to imposed tectonic conditions, illustrating an important feedback between evolution of topography and the mechanisms of channel incision: as the mountains rise, erosion becomes more effective. This preliminary evidence for dynamic adjustment highlights the need for further study of the roles of channel narrowing, changing erosion processes, and changing sediment load as response mechanisms in bedrock channels. We caution that the degree of dynamic adjustment of K may be strongly dependent on lithologic, tectonic, and climatic conditions.

The King Range high-uplift zone channels support the observation, made in other orogens, that rivers have a remarkable ability to keep pace with tectonic base-level forcing (e.g., Burbank et al., 1996). The studied channels appear to have achieved a new steady state in response to an eightfold change in uplift rate in ~100 k.y., a result supported by observations of longitudinal profiles and a simple calculation of response time. This rapid response likely results from dynamic adjustment of factors controlling bedrock-incision rate, including increased precipitation, and possibly changes in channel width, sediment load, and debris-flow frequency. These complicated responses to changes in boundary conditions underscore the need for future work in other areas to generalize the shear-stress incision model.

ACKNOWLEDGMENTS

This research was funded by National Science Foundation grants EAR-9725723 to Whipple and EAR-9725348 to Merritts. We thank Jason Nicholas, Erin Carlson, Emily Himmelstoss, and Simon Brocklehurst for field assistance, Steve Ellen for aerial-photograph analysis, and Jeff Niemann for discussions that helped motivate our interest in returning to the Mendocino triple junction area. The manuscript benefited greatly from thorough reviews by David Montgomery, Frank Pazzaglia, and Ellen Wohl.

REFERENCES CITED

Anderson, R.S., 1994, The growth and decay of the Santa Cruz Mountains: Journal of Geophysical Research, v. 99, p. 20161–20180.

Beaumont, C., Fullsack, P., and Hamilton, J., 1992, Erosional control of active compressional orogens, *in* McClay, K.R., ed., Thrust tectonics: London, Chapman and Hall, p. 1–18.

Beutner, E.C., McLaughlin, R.J., Ohlin, H.N., and Sorg, D.H., 1980, Geologic map of the King Range and Chemise Mountain instant study areas, northern California: U.S. Geological Survey, scale 1:62500.

Burbank, D.W., Leland, J., Fielding, E., Anderson, R.S., Brozovic, N., Reid, M.R., and Duncan, C., 1996, Bedrock incision, rock uplift and threshold hillslopes in the northwestern Himalayas: Nature, v. 379, p. 505–510.

Dietrich, W.E., Wilson, C.J., Montgomery, D.R., and McKean, J., 1993, Analysis of erosion thresholds, channel networks, and landscape morphology using a digital terrain model: Journal of Geology, v. 101, p. 259–278.

Dunne, T., and Leopold, L.B., 1978, Water in environmental planning: New York, W.H. Freeman and Company, 818 p.

Flint, J.J., 1974, Stream gradient as a function of order, magnitude, and discharge: Water Resources Research, v. 10, p. 969–973.

Foley, M.G., 1980, Bedrock incision by streams: Geological Society of America Bulletin, Part II, v. 91, p. 2189–2213.

Goldrick, G., and Bishop, P., 1995, Differentiating the roles of lithology and uplift in the steepening of bedrock river long profiles: An example from southeastern Australia: Journal of Geology, v. 103, p. 227–231.

Hack, J.T., 1957, Studies of longitudinal stream profiles in Virginia and Maryland: U.S. Geological Survey Professional Paper 294-B, p. 42–97.

Hack, J.T., 1973, Stream profile analysis and stream-gradient index: U.S. Geological Survey Journal of Research, v. 1, p. 421–429.

Hancock, G.S., Anderson, R.S., and Whipple, K.X., 1998, Beyond power: Bedrock incision process and form, *in* Tinkler, K.J., and Wohl, E.E., eds., Rivers over rock: Fluvial processes in bedrock channels: American Geophysical Union Geophysical Monograph 107, p. 35–60.

Hoffman, P.F., and Grotzinger, J.P., 1993, Orographic precipitation, erosional unloading, and tectonic style: Geology, v. 21, p. 195–198.

Howard, A.D., 1994, A detachment-limited model of drainage basin evolution: Water Resources Research, v. 30, p. 2261–2285.
Howard, A.D., 1998, Long profile development of bedrock channels: Interaction of weathering, mass wasting, bed erosion, and sediment transport, *in* Tinkler, K.J., and Wohl, E.E., eds., Rivers over rock: Fluvial processes in bedrock channels: American Geophysical Union Geophysical Monograph 107, p. 297–320.
Howard, A.D., and Kerby, G., 1983, Channel changes in badlands: Geological Society of America Bulletin, v. 94, p. 739–752.
Howard, A.D., Seidl, M.A., and Dietrich, W.E., 1994, Modeling fluvial erosion on regional to continental scales: Journal of Geophysical Research, v. 99, p. 13971–13986.
Johnson, D.L., 1977, The late Quaternary climate of coastal California: Evidence for an ice age refugium: Quaternary Research, v. 8, p. 154–179.
Kooi, H., and Beaumont, C., 1996, Large-scale geomorphology: classical concepts reconciled and integrated with contemporary ideas via a surface processes model: Journal of Geophysical Research, v. 101, no. B2, p. 3361–3386.
Koons, P.O., 1995, Modeling the topographic evolution of collisional belts: Annual Reviews of Earth and Planetary Science, v. 23, p. 375–408.
Leopold, L.B., and Miller, J.P., 1956, Ephemeral streams—Hydraulic factors and their relation to the drainage net: U.S. Geological Survey Professional Paper 282A, p. 1–37.
McLaughlin, R.J., Lajoie, K.R., Sorg, D.H., Morrison, S.D., and Wolfe, J.A., 1983, Tectonic uplift of a middle Wisconsin marine platform near the Mendocino triple junction, California: Geology, v. 11, p. 35–39.
McLaughlin, R.J., Sliter, W.V., Frederiksen, N.O., Harbert, W.P., and McCulloch, D.S., 1994, Plate motions recorded in tectonostratigraphic terranes of the Franciscan complex and evolution of the Mendocino triple junction, northwestern California: U.S. Geological Survey Bulletin 1997, 60 p.
Merritts, D.J., 1996, The Mendocino triple junction: Active faults, episodic coastal emergence, and rapid uplift. Journal of Geophysical Research, v. 101, no. B3, p. 6051–6070.
Merritts, D., and Bull, W.B., 1989, Interpreting Quaternary uplift rates at the Mendocino triple junction, northern California, from uplifted marine terraces: Geology, v. 17, p. 1020–1024
Merritts, D., and Ellis, M., 1994, Introduction to special section on tectonics and topography: Journal of Geophysical Research, v. 99, no. B6, p. 12135–12141.
Merritts, D., and Vincent, K.R., 1989, Geomorphic response of coastal streams to low, intermediate, and high rates of uplift, Mendocino junction region, northern California: Geological Society of America Bulletin, v. 101, p. 1373–1388.
Moglen, G.E., and Bras, R.L., 1995, The importance of spatially heterogeneous erosivity and the cumulative area distribution within a basin evolution model: Geomorphology, v. 12, p. 173–185.
Molnar, P., and England, P., 1990, Late Cenozoic uplift of mountain ranges and global climate change: Chicken or egg?: Nature, v. 346, p. 29–34.
Montgomery, D.R., and Buffington, J.M., 1997, Channel-reach morphology in mountain drainage basins: Geological Society of America Bulletin, v. 109, p. 596–611
Montgomery, D.R., and Foufoula-Georgiou, E., 1993, Channel network source representation using digital elevation models: Water Resources Research, v. 29, p. 1178–1191.
Pazzaglia, F.J., Gardner, T.W., and Merritts, D.J., 1998, Bedrock fluvial incision and longitudinal profile development over geologic time scales determined by fluvial terraces, *in* Tinkler, K.J., and Wohl, E.E., eds., Rivers over rock: Fluvial processes in bedrock channels: American Geophysical Union Geophysical Monograph 107, p. 207–236
Prentice, C.S., Merritts, D.J., Beutner, E.C., Bodin, P., Schill, A., and Muller, J.R., 1999, Northern San Andreas fault near Shelter Cove, California: Geological Society of America Bulletin, v. 111, p. 512–523.
Rantz, S.E., 1968, Average annual precipitation and runoff in north coastal California: U.S. Geological Survey Hydrologic Investigations Atlas HA-298, scale 1:1 000 000, 1 sheet, 4 p
Raymo, M.E., and Ruddiman, W.F., 1992, Tectonic forcing of late Cenozoic climate: Nature, v. 359, p. 117–122.
Rosenbloom, N.A., and Anderson, R.S., 1994, Evolution of the marine terraced landscape, Santa Cruz, California: Journal of Geophysical Research, v. 99, p. 14013–14030.
Seidl, M.A., and Dietrich, W.E., 1992, The problem of channel erosion into bedrock: Catena, supplement, v. 23, p. 101–124.
Sklar, L., and Dietrich, W.E., 1998, River longitudinal profiles and bedrock incision models: Stream power and the influence of sediment supply, *in* Tinkler, K.J., and Wohl, E.E., eds., Rivers over rock: Fluvial processes in bedrock channels: American Geophysical Union Geophysical Monograph 107, p. 237–260
Slingerland, R., Willett, S.D., and Hovius, N., 1998, Slope-area scaling as a test of fluvial bedrock erosion laws [abs.]: Eos (Transactions, American Geophysical Union), v. 79, no. 45, p. F358.
Stock, J.D., and Dietrich, W.E., 1998, Channel incision by debris flows: A missing erosion law?. Eos (Transactions, American Geophysical Union), v. 79, no. 45, p. F366.
Stock, J.D., and Montgomery, D.R., 1999, Geologic constraints on bedrock river incision using the stream power law: Journal of Geophysical Research, v. 104, p. 4983–4993.
Talling, P.J., and Sowter, M.J., 1998, Erosion, deposition and basin-wide variations in stream power and bed shear stress: Basin Research, v. 10, p. 87–108.
Tarboton, D.G., Bras, R.L., and Rodriguez-Iturbe, I., 1991, On the extraction of channel networks from digital elevation data: Hydrological Processes, v. 5, p. 81–100.
Tucker, G.E., 1996, Modeling the regional-scale interaction of climate, tectonics and topography: Pennsylvania State University Earth System Science Center Technical Report 96-003, 267 p.
Tucker, G.E., and Bras, R.L., 1998, Hillslope processes, drainage density, and landscape morphology: Water Resources Research, v. 34, p. 2751–2764.
Tucker, G.E., and Slingerland, R.L., 1994, Erosional dynamics, flexural isostasy, and long-lived escarpments: A numerical modeling study: Journal of Geophysical Research, v. 99, p. 12229–12243.
Weissel, J.K., and Seidl, M.A., 1998, Inland propagation of erosional escarpments and river profile evolution across the southeast Australia passive continental margin, *in* Tinkler, K.J., and Wohl, E.E., eds., Rivers over rock: Fluvial processes in bedrock channels: American Geophysical Union Geophysical Monograph 107, p. 189–206.
Whipple, K.X., and Tucker, G.E., 1999, Dynamics of the stream-power river incision model: Implications for the height limits of mountain ranges, landscape response time scales, and research needs: Journal of Geophysical Research, v. 104, no. B8, p. 17661–17674.
Whipple, Kelin X., Hancock, Gregory S., and Anderson, Robert A., 2000, River incision into bedrock: Mechanics and relative efficacy of plucking, abrasion, and cavitation: Geological Society of America Bulletin, v. 112, p. 490–503.
Willgoose, G., 1994, A statistic for testing the elevation characteristics of landscape simulation models: Journal of Geophysical Research, v. 99, no. B7, p. 13987–13996.
Willgoose, G., Bras, R.L., and Rodriguez-Iturbe, I., 1990, A model of river basin evolution: Eos (Transactions, American Geophysical Union), v. 71, p. 1806–1807.
Wohl, E.E., 1998, Bedrock channel morphology in relation to erosional processes, *in* Tinkler, K.J., and Wohl, E.E., eds., Rivers over rock: Fluvial processes in bedrock channels: American Geophysical Union Geophysical Monograph 107, p. 133–151.
Wolman, M.G., and Miller, J.P., 1960, Magnitude and frequency of forces in geomorphic processes. Journal of Geology, v. 68, p. 54–74.

MANUSCRIPT RECEIVED BY THE SOCIETY MARCH 18, 1999
REVISED MANUSCRIPT RECEIVED SEPTEMBER 28, 1999
MANUSCRIPT ACCEPTED NOVEMBER 1, 1999

Printed in USA

3. Channel response to tectonic forcing: Analysis of stream morphology and hydrology in the Mendocino triple junction region, northern California

Noah P. Snyder and Kelin X Whipple
Department of Earth, Atmospheric and Planetary Sciences, Massachusetts Institute of Technology, Cambridge, MA 02139-4307, USA

Gregory E. Tucker
School of Geography and the Environment, University of Oxford, Oxford OX1 3TB, England

Dorothy J. Merritts
Geosciences Department, Franklin and Marshall College, Lancaster, PA 17604-3003, USA

Abstract

An empirical calibration of the shear-stress model for bedrock incision is presented, using field and hydrologic data from a series of small, coastal drainage basins near the Mendocino triple junction in northern California. Previous work comparing basins from the high-uplift zone (HUZ, uplift rates around 4 mm/yr) to ones in the low-uplift zone (LUZ, ~0.5 mm/yr) indicates that the HUZ channels are about twice as steep for a given drainage area. This observation suggests that incision processes are more effective in the HUZ. It motivates a detailed field study of channel morphology in the differing tectonic settings, to test whether various factors that are hypothesized to influence incision rates (discharge, channel width, lithology, sediment load) change in response to uplift or otherwise differ between the HUZ and LUZ. Analysis of regional stream-gauging data for mean annual discharge and individual floods yield a linear relationship between discharge and drainage area. Increased orographic precipitation in the HUZ accounts for about a two-fold increase in discharge in this area, corresponding to an assumed increase in the erosional efficiency of the streams. Field measurements of channel width indicate a power-law relationship between width and drainage area with an exponent of ~0.4, and no significant change in width between the uplift-rate zones, although interpretation is hampered by a difference in land use between the zones. The HUZ channel-width dataset reveals a scaling break interpreted to be the transition between colluvial- and fluvial-dominated incision processes. Assessments of lithologic resistance using a Schmidt hammer and joint surveys show that the rocks of the study area should be fairly similar in their susceptibility to erosion. The HUZ channels generally have more exposed bedrock than those in the LUZ, which is consistent with

protection by sediment cover inhibiting incision in the LUZ. However, this difference is likely the result of a recent pulse of sediment due to land use in the LUZ. Therefore, the role of sediment flux in setting incision rates cannot be constrained with any certainty. To summarize, of the four response mechanisms analyzed, the only factor that demonstrably varies between uplift-rate zones is discharge, although this change is likely insufficient to explain the relationship between channel slope and uplift rate. The calibrated model allows us to make a prediction of channel concavity that is consistent with a previous estimate from slope—drainage area data. We show that the inclusion of nonzero values of critical shear stress in the model has important implications for the theoretical relationship between steady-state slope and uplift rate and might provide an explanation for the observations. This analysis underscores the importance of further work to constrain quantitatively threshold shear stress for bedrock incision.

1. Introduction

The response of river systems to tectonic, climatic, and land-use perturbations is an area of active research in geomorphology (*e.g.* Merritts and Vincent, 1989; Tucker and Slingerland, 1997; Harbor, 1998; Tinkler and Wohl, 1998; Lavé and Avouac, 2000; Schumm *et al.*, 2000; Kirby and Whipple, 2001). These efforts are motivated by the desire to develop a quantitative theory of the processes and styles of channel response, so that present-day stream morphology can be used to understand past disturbances. Bedrock rivers are particularly important to the goal of understanding tectonic—climatic—topographic interactions because incision into bedrock and transport of sediment control the rates that (1) base-level signals, generated by tectonic, eustatic or climatic forcings are transmitted through the landscape, and (2) sediment is delivered from highlands to basins (Whipple and Tucker, 1999). To use bedrock rivers to gain insight into tectonic or climatic conditions, we must first understand how known changes in these forcings affect the channel morphology. Here we present field data from a site where the tectonic and climatic conditions are well known.

In a previous study of streams in the vicinity of the Mendocino triple junction region of northern California (Snyder *et al.*, 2000), we used data from digital elevation models (DEMs) to compare stream longitudinal profiles from basins undergoing varying rock-uplift rates, in terms of the

shear-stress model for bedrock incision. We found that the topography of the area was not easily explained by the simplest form of the model. Specifically, the streams showed an approximately twofold increase in slope (at a given drainage area) in response to an eightfold increase in rock-uplift rate. This is considerably less steep than expected from the simplest form of the model, which assumes that (1) climate and lithology are the same throughout the field area, (2) channels respond to changes in rock-uplift rate through adjustments in channel gradient only, and (3) the critical shear stress to initiate incision is negligible. This paper investigates the first two assumptions in detail using field data. It is beyond the scope of this work to provide quantitative constraints on critical shear stress, but we do discuss the modeling implications of nonzero values of this parameter.

The observation that the channels do not exhibit a greater contrast in gradient can be interpreted to mean that as rates of tectonic uplift increase, incision processes act more effectively. This paper tests hypotheses that this incision-rate change might be the result of the response of four basic factors that control erosion rates: (1) increases in stream discharge because of orographic precipitation in the HUZ; (2) narrowing of channel width in the HUZ; (3) different lithologic resistance throughout the study area (weaker rocks in the LUZ); and (4) changes in sediment flux (greater in the HUZ) or bed cover (greater in the LUZ). Below, we outline briefly how these adjustments might influence response to tectonic and climatic perturbations, and introduce means for field testing these hypotheses.

Bedrock-channel incision is driven by flood events (*e.g.* Baker and Kale, 1998). Mountainous topography can enhance the magnitude of large-discharge events by increasing precipitation through orographic lifting of moist storm air masses (*e.g.* Barros and Lettenmaier, 1993). Therefore, mountain building by accelerated rock-uplift rates can enhance incision processes. Through analysis of stream-discharge records in varying settings, we can begin to quantify this tectonic—climatic—erosion feedback loop.

Rivers have been shown to respond to perturbations through adjustments in channel width (*e.g.* Harbor, 1998; Lavé and Avouac, 2000; Hancock and Anderson, 2001). Entrenchment within wide valley bottoms increases flow depth, therefore increasing basal shear stress, which drives incision. Previously, we speculated that channels undergoing high uplift rates might be

systematically narrower (Snyder *et al.*, 2000). Here we test this hypothesis by measuring channel widths throughout the field area. We also evaluate whether width—discharge—area scaling relations that are well known in alluvial rivers (Leopold and Maddock, 1953) hold for bedrock rivers (Montgomery and Gran, 2001), as often assumed in landscape evolution models. In addition, these scaling relations yield insight into the study of downstream process transitions.

Any regional comparison of bedrock-channel morphology must carefully evaluate lithologic resistance (*e.g.* Tinkler and Wohl, 1998). Harder, less-fractured rocks will erode slowly, and weaker, more-fractured rocks will erode more rapidly. Differing tectonic regimes might lead to different rock types, simply by juxtaposing distinct lithologic packages. In addition, topographic stresses set up by increased relief might drive fracturing of rocks in valley bottoms, as hypothesized by Miller and Dunne (1996). Quantification of lithologic resistance is difficult (Selby, 1993), and here we primarily attempt to discern whether or not important variations in rock strength exist in the field area.

If incision is driven by particle impacts with the bed, then sediment flux may influence bedrock incision rates and channel gradients (Sklar and Dietrich, 1998). At low sediment flux, the stream might have insufficient tools to incise the bed, whereas at higher sediment-flux rates, incision might be optimized. However, if the sediment-flux rate exceeds the transport capacity of the stream, then the bed might be protected—*i.e.* armored from incision by stored alluvium. These effects are difficult to quantify with field data, and perhaps the most promising avenues of research are through laboratory experiments (Sklar and Dietrich, 1999). Here, we make observations of channel-bed morphology to gain some qualitative insight as to whether or not sediment flux plays an important role in setting incision rates throughout the field area.

The purpose of this paper is to provide a field-based empirical calibration of the shear-stress bedrock-incision model, with emphasis placed on testing hypothesized response mechanisms of streams to tectonics. We begin with a review of the model, with specific reference to which model parameters can be estimated from field data, and which are unknown (part 2). Part 3 is brief description of the important aspects of the tectonics and fluvial geomorphology of the field area. The empirical calibration is presented in part 4, with four sections on stream discharge, channel width, lithologic resistance, and channel-bed morphology. Each of these sections is

divided into subsections on background, methods, results and interpretations. In part 5, the results of the calibration are discussed in terms of process transitions in the landscape, our previous work on longitudinal profiles and channel concavity (Snyder *et al.*, 2000), and the role of threshold shear stresses in the model. Finally, we assess overall response of the channels to variable tectonic forcing, and suggest a few avenues for further investigations.

2. Theoretical Background

Many workers have postulated that detachment-limited fluvial bedrock incision rate (E) is a power-law function of excess shear stress (*e.g.* Howard and Kerby, 1983; Howard, 1994; Parker and Izumi, 2000):

$$E = k_e(\tau_b - \tau_c)^a, \tag{1}$$

where τ_b is shear stress at the channel bed, τ_c is a threshold (or critical) shear stress for detachment of bedrock blocks, k_e is a dimensional coefficient, and a is an exponent, assumed to be positive and constant. In this study, k_e, a and τ_c are unknown parameters.

The value of a depends on the incision process. Theoretical considerations suggest that the shear-stress exponent (a) should be around 3/2 for plucking of intact bedrock blocks, 5/2 for suspended-load (sand) abrasion, and possibly higher for cavitation (Whipple *et al.*, 2000a). For this study, we assume incision process (and therefore a) is constant throughout the studied channels.

The shear-stress coefficient (k_e) depends on several factors:

$$k_e = k_e \text{ (erosion process, lithologic resistance, sediment flux, intermittency factor).} \tag{2}$$

Just as the exponent (a) varies with erosion process, so must the coefficient (k_e). Lithologic resistance will of course directly influence the rate that rivers can incise, with more resistant rocks (harder, less jointed) corresponding to slower (low k_e) rates. Sediment flux and associated sediment carrying capacity of a river might be important controls on bedrock-incision rate, as hypothesized by Sklar and Dietrich (1998). The intermittency factor is necessary in this

approach, because incision is assumed to happen during representative events, which occur only during some small fraction of time (Paola *et al.*, 1992; Tucker and Slingerland, 1997). Here we evaluate carefully how the factors that make up k_e can be expected to vary throughout a field area and in response to changes in tectonic regime.

Threshold shear stress (τ_c) is the minimum bed shear stress (τ_b) required to initiate detachment of bedrock blocks. It is often assumed that large flood events are responsible for most bedrock erosion, and that τ_b is much greater than τ_c during such events, so τ_c is negligible in modeling efforts. We do not make this assumption in our analysis, because, as we show below, the inclusion of a nonzero critical shear stress importantly influences the relationship between steady-state channel slope (S_e) and rock uplift rate (U). Like k_e, τ_c is expected to be a function of erosion process and lithologic resistance, as well as size of bed sediment.

We now place equation 1 in terms of more easily measured quantities, specifically drainage area (A) and local channel slope (S). We follow the basic approach of Howard and Kerby (1983). The purpose of reviewing this derivation is to highlight the components of the model that can be measured from field data. The assumptions of steady and uniform flow, and conservation of momentum and water mass, combined with the Manning equation, yield the following relation for shear stress (τ_b):

$$\tau_b = \rho g N^{\alpha} \left(\frac{Q}{w} \right)^{\alpha} S^{\beta}, \tag{3}$$

where ρ is the density of water, g is the acceleration due to gravity, Q is stream discharge, w is channel width, S is local channel gradient, and α and β are positive, constant exponents. In the roughness approach used here, α=3/5, β=7/10, and N is the Manning coefficient (also used by Tucker and Bras, 2000). An alternative formulation using a dimensionless Darcy-Weisbach friction factor gives α=β=2/3 (Tucker and Slingerland, 1997; Whipple and Tucker, 1999; Snyder *et al.*, 2000). We use the Manning-equation formulation because it includes a dependence of flow discharge on flow depth that is likely to be appropriate for the rugged channels of the field area. This possibility is developed further in the discussion.

Next we put discharge (Q) and width (w) in terms of drainage area (A) via power-law relationships for basin hydrology,

$$Q = k_q A^c, \tag{4}$$

and hydraulic geometry:

$$w = k_w Q^b = k_w k_q{}^b A^{bc} = k_{w'} A^{b'}, \tag{5}$$

where k_w and k_q are dimensional coefficients, b and c are exponents, and $k'_w = k_w k_q{}^b$ and $b' = bc$. In this approach, the coefficient k_q corresponds to a dominant discharge event, responsible for most of the channel incision. The intermittency factor in equation 2 is time fraction of this discharge event. We present empirical data to constrain k_q, k'_w, c, and b' using power-law regressions in the next section.

Combining equations 1 and 3-5, we obtain the following relation for bed shear stress:

$$\tau_b = k_t A^{\alpha(c-b')} S^{\beta}, \tag{6}$$

where $k_t = \rho g N^{\alpha} (k_q / k'_w)^{\alpha}$, by definition. This approach implicitly assumes that the width exponent (b) is the same for downstream and at-a-station variations in channel width. If Q is a specific discharge event this assumption is unimportant, but for general Q, both estimates of b are needed. Equation 6 can be substituted into equation 1, to obtain the relation for channel incision as a function of drainage area (A), slope (S), and critical shear stress (τ_c):

$$E = k_e (k_t A^{\alpha(c-b')} S^{\beta} - \tau_c)^a. \tag{7}$$

The relationship in equation 7, the shear-stress model for bedrock incision by rivers, includes a nonzero critical shear stress term. Setting $\tau_c = 0$, we obtain the familiar version of this equation:

$$E = K A^m S^n, \tag{8}$$

where the coefficient of incision, K equals $k_e k_t{}^a$, the area exponent, m equals $\alpha a(c-b')$, and the slope exponent, n equals βa.

In the case of steady-state incision, where rock uplift (U) is perfectly balanced by channel incision (E), we can solve equation 7 for steady-state slope (S_e):

$$S_e = \left[\left(\frac{U}{K}\right)^{1/a} + \left(\frac{\tau_c}{k_t}\right)\right]^{1/\beta} A^{-\frac{\alpha}{\beta}(c-b')}. \quad (9)$$

For τ_c=0, equation 9 reduces to the more familiar form:

$$E = \left(\frac{U}{K}\right)^{1\ n} A^{-m\ n}. \quad (10)$$

These equations predict a power-law relationship between slope (S) and area (A) that commonly is observed in rivers (*e.g.* Hack, 1973; Snyder *et al.*, 2000). In the case of study-state channels, with spatially constant uplift rate (U) and other parameters (see discussion of steady-state channels in Snyder *et al.* (2000), stream-profile concavity is given by the exponent on area ($(\alpha/\beta)(c\text{-}b')=m/n$), and channel steepness is given by the coefficient ($[(U/K)^{1/a}+(\tau_c/k_t)]^{1/\beta}$ or $(U/K)^{1/n}$). Importantly, these relations predict that because channel concavity does not depend on a, it should be independent of incision process (Whipple and Tucker, 1999). Because the values of α and β are known, we can measure c and b' with power-law regressions of field data to get an empirical estimate of the channel concavity. Later in this paper, we compare this calibrated concavity to empirically derived values from longitudinal profiles (Snyder *et al.*, 2000).

3. Field area and previous work

The field area comprises a series of small drainage basins along the northern California coast from Cape Mendocino south to Westport (Figure 1). The region has a maritime, humid climate, with wet winter and dry summers. These streams first were analyzed by Merritts and Vincent (1989) and subsequently by Snyder *et al.* (2000). The reader is referred to these sources for a full description of the area. Rock-uplift rates vary in the field area from ~0.5 mm/yr in the south to 4 mm/yr in the King Range (Figure 2). These rates were obtained from studies of a flight of Quaternary marine terraces exposed in the region (Merritts and Bull, 1989; Merritts and Vincent,

1989; Merritts, 1996). Following the terminology of Snyder *et al.* (2000) we divide the field area into four uplift rate zones (Figure 2). In this study, we present field data from four streams in the high-uplift zone (HUZ; Oat, Kinsey, Shipman, and Gitchell), two streams in the low-uplift zone (LUZ; Hardy and Juan), and one stream in the zone of intermediate uplift rate that lies between the HUZ and the LUZ (Horse Mountain; Figure 1). These basins were chosen because their profiles are representative of the uplift-rate zones (Snyder *et al.*, 2000) and they are relatively easy to access. Rock-uplift rates in the HUZ accelerated from 0.5-1 mm/yr to the present rate around 100 ka (Merritts and Bull, 1989).

The basins are small (drainage area 4-19 km^2), steep (up to 1200 m of relief), and forested. Near drainage divides, the streams begin as colluvial channels. Downstream, in the fluvial part of the system the channel morphology is a locally variable mix of bedrock, step-pool, forced step-pool, boulder-cascade conditions (classifications of Montgomery and Buffington, 1997). The mouths of most of the basins studied (particularly Shipman, Hardy and Juan Creeks) have cobble to pebble plane-bed reaches. The LUZ basins are covered by dense forests, dominated by coast redwoods (*Sequoia sempervirens*), with immature riparian forests on floodplains near mouths. The HUZ basins have grassy ridgetops, and hillslopes covered by Douglas fir (*Pseudotsuga menziesii*).

In our previous study (Snyder *et al.*, 2000), we analyzed stream-longitudinal-profile data, derived from digital elevation models, for a series of 21 streams in the study area. This analysis, based on the standard shear-stress model (τ_c=0, equations 8 and 10), demonstrated that the observed relationship between channel slope and uplift rate could be explained only by either an unrealistically high value of the slope exponent (n≈4), or a significant increase in the coefficient of erosion (K) in the HUZ. This result implies that erosion processes are acting more efficiently in the HUZ—a conclusion that motivates further analysis of channel response mechanisms and feedbacks. We also included an attempt to characterize, to first order, the role of precipitation differences between the LUZ and HUZ. We found that orographic enhancement of stream discharge could only partially explain the observed channel slope—uplift rate relationship. We also included some preliminary channel-width data from the HUZ. Here, we expand significantly on these prior analyses, by using a more complete suite of field and hydrologic data, as well as a fuller version of the shear-stress model.

4. Empirical calibration of the shear-stress model

To gain a quantitative understanding of channel response to differing rock-uplift rates in terms of the shear-stress model, we evaluate four parameters of the study area: stream discharge, channel width, lithologic resistance, and stream-bed morphology. Below, we present data and analysis pertinent to each of these four factors. Each analysis is divided into four subsections. In the background subsection, we look at: (1) previous empirical and/or theoretical work, both in general and in adjacent field areas; and (2) how the parameters may be affected by differing rock-uplift rates. The subsection on methods describes the data collection and analysis techniques. Each part closes with results and interpretations subsections.

4.1. Discharge

Background. Many previous studies have shown that stream discharge increases with drainage area for streams in non-arid regions. Equation 4 is a commonly assumed and observed empirical relationship between drainage area (A) and stream discharge (Q) (Leopold *et al.*, 1964; Dunne and Leopold, 1978; Talling, 2000). Empirical values for the exponent c depend on the discharge measurement: from c=1 for mean-annual discharge, to c≈0.7-0.9 for bankfull discharge in alluvial channels (Dunne and Leopold, 1978). Values of c for individual flood events have received less attention in the literature, although because these are likely the important erosive events (Baker and Kale, 1998), we suspect that this discharge measurement may be most useful for our purposes.

In the simplest case of constant rainfall intensity over an entire basin with complete runoff (either through saturation or Horton overland flow), the value of the exponent c is unity, and the value of the coefficient (k_q) will simply be the rainfall intensity (Dunne and Leopold, 1978). However, particularly in larger basins and/or short rainfall events, storm contributions to stream discharge might not be equal throughout the entire basin, causing c to be less than 1. This can happen for at least two reasons: (1) water storage and slow transport in the subsurface, and (2) variations in rainfall intensity throughout a basin (Leopold *et al.*, 1964). These effects are attenuated by long-term averaging, hence the linear relationship observed for mean-annual discharge (Dunne and Leopold, 1978).

Significant rainfall gradients exist in the Mendocino triple junction area, because of orographic enhancement of precipitation by mountains. This is particularly true in the high-uplift zone (HUZ), which is one of the wettest places in California (Rantz, 1968). Monitoring stations in Honeydew and Whitethorn, just inland from the crest of the King Range, receive 2.7 to 3.5 m/yr of precipitation (National Climatic Data Center; Bureau of Land Management), compared with 0.98 m/yr in Eureka and 1.01 m/yr in Fort Bragg (Western Regional Climate Data Center), just to the north and south of the field area, respectively (Figure 1). This contrast led us to make the simple assumption that the value of k_q may be as much as three times higher in the HUZ than the LUZ (Snyder *et al.*, 2000). Here we test this assumption through the use of stream-gauging data. This analysis assumes that the relative differences seen in the current climate of the area are representative of the role of orography over the past ~100 kyr.

Methods. To parameterize equation 4, we regressed discharge against drainage area. Because we suspected that c should be near unity, we calculated both a power-law and a linear least-squares best fit, and associated 95% confidence intervals on the parameters (Hamilton, 1992). For the linear model, the intercept was forced at zero, because Q must be zero with no upstream contributing area.

The U.S. Geological Survey maintains numerous stream-gauging stations throughout northern California. Unfortunately, none of the small coastal streams within the study area are monitored. Therefore, to find values of k_q and c, we needed to use data from elsewhere in the region as a proxy. We compiled data from thirteen gauging stations that surround the study area (Figure 1). These stations span a range of drainage area from 0.4 km^2 to 1,840 km^2 (Table 1). The time series of measurements available from the USGS differs for each of the gauging stations. Because of the northwest, coast-parallel flow direction of the South Fork of the Eel River, it is concentric to the entire field area, and we use its course as an outer border of the stations involved in the analysis (Figure 1). Therefore, these stations do not include drainage area that is too far away from the study area, ensuring that the climate and hydrology is roughly constant throughout the region. We intentionally did not use data from the main trunk of the Eel River in the analysis, because this river samples an area that extends far inland (Figure 1; Table 1).

Because we are concerned with the relative difference in k_q between the HUZ and the LUZ (Snyder *et al.*, 2000), we compared the discharge measured at Honeydew Creek in Honeydew, California to the regression line for the other stations. The drainage area for Honeydew Creek is the east side of the King Range, so this station is likely to be the best representation of the HUZ drainages (Figure 1). Unfortunately, only four years of data are available for Honeydew Creek (1973-1976; Table 1). Because most incision is likely to happen during storm events (Tinkler and Wohl, 1998), we compare the two largest floods gauged at Honeydew (January 15, 1974 and March 17, 1975) to data from the other stations during these events. In addition, we calculated mean annual discharge for the period of record on Honeydew Creek. Finally, to constrain the values of k_q and c for a major event, we compiled available data for the December 20-22, 1964 event, the largest flood on record for most of the stations in the region (Table 1; Wannanen *et al.*, 1971).

Results. Figure 3 shows the power-law and linear regressions of discharge against drainage area for three floods and the mean-annual discharge in 1973-1976. All the datasets show linear trends in logarithmic space, and the power-law regressions indicate values of c that are indistinguishable from unity. The more complete discharge dataset from the December 1964 flood indicates that the scaling trend holds over four orders of magnitude in drainage area, including smaller basins on the order of those studied here (0.1-20 km^2; Figure 3a).

Interpretations. We find that for this field area, discharge has a linear relationship with drainage area, and the values of k_q for the linear model are most appropriate to use. The value of k_q from the regression lines corresponds to the magnitude of the associated flood, with the December 1964 event by far the largest.

For Honeydew Creek gauge data, the discharge—area coordinate values lie above the regression line (Figure 3b-d), consistent with the increase in precipitation observed at nearby rain gauges. Table 2 shows values of k_q for Honeydew Creek, calculated using an assumed linear relationship between discharge and drainage area. With the best-fit values of k_q from the regression lines, Honeydew Creek transmits 1.3 to 2.3 times more discharge (relative to unit drainage area) than the rest of the area (Table 2). Taking the maximum cases from the confidence intervals on k_q, the range is 1.2 to 3.6. The threefold variation in k_q assumed by Snyder *et al.* (2000) is at the high

end of these ranges. The flood of March 17, 1975 was the largest event of the short record for Honeydew Creek, and clearly a more significant event there than at other stations (ranking fifth at the adjacent Mattole River station, and not more than eight elsewhere; Table 1). However, the best-fit k_q for this event implies only a 1.9-times variation between Honeydew Creek and elsewhere, which is not quite as significant as might be expected (Table 2). The mean annual discharge data for Honeydew Creek shows the greatest deviation from the regression line of regional data, suggesting that Honeydew Creek has a significantly higher base flow than other streams in the region. This regression also has a closer match to the observed differences in annual precipitation.

Although we have no discharge data directly from the study-area channels, the proxy data from nearby streams suggest that we should expect an approximately twofold variation in the value of k_q between the HUZ and the LUZ. This interpretation is uncertain, because we do not know whether the west side of the King Range is actually receiving more precipitation than the east side, where Honeydew Creek is located. This situation might be expected, because the orographic effect is usually most pronounced on the seaward side of mountain ranges. However, three observations suggest that this may not be the case in this field area. First, the seaward side of the range is so narrow (<5 km) and steep that it might act as a barrier to precipitation, deflecting storms to the north, and up the Mattole and Honeydew Valleys (Figure 1). This is certainly the behavior exhibited by the ubiquitous northern California coastal fog in the area. Second, vegetation on the west side of the King Range is characteristic of a drier climate than that on the east side, although this might be a function of windier conditions and steeper slopes. Finally, the steep topographic gradient of the King Range might enhance precipitation through lifting of air masses, but because of the small width of the seaward side, much of this precipitation might actually fall on the leeward side. For these reasons, the Honeydew Creek basin might actually receive more rainfall that the studied HUZ channels. Therefore, estimates of orographic enhancement of discharge presented in Table 2 are likely maxima when applied to the HUZ.

These uncertainties stated, we consider it reasonable to assume a twofold variation in flood-event k_q between the HUZ and LUZ, somewhat less than the up to threefold variation in annual precipitation. However, we are unable to place any constraints on the absolute magnitude of k_q,

because to do so would assume a dominant discharge that is responsible for most channel incision. This value of k_q could correspond to a small-magnitude, high-recurrence flood (like the 1974 and 1975 events) or a very large, catastrophic event (perhaps greater than the 1964 event). This limitation is investigated further in the discussion section, below.

4.2 Channel width

Background. Hydraulic geometry in alluvial channels (relations among channel width, depth, and discharge) has received much research attention over the past 50 years (*e.g.* Leopold and Maddock, 1953; Richards, 1982). Equation 5 describes the downstream trend in channel width with discharge (or via equation 4, area). The value of the exponent (b) has been shown to be approximately 0.5 in many studies of width and discharge in alluvial rivers (*e.g.* Leopold and Maddock, 1953), but comparably little research has been done for bedrock-incision-dominated, mountain channels, like the ones in the study area, although a value of 0.5 is often assumed in models (*e.g.* Tucker and Bras, 2000). Recent interest in bedrock-channel processes has yielded some studies of the equation 5 relationship for bedrock rivers (Pazzaglia *et al.*, 1998; Snyder *et al.*, 2000; Montgomery and Gran, 2001). In the most detailed study to date, Montgomery and Gran (2001) present width—drainage area data from a variety of mountain rivers in Washington, Oregon, and California indicating best-fit values of b' from 0.32 to 0.53. The value of the width coefficient, k_w, should depend on a variety of factors including the location of the width measurement (high-flow channel, valley bottom, see below), the type of river (bedrock, plane bed, meandering, etc.), and the substrate (bedrock, fine or coarse alluvium).

Width adjustments are an important way in which fluvial systems might respond to perturbations (*e.g.* Harbor, 1998; Lavé and Avouac, 2000; Schumm *et al.*, 2000; Hancock and Anderson, 2001). In our previous work, we speculated that bedrock channels are likely to narrow in response to increased gradients associated with higher uplift rates (Snyder *et al.*, 2000). Like orographic precipitation, this is a feedback mechanism that would make incision processes more effective in concert with higher uplift rates. This hypothesis predicts a lower value of k_w in the HUZ than in the LUZ, and is easily testable with field data.

Methods. During the summers of 1998, 1999 and 2000, we conducted field surveys of seven study-area creeks (from north to south): Oat, Kinsey, Shipman, Gitchell, Horse Mountain, Hardy

and Juan (Table 3). During these surveys, we collected several sets of data through measurements and observations: streamwise distance (using a hip chain) and local slope (using a hand inclinometer); channel width at stations spaced every 50 m in stream distance; rock strength and jointing (discussed in Section 4.3); stream-bed morphology (discussed in section 4.4); and terrace type (strath, fill) and height. At each station, three channel-width measurements were made. (1) Low-flow width, defined by the water in the channel during summer baseflow conditions. (2) High-flow width, defined as the zone of active scour between channel banks, generally seen as the area without vegetation. This width is analogous to the bankfull width of an alluvial river, and it is the measurement reported by Montgomery and Gran (2001). However, unlike Montgomery and Gran, we do not separate bedrock-channel from alluvial-channel reaches. (3) Valley-bottom width from side wall to side wall, including strath and fill terraces to 3-4 m height above the stream bed. To further characterize local variability, a second set of high-flow width (and in Hardy Creek, valley width) measurements were made at each station during our later field seasons (including upper Oat, upper Kinsey, Gitchell, Horse Mountain, and Hardy Creeks). Most width measurements were made using a plastic tape measure, with an accuracy of 0.1 m. In some cases, valley width was found using a laser rangefinder (±1 m) or visually estimated. Some sections of Kinsey, Shipman, and Gitchell Creeks could not be accessed, usually because of waterfalls (Table 3). The lower parts of Hardy and Juan Creeks were not accessed because of land-ownership and time constraints, respectively (Table 3). To further augment our data, we collected data from several tributary channels, selected because they appeared representative of the overall stream morphology and/or filled gaps in the span of drainage area surveyed (Table 3).

Because there are no gauging stations on the study area streams, we plotted width against drainage using equation 5 as a regression model. Drainage areas were calculated from DEMs and carefully registered to the field surveys. This process was checked by matching tributary junctions, which were recorded on field surveys and are easily recognized as step-function changes in drainage area. The regression analysis includes only data with $A>10^5$ m^2, as this is the zone of fluvial-process dominance in these channels identified by Snyder *et al.* (2000). We do not present data for the low-flow width, because this is not geomorphically relevant and depends on the hydrologic conditions at the time of the measurement. The values of b' produced by the

regressions were compared using the 95% confidence intervals on the regression parameter (Hamilton, 1992). Values of k'_w covary strongly with b', so we compared the widths predicted by the regressions at a reference drainage area of 10^6 m^2 (1 km^2), to test for systematic differences in channel width between the uplift-rate zones. The ranges of predicted mean-width values were compared using the 95% confidence hyperbolae on the regression (Table 3; Hamilton, 1992).

Results. Regressions of high-flow width against drainage area for individual streams yielded best-fit values of b' from 0.21 to 0.56, and valley-width regressions ranged from 0.29 to 0.50 (Table 3). To increase the span of drainage areas included in the regressions, and to characterize overall study-area trends, we pooled data from the four HUZ streams surveyed (Oat, Kinsey, Shipman and Gitchell Creeks) and the two LUZ streams (Hardy and Juan Creeks; Figure 4; Table 3). These combined datasets yielded b' values of 0.35±0.04 and 0.28±0.02 for high-flow width of HUZ and LUZ streams, respectively. These ranges are significantly different. The combined datasets indicate valley-width b' values of 0.42±0.05 and 0.35±0.03, respectively, which are not significantly different. The regression lines give best-fit high-flow widths of 5.4 m and 4.0 m at the reference drainage area (1 km^2), respectively, with ranges that do not overlap within 95% confidence intervals (Figure 4; Table 3). Valley widths are 7.9 m and 8.9 m, respectively, which do overlap (Figure 4; Table 3).

Interpretations. The channel-width measurements are quite variable, with nearly an order of magnitude of scatter at any drainage area (Figure 4). Both the scatter and the range of b' values are in good agreement with the data presented by Montgomery and Gran (2001). Combining the data from channels within uplift-rate zones generally improves the regressions, and more importantly, allows us to analyze data over a larger span of drainage area in the HUZ (Table 3). For these reasons, we focus this discussion on the pooled-data regressions.

Comparison of b' values for high-flow width data from the two uplift-rate zones indicates that the regressions are significantly different, with a stronger relationship between width and area in the HUZ (Figure 4). Surprisingly, the HUZ channels are significantly wider (at a given drainage area) than the LUZ channels, counter to the expected narrowing (Table 3; Snyder *et al.*, 2000). Unfortunately, differences in recent land-use practices in the two zones complicate interpretation of these data. The more accessible topography and larger trees of the low-uplift zone have made

this area more attractive for logging. The four studied HUZ basins have never been logged significantly, whereas Juan and Hardy Creeks have had large-scale timber harvests for over a century. Past logging activity included the construction of an elevated railroad in the channel bottom of Hardy Creek and a road next to the channel in Juan Creek (Figure 5). The channel morphology of Hardy and Juan Creeks reflects these land-use practices, with ubiquitous fill terraces 1-2.5 m high that are likely the result of increased sediment flux from harvested hillslopes and valley-wall excavation for road construction. The terraces record recent entrenchment by the channel and are likely to be the reason the LUZ channels are narrower at present. Unfortunately, no low-uplift channels in the field area share the land-use history of the high-uplift channels, and vice versa.

Horse Mountain Creek basin also was logged in the 1950s and 1960s, and exhibits morphology similar to that of Hardy and Juan Creeks. Horse Mountain Creek has a high-flow width of 4.2-4.8 m at 1 km^2, overlapping with the range seen on the LUZ creeks (Table 3). For these reasons, we believe that the differences between high-flow widths throughout the field area should not be viewed as the result of differing response to uplift rates.

We next turn to the valley-width data, which are less likely to be affected by land-use differences. The values of b' from the regressions for the high-uplift and low-uplift zone channels overlap within 95% confidence bounds at b'=0.37-0.38 (Figure 4). These regressions also yield similar values of k'_w and width at the reference drainage area, suggesting that the valley-width data, although scattered, are not significantly different between different uplift-rate zones. In the LUZ, the regressions for Juan and Hardy are quite different, with the parameters for Juan Creek more similar to the other study-area streams, and better constrained (R^2=0.60). This might again reflect land-use differences, particularly because of in-channel railroad construction in Hardy Creek, but we have no basis to say this with certainty. At the southern end of the HUZ, Gitchell Creek is proportionally somewhat wider and has a lower value of b' than the other HUZ channels, with a regression similar to Hardy Creek (Table 3). The only discernible difference in channel morphology for this stream was the presence of large (1-3 m diameter) sandstone boulders, which were not seen as extensively in adjacent drainages (Figure 6). These boulders are sourced from the ridge to the east of the creek, a different unit from that of the rest of the

studied channels (McLaughlin *et al.*, 2000). We can offer no speculation as to how this might explain the apparently anomalous valley-width data of Gitchell Creek.

Taking the width regressions as a whole, we use a value of b' of 0.4 for subsequent calculations, because this value is representative of most of the valley-width measurements, and the high-flow width measurements least affected by land use (Oat, Kinsey and Shipman Creeks). This is in contrast to the preliminary results presented in our previous paper (Snyder *et al.*, 2000). We also are unable to discern any important difference in valley width between the uplift-rate zones, so we believe that assuming that k'_w is constant throughout the study area is acceptable.

4.3 Lithologic resistance

Background. The coefficient relating excess shear stress to incision rate (k_e, equations 1 and 2) depends on fluvial-incision process, lithologic resistance, and possibly sediment flux. Here, we assume that incision processes are constant throughout the area, so that they do not contribute to variations in k_e. We consider the role of sediment flux in the next section. The possibility of systematic variations in lithologic resistance to erosion must be considered through the use of careful field analysis. Because measurable bedrock incision by rivers occurs over long time periods and/or during large events, we cannot make empirical estimations of the value of k_e directly. We can, however, search for evidence of important variations in lithologic resistance that would contribute to changes in k_e throughout the study area. For simplicity and brevity, we assume that changes in k_e due to lithology would also yield changes in critical shear stress (τ_c). Our analysis focuses on the former but can expected to apply equally well to the latter.

Lithology clearly plays an important role in setting bedrock incision rates (Wohl, 1998; Stock and Montgomery, 1999; Whipple *et al.*, 2000a; Whipple *et al.*, 2000b). Bedrock in the study area is entirely within the Cretaceous—Tertiary Coastal Belt of the Franciscan Complex, a highly sheared and folded mix of argillite and sandstone, with some conglomerate and igneous rocks (Jennings and Strand, 1960; Strand, 1962; McLaughlin *et al.*, 2000). Broadly speaking, resistance varies locally, but overall the rocks are fractured and weak. From detailed aerial-photograph interpretation and mapping of rocks in the HUZ of the King Range terrane, McLaughlin *et al.* (2000) divided the lithologies of the area into discrete zones based on hillslope morphology. Similar aerial-photograph interpretation has been done by Ellen for the region south

of the McLaughlin *et al.* study area, including the basins of the LUZ (S. Ellen, unpublished mapping, USGS 1:100,000-scale Covelo quadrangle). For the most part, the HUZ channels lie in the zone dominated by argillite with "irregular [hillslope] topography, lacking a well-incised system of sidehill drainages" (McLaughlin *et al.*, 2000), while the high-relief King Range crest area (upper parts of Big, Big Flat, and Shipman Creeks, Figure 1) are in the category of hillslope morphology characterized by "sharp-crested topography, with a regular, well-incised system of sidehill drainages." The LUZ channels generally lie in a zone characterized by hillslope morphology similar to the latter case (Ellen, unpublished mapping).

Methods. Here, we use detailed measurements of rock-mass strength and jointing of channel bedrock outcrops to assess whether important variations in rock resistance can be found. To first order, lithologic resistance depends of two related factors: intact rock mass strength, and degree of fracturing due to weathering and jointing (Selby, 1993). Both of these factors can be estimated in the field. To assess rock resistance in the field, we use two techniques: Schmidt hammer measurements of rock mass strength, and visual estimates of characteristic joint spacing. Our analysis of the former includes statistical tests of various sample subsets.

Mass strength of intact rock can be measured in the field with a Schmidt hammer (Selby, 1993). Because measurements near fractures are highly variable and difficult to treat in a quantitative way, we attempted to limit our survey to outcrops large enough to provide at least ten different measurements of intact rock. We report our data in Schmidt hammer R units, uncorrected for inclination of the hammer. We neglect this correction because we find that the correction is small (<4 R units) compared with the scatter inherent in the data. We omit measurements less than 11 R units (10 is the minimum reading) and those that are clearly influenced by fractures in the rock (generally identified by hollow-sounding impacts). During our field surveys of channel morphology, we made Schmidt hammer measurements at stations spaced approximately 100 m apart, where outcrop permitted. At most stations, we took 25-50 readings. We then compared these measurements both within a basin, and between zones within the field area.

Schmidt hammer measurements from channels in different settings can be compared through statistical analysis, after some data reduction. Because we took different numbers of readings at each station, we compare mean values of each station, creating samples of basin-wide station-

mean values. To assess rock mass strength of basins and zones as a whole, we compiled histograms of the mean values for each station. When looking at basin-wide data, we include only readings from bedrock in channels likely to be dominated by fluvial processes, so as with other analyses, we work only with data from locations with $A>0.1$ km^2. The station mean values were also subdivided into those at locations with distinct bedrock steps (small waterfalls or knickpoints at least 0.5 m high) and those without bedrock steps. We tested the hypothesis that two samples are from the same distribution using Kolmogorov-Smirnov nonparametric methods (Davis, 1986; Rock, 1988), with the criteria that the hypothesis can be rejected if $p<0.05$. The Kolmogorov-Smirnov test is useful because it does not require that the two samples come from normal distributions (Davis, 1986; Rock, 1988). To look at intrabasin variability, we plotted Schmidt hammer means, maxima and standard deviations along profiles. We also separated out stations at bedrock steps or knickpoints ≥0.5 m high to test whether these features were formed on disproportionally harder lithologies.

Our analysis of the degree of jointing consisted of visual estimates of the range of joint spacing in each outcrop. The goal of this methodology was simply to get an idea of the size of blocks that could be created by erosion of the bedrock. This technique is qualitative, and not sufficient to characterize the overall contribution to lithologic resistance due to weathering and jointing. Nonetheless, we include our observations in the results presented here, because they give at least a rough idea of the degree of fracturing of the rock throughout the study area.

Results. The basin-wide Schmidt hammer data are presented in Table 4. As with the channel-width data, we focus on the pooled data for the HUZ and the LUZ, which increases sample size (Figure 7; Table 4). The Schmidt hammer R mean value for the HUZ is 47.5±10.1 (all errors are 1σ unless otherwise noted), and the LUZ is 44.5±7.2 R. Comparing the pooled samples from the LUZ and HUZ, the Kolmogorov-Smirnov (K-S) test indicates that we must reject the hypothesis that they are from the same distribution, indicating that there is a statistical difference ($p=2.5\times10^{-4}$) between the rock-mass strength in the two uplift-rate zones (Figure 7a-b). Plots of Schmidt hammer maxima, mean, and standard deviation at each station along a channel show that outcrops have fairly random, variable resistance (Figures 8b-10b).

In the HUZ, the stations located at bedrock steps ≥0.5 m yield a mean value of 54.9±8.3 R

(Figures 7-8; Table 4). This mean is compared to a mean of 45.4±9.7 R for stations without significant bedrock steps. A K-S test indicates that the hypothesis that these samples are from the same distribution can be rejected ($p=2.7\times10^{-4}$). In the LUZ, the stations with a bedrock step have a mean of 47.0±6.4 R, and those without steps have 43.5±7.3 R. Here, the K-S test suggests that these samples may be from the same distribution ($p=0.149$).

Basin-wide joint spacing calculations indicate mean minimum spacings of 2-3 cm in the HUZ and 4-5 cm in the LUZ, and mean maximum spacings of 20-28 cm and 46-49 cm, respectively (Table 5; Figures 8c-10c). Horse Mountain Creek, between the uplift-rate zones, has a mean joint spacing range of 2-17 cm.

Interpretations. The Schmidt hammer data indicate that rocks of the HUZ are slightly harder than those of the LUZ, with a higher mean and mode (Table 4; Figure 7). However, the difference in means is small, as the standard deviations overlap considerably. Conversely, the joint-spacing data indicate that the HUZ rocks are somewhat more fractured than LUZ rocks (Table 5; Figures 8c-10c). This is broadly consistent with the model proposed by Miller and Dunne (1996) that valley bottoms in areas of greater relief should be more fractured simply because of topographic perturbations of the stress field. However, we have not made the required systematic measurements of joint spacing and orientation to test their hypothesized feedback between relief production and bedrock fracturing.

Separating the Schmidt hammer station data into samples at ≥0.5 m bedrock steps and those not at steps shows that the knickpoints in the HUZ are controlled by areas of particularly resistant rock, with a significantly different distributions and greater sample mean (Figure 7d, f; Table 4). This is not the situation in the LUZ, where the bedrock-step sample is only slightly harder than the non-step sample (Figure 7c, e; Table 4). This difference may be related to the increased erosion rates of the HUZ, which might (1) emphasize the importance of zones of more resistant rock as a channel responds to higher rates of rock uplift and/or (2) give less opportunity for preparation and fracturing of bedrock by weathering. Alternatively, this difference may be a reflection of the somewhat greater distribution of resistant (high mean R value) areas of rock in the HUZ, which is clearly indicated by the left-skewed appearance of the histograms for the overall HUZ sample (Figure 7b) and bedrock-step HUZ sample (Figure 7d). This suggestion is

supported by the observation that the non-bedrock step HUZ sample is more similar to the LUZ samples, in that it has a lower mean and is less skewed (Figure 7f). In any case, zones of resistant rock appear to play an important role in controlling the location of channel knickpoints, particularly in the HUZ.

Unfortunately, none of our channel surveys cross any of the significant hillslope morphologic contacts mapped by McLaughlin *et al.* (2000) or Ellen (unpublished), so we cannot assess the importance of these potential intrabasin variations in hillslope morphologic expression. However, we can say that the gradients of stream channels that cross these transitions in the King Range (Big, Big Flat, and Shipman Creeks) do not seem to be affected by this change in hillslope morphology (Snyder *et al.*, 2000). We also can speculate that the differences we observe in mass strength (greater in the HUZ) and joint spacing (greater in the LUZ) could be broadly consistent with the mapping by McLaughlin *et al.* (2000) and Ellen, which put these channels in different hillslope-morphology zones.

Importantly, the lower, south-flowing, part of Horse Mountain Creek follows a major shear zone (McLaughlin *et al.*, 2000). This shear zone is on strike with and just north of the mapped active trace of the San Andreas Fault (Figure 1; Prentice *et al.*, 1999). Channel slopes in this area are anomalously low (Snyder *et al.*, 2000). This zone is characterized by particularly fractured rocks, with a corresponding decrease in rock mass strength and joint spacing (Figure 10). Relatively little data could be collected in this area because of a paucity of outcrops of sufficient size and competence for Schmidt hammer measurements. Joint spacings in the 1.5 km section of channel near the mouth of Horse Mountain Creek are consistently in the 1-10 cm or 1-5 cm categories (Figure 10c), and station mean Schmidt hammer R values are around 30, well below the basin-wide average of 41.8. These observations confirm that the analysis is capable of picking up important, systematic variations in rock resistance.

The central question of the analysis of lithologic resistance can be stated as follows: are there systematic differences between rocks of the HUZ and LUZ that could affect the values of k_e and τ_c? One interpretation of the Snyder *et al.* (2000) analysis is that rocks of the HUZ might be more easily eroded than rocks of the LUZ, yielding more efficient incision processes (higher k_e and K). The jointing data are consistent with this situation, but the data on rock-mass strength are

not. The latter data are clearly more robust than the jointing data, and they suggest that, if anything, rocks within the HUZ are (at least locally) harder and therefore presumably more difficult to erode (lower k_e). We cannot discern with certainty if either factor is significantly affecting incision rates throughout the study area. Because the analysis presented here does not provide evidence for what we might suspect to be major differences in mass strength or jointing, however, we proceed with the assumption that k_e and τ_c do not vary due to variations in rock resistance.

4.4 Channel-bed morphology

Background. Sediment flux is likely to be an important control on the ability of a stream to incise its bed, and hence on possible rates of incision. Sklar and Dietrich (1998) propose a model for stream incision by particle (sediment) impacts on the bed. In their model, low sediment flux gives rise to a "tool-starved" condition, with insufficient impacts to break apart and transport channel bedrock. At the other end of the spectrum, sediment flux greater than transport capacity buries the channel bedrock, reducing erosion rates to include only rare, catastrophic events that can move the bed material. This gives rise to transport-limited-incision or depositional conditions. In between these two cases is a situation where an optimal sediment flux yields the most effective bedrock incision. On an intuitive level, this simple presentation of the Sklar and Dietrich argument is likely to be correct, so the question becomes: is this effect important in this field setting? For the purposes of this paper, we propose that sediment flux through the channel might influence the value of k_e (equation 2; Whipple and Tucker, 1999).

In our previous paper (Snyder *et al.*, 2000), we argued that the main-trunk channels of the study area are likely to be eroding at the same rate that the land surface is uplifting. We are less confident, however, about the response of tributaries and hillslopes. Throughout the study area, and particularly in the HUZ, we see inner gorges and "hanging" tributaries that have a pronounced convexity at their junction with the main channel (Snyder *et al.*, 1999). These observations suggest the possibility that the main channels might have been more rapid in their response to increased rock uplift rates than the channels throughout the rest of the basins. Put simply, we are not confident that the steady-state model we believe applies to the main channels is appropriate for the entire drainage basins. Therefore, although we might assume that the

steeper hillslopes and tributaries of the HUZ indicate greater sediment flux out of the system than the LUZ, we cannot say this with any quantitative confidence.

We are left with taking an essentially qualitative approach to the problem of sediment flux, by making observations of the present morphology of the channel bed throughout the study area. We suggest two cases for how the value of k_e might be affected by sediment flux. First, if the bed is mostly covered by alluvium, sediment flux rate might slow incision rates because bedload impact energy would be spent reducing the size of bed sediment, not incising bedrock. Conversely, if the bed is composed mostly of exposed bedrock outcrop, then either sediment flux is enhancing bedrock incision or is playing a small role in setting bedrock incision rates. In the first situation, k_e is likely to be reduced because of increased sediment flux. In the second case, the value k_e will either be unaffected by sediment flux or be increased.

Methods. During our field surveys, we made detailed observations of the stream morphology, including: channel-type classification (Montgomery and Buffington, 1997); size and source (alluvial or colluvial) of bed sediment; size, type and distribution of terraces; and the presence of bedrock outcrops. As we surveyed each ~25 m reach of channel, we made visual assessments of the percentage of the bed and sidewalls was that was composed of exposed bedrock. Each reach fell into one of eight categories: 0% for no exposed bedrock; 1% for a trace; 10%, 25%, 50%, 75%, and 90% for varying degrees of exposure; and 100% for bedrock channel with no continuous sediment deposits. These values were plotted on the channel longitudinal profiles, and integrated in the horizontal (distance, x) and vertical (elevation, z) directions to calculate an overall percentage of channel bedrock for the fluvial part of the system ($A > 0.1$ km^2). Although this technique is only semiquantitative, it does provide a relative measure of the channel morphology to allow interbasin comparison.

Results. Horizontally integrated channel bedrock ranges from 2.6-2.7% in Gitchell and Juan Creeks to 27% in Oat Creek (Figures 8a-10a; Table 5). For integration in the vertical direction, bedrock percentages range from 2.0% in Juan Creek, to 31% in Oat Creek. Plots of channel bedrock percentage along the stream profiles show that outcrops are distributed throughout the channels, with perhaps a slightly increased percentage in the upper half of the profiles (Figures 8a-10a).

Interpretations. In five of the six channels studied, the percentage of channel bedrock is greater in the vertical integration than the horizontal (Table 5). This simply shows that, in general, bedrock channel segments are steeper than sediment-mantled segments. The wide distribution of bedrock outcrops throughout the channels indicates that any alluvial cover is a thin mantle (<3 m) and reinforces the interpretation that the longitudinal profiles of these streams are controlled by their ability to incise bedrock (Figures 8a-10a; Snyder *et al.*, 2000).

In general, high-uplift zone channels have more exposed bedrock than low-uplift zone channels (Table 5). This is particularly true when Oat and Kinsey Creeks are compared to Hardy and Juan Creeks. Gitchell Creek seems to have an anomalously low percentage of exposed bedrock, reflecting the large sandstone boulders that make up the channel bed material in many places (Figure 6). These boulders might effectively act as bedrock for this channel, with incision limited by the ability of the channel to detach pieces from them. The boulders might have an effect on channel width and bedrock in Gitchell Creek, but they do not appear to affect the longitudinal profile, which is consistent with adjacent HUZ creeks (Snyder *et al.*, 2000). We set aside Gitchell Creek, in order to address the general trend that HUZ channels have much more exposed bedrock than LUZ channels.

Taken at face value, these data suggest that the LUZ channels are in a situation where incision is limited by bed protection by sediment cover, suggesting a low value of k_e, or perhaps even transport-limited conditions. At the same time, the HUZ channels appear to have ample opportunity to erode bedrock, not limited by their (presumably somewhat higher in the long term) sediment flux rate. However, as with the channel-width signal, the land-use differences between the two areas are likely to play an important role in setting the present-day channel morphology. The LUZ channels clearly show the signs of a recent period of high sediment flux due to activities related to timber harvesting (Figure 5). The ubiquitous young (<100 years old) fill terraces of Hardy and Juan Creeks indicate that the main channels are trenching actively through this sediment. This recent signal is likely the dominant control on bed morphology in the LUZ. In fact, if we consider the possibility that the recent pulse of sediment has yielded a greater short-term sediment flux rate in the LUZ than in the HUZ, then the LUZ is presently an example of bedrock incision limited by an overabundance of sediment. However this is likely a short-term perturbation, and in the absence of comparable HUZ and LUZ channel morphologies, we are

unable to make any inferences about the role of sediment flux as a response mechanism.

To summarize, although a model for k_e changing as a function of sediment flux is plausible for this field area (equation 2), we cannot draw any firm conclusions, because of land-use differences. However, if no other cause of a change in k_e (or other factors) can explain the observed relationship between steady-state channel slope (S_e) and uplift rate (U; equations 9-10; Snyder *et al.*, 2000), then we might conclude that incision rate is dependent on the presumed long-term difference in sediment-flux rate between the HUZ and LUZ. Conversely, if other plausible mechanisms can explain the S_e-U data adequately (for instance τ_c), then perhaps sediment flux is not an important control on incision rates in this field area.

5. Discussion

5.1 Inferences about process transitions from channel-width data

The full, divide-to-mouth channel width datasets, paired with observations of channel morphology, provide some insight into downstream process transitions (*e.g.* Dietrich *et al.*, 1993). The width—drainage area scaling appears to break down at a drainage area of ~10^5 m^2 (0.1 km^2; Figure 4). This is at the same value as the break in channel slope—drainage area observed by Snyder *et al.*(2000). In the field, this is typically the place where two ephemeral gullies come together, doubling the drainage area, to form a perennial stream (Figure 11). Downstream from this junction, channel sediment and bedrock outcrops exhibit clear signs of fluvial reworking (organization into bedforms, and rounding and fluting, respectively), whereas these morphologies are rare in upstream gullies. We suggest that this break reflects the switch from colluvial-dominated (mostly debris flows; Stock and Dietrich, 1998) to alluvial-flood-dominated incision processes, although both sets of processes are certainly active in both areas.

The scaling break is observed most strongly in the HUZ channels (Figure 4), which may be related to two factors. First, erosional rills and gullies, with thin veneers (<<1 m) of sediment stored in the channel, occupy the first 100-300 m downstream from the divide in the HUZ. This is generally not the case in the LUZ, where several hundred meters of rounded, convex-up hillslopes and intermittent sediment-filled colluvial hollows characterize ridge crests. Second,

Hardy and Juan Creeks have numerous roads running on and just below the ridges, which greatly influence local channel morphology, often diverting flow out of ephemeral gullies. Both factors mean that in many cases data collection is impossible because the rills or gullies cannot be followed or are not defined enough to permit width measurement with any certainty in the LUZ channels. This is reflected by the comparative lack of data from drainage areas less than about 2×10^4 m^2 (0.02 km^2) in the LUZ (Figure 4). We surveyed upper tributaries in both Juan Creek and Hardy Creek in an unsuccessful attempt to fill in this data gap (Table 3).

5.2 Channel concavity

Steady-state channel concavity is given by the area (A) exponent in equations 9 and 10 ($(\alpha/\beta)(c-b')=m/n$, hereafter m/n). Using slope—area regressions from longitudinal-profile data, we found previously that the true mean channel concavity (θ) of the 21 study area streams was 0.43±0.11 (1σ), and that these streams were likely close to steady state (Snyder *et al.*, 2000). Using the empirical calibrations presented here (c=1; $b'\approx$0.4; Table 6), equations 9 and 10 predict that the steady-state concavity of these streams should be around 0.51. This calibrated theoretical value matches the previous empirical estimate of θ (from longitudinal-profile data) within 1σ uncertainty, although it does suggest that the true concavity is somewhat less than theory would predict. Previously, we presented preliminary channel-width data that was more consistent with b'=0.6, which provided a more satisfying match to the observed concavity (Snyder *et al.*, 2000). However, the more complete investigation of channel width does not support this higher value of b'.

Although our empirically calibrated theoretical prediction for m/n is reasonably close to the observed value of θ, an investigation of the assumptions associated with this prediction is warranted. The basic premise of equations 9 and 10 is that at steady state (and spatially constant U and K), the channel slope has adjusted so that excess shear stress (or shear stress, if τ_c=0) is constant downstream (Snyder *et al.*, 2000). If the true concavity is less than the value predicted in equations 9 and 10, this suggests that either shear stress is actually decreasing downstream or the derivation of equations 2, 9 and 10 is incomplete or oversimplified. Here we address a set of possible explanations, which could result from a variety of violations of the basic assumptions of equations 9 and 10.

(1) The system may not be in steady state, for instance a wave of incision could be migrating headward through the channels. This is conceivable, although we would expect a distinct break in the slope—area relationship that is not observed (Snyder *et al.*, 2000).

(2) The rock uplift rate (U) may not be constant throughout the basin. An increase in U downstream could explain the observed concavity (*e.g.* Kirby and Whipple, 2001), but the wide (≤1 km), flat emergent marine terraces in the northern and southern parts of the study area are not consistent with significant tectonic tilting (Merritts *et al.*, 1992; Snyder *et al.*, 2000). Differential motion along discrete faults crossing channels could also cause intrabasin changes in uplift rate, but no structures that would lead one to suspect this situation have been identified, except possibly the shear zone in Horse Mountain Creek (McLaughlin *et al.*, 2000).

(3) Downstream from the divide, the bed may be progressively buried and therefore protected by sediment, lowering the value of k_e. Most of the surveys are consistent with this possibility, with more bedrock exposed in the upper parts of the channels (Figures 8a-10a).

(4) Holocene eustatic sea-level rise might be causing some reduction in sediment-carrying capacity in the lower parts of the basin. This is most likely in the low-uplift zone, where rock-uplift rates are less than recent rates of sea-level rise. Indeed, these channels are more alluviated in the lower reaches (Figure 9a), and for this reason, these areas were not included in the calculations of concavity from longitudinal profiles by Snyder *et al.* (2000).

(5) Intrabasin orographically driven gradients in precipitation might affect stream discharge in a way not captured by the analysis in Section 4.1. For example, c measured within individual study-area basis could be less than 1, corresponding to a reduction in the predicted concavity. The affect of orographic precipitation on concavity has been investigated by Roe *et al.* (2001).

(6) Perhaps the most likely case is a downstream decrease in the hydraulic roughness parameter (in this case, N). For instance, if N varied from 0.070 $m^{-1/3}s$ at $A=10^5$ m^2 to

0.048 $m^{-1/3}s$ at $A=10^7$ m^2, this would translate into a relationship where N goes as $A^{-0.08}$, and m/n in equations 9 and 10 would be 0.43, matching the value of θ. We present this calculation for heuristic purposes—to illustrate the point that minor downstream variations in channel roughness could explain the slight data mismatch. Variations in Manning's N on this order as the stream makes the transition from a steep mountain channel choked with woody debris and boulders delivered from mass wasting on adjacent hillslopes (*i.e.* $A=10^5$ m^2), to a 10-m-wide, pool—riffle or plane-bed channel with well-formed smooth banks ($A=10^7$ m^2) seems like a reasonable possibility, consistent with other field observations of downstream changes in morphology (Barnes, 1967; Richards, 1982; Montgomery and Buffington, 1997; Buffington and Montgomery, 1999). Unfortunately, we do not have the required field measurements of N to test this hypothesis.

5.3 The importance of critical shear stress

Most models of bedrock channel incision neglect the critical-shear-stress term (τ_c) in equation 1, and therefore use a form of equation 8 to describe channel evolution. Recently, Tucker and Bras (2000) used a fluvial erosion model forced by a stochastic distribution of storms to show that in the absence of a threshold term, for reasonable (<2) values of a, the highest erosion rates occurred in the least variable climatic conditions—*i.e.* constant gentle rain. This is in direct opposition to the basic assumption usually used to justify ignoring the τ_c term—that the big storms do most of the work and produce shear stresses that far exceed τ_c. This observation spurred our initial interest in investigating the role of the threshold shear stress term.

A cursory comparison of equations 9 and 10 reveals that nonzero values of τ_c influence the expected relationship between steady-state slope (S_e) and rock-uplift rate (U). To illustrate, we consider S_e at a reference drainage area ($A_{ref}=10^6$ $m^2=1$ km^2; Figure 12; Table 6). We use the mean cases from the longitudinal profile analysis in Snyder *et al.* (2000), for values of S_1 and S_2, the slopes at A_{ref} for the LUZ and HUZ, respectively. When $\tau_c=0$ is assumed (equation 10), with $n=1$ (erosion rate linear in slope; $a=10/7$), steady-state slope varies linearly with uplift rate (U). In our previous analysis (Snyder *et al.*, 2000), we found that one value of K cannot match the observed relationships between slope and uplift rate for both the LUZ and HUZ (unless $n\approx4$),

implying that K must vary between the zones (Figure 12). However, simply the presence of the non-zero τ_c term in equation 9 makes the relationship between S and U nonlinear, and K need not vary to explain the data (Figure 12).

Unfortunately, an infinite set of combinations of τ_c, k_e, and k_q can explain the data (for any given value of a or n), so we are unable to place constraints on these key unknown parameters. The model presented here assumes the existence of a dominant erosive flood event of unknown magnitude (parameterized by k_q). For any value of k_q, a corresponding value of τ_c can be found. A minimum value of τ_c would be the Shields shear stress required to move the larger blocks of sediment (20-30 cm diameter, similar to typical joint spacing) observed on the bed (100-300 Pa). However, we cannot further constrain this value with the present model. The approach of Tucker and Bras (2000) presents a solution to this problem, because using a stochastic distribution of storms eliminates the need to assume a dominant discharge (k_q), thereby allowing back calculation of τ_c and k_e. At present, we can conclude only that a nonzero threshold shear stress for incision provides a plausible alternative to systematic variations in k_e.

6. Conclusions: channel response to tectonic forcing

The streams of the Mendocino triple junction region offer the opportunity to look at the effects of a major change in rock-uplift rate. We evaluate the responses of fluvial systems to this change, with specific reference to how these changes will affect the shear-stress-model parameters. We find that the most important difference between the HUZ and LUZ watersheds is the increased stream discharge in the HUZ due to orographic enhancement of precipitation by higher mountains. Comparison of discharge records from Honeydew Creek, just east of the HUZ to gauging-station data from throughout the region, indicates that Honeydew creek receives about twice as much flow as the rest of region, corresponding to likely twofold increase in the value of k_q, less than the value assumed by Snyder *et al.* (2000).

Land-use differences between the HUZ and LUZ limit our ability to assess potential changes in channel width and role of sediment flux. As a partial solution to this problem, we emphasize our valley-width data, for this is likely to be less affected by land use. Our analysis of channel-width

data is consistent with assuming that k'_w and b' are constant throughout the study area. We cannot directly say anything conclusive about the importance of sediment flux in controlling incision rate. This situation provides a nice illustration of the importance of the timescale of response to perturbations. Because of higher-uplift rates over the past ~100 kyr, we expect narrower channels in HUZ. However, most likely because of a sediment pulse in the past ~100 yr, we observe narrower high-flow channels in the LUZ. The same is true of channel morphology. We might expect the onset of high hillslope erosion rates, responding to stream incision, to begin to bury the HUZ channels in alluvium. However, we see this situation in the LUZ, again because of a recent, short-term perturbation in sediment flux.

Our analysis of channel bedrock outcrops indicates that rocks of the HUZ have slightly greater mass strength than those of the LUZ but are also somewhat more fractured. Therefore, we conclude that k_e and τ_c are likely to be approximately constant throughout the study area.

Previously, we placed constraints on the value of n for the case where τ_c=0 (equation 8; Snyder *et al.*, 2000). The data presented here does not significantly change this analysis: we have no evidence for changes in K other than the variation in discharge (k_{ql}/k_{ql}=½; Table 6), which suggests that a model with n=1.5-2.3 can explain the data. However, we hasten to point out that we now believe this analysis to be oversimplified because values of τ_c>0 significantly change the model prediction for steady-state channels, and can explain the S—U data without appealing to unexplained variations in other parameters, particularly k_e. Because we have little knowledge of what value of τ_c (or k_q) is appropriate for the study area, we are unable to place any additional constraints on the values of n or a. Further work on the importance of threshold shear stress in bedrock-channel incision is needed to more fully calibrate the model.

Acknowledgments

This research was funded by National Science Foundation grants EAR-9725723 to Whipple and EAR-9725348 to Merritts. We wish to express our deep gratitude to three years of excellent field crews: Simon Brocklehurst, Erin Carlson, Ben Crosby, Emily Himmelstoss, Jason Nicholas, Jeff Niemann, Jim Partan, Kim Sunderlin, Galen Whipple, and Jesse Yoburn. We also thank: the Mendocino Redwood Company and Dale Meese for land access and assistance; David Fuller and Henry Harrison at the Bureau of Land Management in Arcata for climate data, land-use histories,

and land access; Richard Stein at the Humboldt County Department of Public Works for access to historical aerial photos; and Steve Ellen of the U.S. Geological Survey in Menlo Park for sharing lithologic mapping and insights. This manuscript benefited from reviews by John Southard and Rafael Bras.

References Cited

Baker, V.R., and Kale, V.S., 1998, The role of extreme floods in shaping bedrock channels, *in* Tinkler, K.J., and Wohl, E.E., eds., Rivers Over Rock: Fluvial Processes in Bedrock Channels, Volume 107: Geophysical Monograph: Washington, American Geophysical Union, p. 153-165.

Barnes, H.H., 1967, Roughness characteristics of natural channels: U.S. Geological Survey Water-Supply Paper 1849, 213 p.

Barros, A., and Lettenmaier, D., 1993, Dynamic modeling of orographically induced precipitation: Reviews of Geophysics, v. 32, p. 265-284.

Buffington, J.M., and Montgomery, D.R., 1999, Effects of hydraulic roughness on surface textures of gravel-bed rivers: Water Resources Research, v. 35, p. 3507-3521.

Davis, J.C., 1986, Statistics and data analysis in geology, New York, John Wiley and Sons, Inc., 646 p.

Dietrich, W.E., Wilson, C.J., Montgomery, D.R., and McKean, J., 1993, Analysis of erosion thresholds, channel networks, and landscape morphology using a digital terrain model: Journal of Geology, v. 101, p. 259-278.

Dunne, T., and Leopold, L.B., 1978, Water in Environmental Planning, New York, W.H. Freeman and Company, 818 p.

Hack, J.T., 1973, Stream profile analysis and stream-gradient index: J. Res. U.S. Geological Survey, v. 1, p. 421-429.

Hamilton, L.C., 1992, Regression with graphics: a second course in applied statistics, Belmont, California, Wadsworth, Inc., 363 p.

Hancock, G.S., and Anderson, R.S., 2001, Numerical modeling of fluvial terrace formation in response to oscillating climate: GSA Bulletin, v. in review.

Harbor, D.J., 1998, Dynamic equilibrium between an active uplift and the Sevier River, Utah: Journal of Geology, v. 106, p. 181-194.

Howard, A.D., and Kerby, G., 1983, Channel changes in badlands: Geological Society of America Bulletin, v. 94, p. 739-752.

Howard, A.D., 1994, A detachment-limited model of drainage basin evolution: Water Resources Research, v. 30, p. 2261-2285.

Jennings, C.W., and Strand, R.G., 1960, Geologic map of California, Ukiah sheet, Department of Conservation, State of California.

Kirby, E., and Whipple, K.X., 2001, Quantifying differential rock-uplift rates via stream profile analysis: Geology, v. 29, p. 415-418.

Lavé, J., and Avouac, J.P., 2000, Active folding of fluvial terraces across the Siwaliks Hills, Himalayas of central Nepal: Journal of Geophysical Research, v. 105, p. 5735-5770.

Leopold, L.B., and Maddock, T., Jr., 1953, The hydraulic geometry of stream channels and some physiographic implications: U.S. Geological Survey Professional Paper 252.

Leopold, L.B., Wolman, M.G., and Miller, J.P., 1964, Fluvial processes in geomorphology, San Francisco, W.H. Freeman and Company, 522 p.

McLaughlin, R.J., Ellen, S.D., Blake, M.C., Jr., Jayko, A.S., Irwin, W.P., Aalton, K.R., Carver, G.A., and Clarke, S.H., Jr., 2000, Geology of Cape Mendocino, Eureka, Garberville, and southwestern part of the Hayfork 30 x 60 minute quadrangles and adjacent offshore area, northern California: U.S. Geological Survey Miscellaneous Field Studies, v. MF-2336.

Merritts, D., and Bull, W.B., 1989, Interpreting Quaternary uplift rates at the Mendocino triple junction, northern California, from uplifted marine terraces: Geology, v. 17, p. 1020-1024.

Merritts, D., and Vincent, K.R., 1989, Geomorphic response of coastal streams to low, intermediate, and high rates of uplift, Mendocino junction region, northern California: Geological Society of America Bulletin, v. 101, p. 1373-1388.

Merritts, D.J., Chadwick, O.A., Hendricks, D.M., Brimhall, G.H., and Lewis, C.J., 1992, The mass balance of soil evolution on late Quaternary marine terraces, northern California: GSA Bulletin, v. 104, p. 1456-1470.

Merritts, D.J., 1996, The Mendocino triple junction: Active faults, episodic coastal emergence, and rapid uplift: Journal of Geophysical Research, v. 101, p. 6051-6070.

Miller, D.J., and Dunne, T., 1996, Topographic perturbations of regional stresses and consequent bedrock fracturing: Journal of Geophysical Research, v. 101, p. 25523-25536.

Montgomery, D.R., and Buffington, J.M., 1997, Channel-reach morphology in mountain drainage basins: Geological Society of America Bulletin, v. 109, p. 596-611.

Montgomery, D.R., and Gran, K.B., 2001, Downstream variations in the width of bedrock channels: Water Resources Research, v. in press.

Paola, C., Heller, P.L., and Angevine, C.L., 1992, The large-scale dynamics of grain-size variation in alluvial basins, 1: Theory: Basin Research, v. 4, p. 73-90.

Parker, G., and Izumi, N., 2000, Purely erosional cyclic and solitary steps created by flow over a cohesive bed: Journal of Fluid Mechanics, v. 419, p. 203-238.

Pazzaglia, F.J., Wegmann, K., and Garcia, A.F., 1998, Bedrock fluvial incision in the tectonically active setting evaluated in the context of the stream power law and the valley-width/channel width ratio: Abstracts with programs, 1998 GSA annual meeting, v. 30, p. P329.

Prentice, C.S., Merritts, D.J., Beutner, E.C., Bodin, P., Schill, A., and Muller, J.R., 1999, Northern San Andreas fault near Shelter Cove, California: Geological Society of America Bulletin, v. 111, p. 512-523.

Rantz, S.E., 1968, Average annual precipitation and runoff in north coastal California, U.S. Geological Survey.

Richards, K., 1982, Rivers, form and process in alluvial channels, New York, Methuen and Co., 361 p.

Rock, N.M.S., 1988, Numerical Geology: Lecture Notes in Earth Sciences 18, New York, Springer-Verlag, 427 p.

Roe, G.H., Montgomery, D.R., and Hallet, B., 2001, Effects of orographic precipitation variations on steady-state river profiles and relief: in preparation.

Schumm, S.A., Dumont, J.F., and Holbrook, J.M., 2000, Active tectonics and alluvial rivers, Cambridge, Cambridge University Press, 276 p.

Selby, M.J., 1993, Hillslope Materials and Processes, Oxford, Oxford University Press, 451 p.

Sklar, L., and Dietrich, W.E., 1998, River longitudinal profiles and bedrock incision models: stream power and the influence of sediment supply, *in* Tinkler, K.J., and Wohl, E.E., eds., Rivers Over Rock: Fluvial Processes in Bedrock Channels: Geophysical Monograph 107: Washington, DC, American Geophysical Union, p. 237-260.

—, 1999, Relating rates of fluvial bedrock erosion to rock strength: an experimental study (abstract): EOS, Transactions, AGU, v. 80, p. F448.

Snyder, N.P., Whipple, K.X., Tucker, G.E., and Merritts, D.J., 1999, Evidence for an equilibrium between main-trunk-channel incision and tectonic uplift: Mendocino triple junction region, northern California: Annual Meeting Expanded Abstracts, Geological Society of America, v. 31, p. 444-445.

—, 2000, Landscape response to tectonic forcing: DEM analysis of stream profiles in the Mendocino triple junction region, northern California: Geological Society of America Bulletin, v. 112, p. 1250-1263.

Stock, J.D., and Dietrich, W.E., 1998, Channel incision by debris flows: a missing erosion law?: Eos, Transactions, American Geophysical Union, v. 79, p. F366.

Stock, J.D., and Montgomery, D.R., 1999, Geologic constraints on bedrock river incision using the stream power law: Journal of Geophysical Research, v. 104, p. 4983-4993.

Strand, R.G., 1962, Geologic map of California, Redding sheet, Department of Conservation, State of California.

Talling, P.J., 2000, Self-organization of river networks to threshold states: Water Resources Research, v. 36, p. 1119-1128.

Tinkler, K.J., and Wohl, E.E., 1998, A primer on bedrock channels, *in* Tinkler, K.J., and Wohl, E.E., eds., Rivers over rock: fluvial processes in bedrock channels, Volume Geophysical Monograph 107: Washington, DC, American Geophysical Union.

Tucker, G.E., and Slingerland, R., 1997, Drainage basin responses to climate change: Water Resources Research, v. 33, p. 2031-2047.

Tucker, G.E., and Bras, R.L., 2000, A stochastic approach to modeling the role of rainfall variability in drainage basin evolution: Water Resources Research, v. 36, p. 1953-1964.

Wannanen, A.O., Harris, D.D., and Williams, R.C., 1971, Floods of December 1964 and January 1965 in the far western states: U.S. Geological Survey Water-supply Paper 1866-A, Washington, U.S. Government Printing Office, 265 p.

Whipple, K.X., and Tucker, G.E., 1999, Dynamics of the stream-power river incision model: Implications for the height limits of mountain ranges, landscape response timescales, and research needs: Journal of Geophysical Research, v. 104, p. 17661-17674.

Whipple, K.X., Anderson, R.A., and Hancock, G.S., 2000a, River incision into bedrock: Mechanics and relative efficacy of plucking, abrasion, and cavitation: Geological Society of America Bulletin, v. 112, p. 490-503.

Whipple, K.X., Snyder, N.P., and Dollenmayer, K., 2000b, Rates and processes of bedrock incision by the Upper Ukak River since the 1912 Novarupta ash flow in the Valley of Ten Thousand Smokes, Alaska: Geology, v. 28, p. 835-838.

Wohl, E.E., 1998, Bedrock channel morphology in relation to erosional processes, *in* Tinkler, K.J., and Wohl, E.E., eds., Rivers over rock: fluvial processes in bedrock channels, Volume Geophysical Monograph 107: Washington, DC, American Geophysical Union.

Table 1. Discharge (Q) data for selected events (see Figure 1 for gauging-station locations).

station	drainage area, A ($\times 10^6$ m^2)	length of record (yr)	12/20-22/64 event Q (m^3/s)	rank	1/15/1974 event Q (m^3/s)	rank	3/17/1975 event Q (m^3/s)	rank	1973-76 mean ann. Q (m^3/s)
Honeydew	*51.1*	*4*	*nd*	*nd*	*130.26*	*2*	*139.32*	*1*	*4.23*
Oil	0.45	12	0.71	1	nd	nd	nd	nd	nd
Squaw	0.89	10	2.46	2	nd	nd	nd	nd	nd
Painter	2.20	12	10.08	1	nd	nd	nd	nd	nd
Dunn	6.45	12	8.10	1	nd	nd	nd	nd	nd
Elder	22.3	32	103.64	1	56.07	4	25.66	9	0.83
Pudding	42.9	9	56.63	1	nd	nd	nd	nd	nd
Bull	96.4	38	184.63	2	165.10	5	93.16	19	3.76
Tenmile-MF	113	10	160.56	1	122.90	2	nd	nd	nd
Eel-SF-Bran	151	29	557.84	2	nd	nd	229.08	11	nd
Noyo	364	47	679.60	2	747.56	2	208.13	22	7.19
Mattole	841	50	2222.87	2	1758.50	3	1732.99	5	40.32
Eel-SF-Leggett	851	34	2228.54	1	1713.20	3	1019.41	8	28.52
Eel-SF-Miranda	1840	59	5635.05	1	3454.70	5	2650.46	9	62.71
Eel-Scotia	*10680*	*87*	*21294.30*	*1*	*10958.60*	*3*	*6541.20*	*26*	*254.92*

Notes: Rank indicates position of event in the series of mean-annual floods over the record of available data for each station. nd, no data available. Tenmile-MF, Middle Fork Tenmile River. Eel-SF, South Fork Eel River. Data for the Eel River at Scotia is included in this table only for comparison purposes because of its long length of record, it is not included in the regression analysis (Figure 3; Table 2).

Table 2. Discharge-area coefficient (k_q) calculations

event	#	c (power law) ±95%	k_q (linear, c=1) (m/s) ±95%	k_q (H) (m/s)	k_q(H)/k_q	k_q(H)/$k_{q\,max}$	k_q(H)/$k_{q\,min}$
12/20-22/64	12	1.01±0.11	2.90±0.35 ($\times10^{-6}$)	nd	nd	nd	nd
1/16/74	7	1.01±0.20	1.93±0.19 ($\times10^{-6}$)	2.55×10^{-6}	1.32	1.46	1.20
2/17/75	7	1.07±0.29	1.47±0.58 ($\times10^{-6}$)	2.73×10^{-6}	1.85	3.05	1.33
1973-76 mean	6	0.99±0.25	3.56±1.27 ($\times10^{-8}$)	8.28×10^{-8}	2.33	3.62	1.71

Notes: k_q (H), best-fit value of k_q for Honeydew Creek. nd, no data available.

Table 3. Channel-width data

creek	uplift rate, *U* (mm/yr)	num	*b'*	k'_w	width @ 1 km^2 (m) (95% range)*	R^2	regression survey range (km^2)**
HIGH-FLOW WIDTH							
1. Oat	4	102	0.34±0.07	0.045±0.077	4.5 (4.2-4.9)	0.51	0.1-4.1
2. Kinsey	4	67	0.56±0.12	0.0026±0.0074	5.8 (5.1-6.5)	0.62	0.1-0.4; 0.9-3.9 0.3-0.4 (upper left trib)
3. Shipman	4	49	0.46±0.32	0.0094±0.7215	5.6 (3.1-10)	0.15	3.3-8.7
4. Gitchell	3.7	193	0.21±0.04	0.354±0.521	6.1 (5.8-6.5)	0.34	0.1-1.6 2.4-8.6
HUZ	**3.7-4**	**411**	**0.35±0.04**	**0.045±0.065**	**5.4 (5.1-5.7)**	**0.49**	**0.1-8.7**
5. Horse Mtn.	2??	181	0.36±0.05	0.031±0.480	4.5 (4.2-4.8)	0.50	0.1-6.8 1.8-3.5 (lower left trib)
6. Hardy	0.5	311	0.22±0.03	0.208±0.296	4.0 (3.9-4.2)	0.36	0.1-10.5 0.1-0.2 (North Fork) 1.2-3.3 (North Fork)
7. Juan	0.5	179	0.33±0.03	0.040±0.057	3.9 (3.6-4.2)	0.69	0.1-13.6; 14.4-19.1 0.1-1.1 (upper left trib)
LUZ	**0.5**	**490**	**0.28±0.02**	**0.090±0.127**	**4.0 (3.8-4.2)**	**0.53**	**0.1-19.1**
VALLEY WIDTH							
1. Oat	4	93	0.41±0.10	0.028±0.067	7.7 (6.9-8.7)	0.42	0.1-4.1
2. Kinsey	4	58	0.50±0.14	0.0072±0.0268	6.9 (6.0-7.9)	0.51	0.1-0.4; 0.9-3.9 0.3-0.4 (upper left trib)
3. Shipman	4	49	0.50±0.47	0.0066±4.8360	6.8 (2.9-16)	0.09	3.3-8.7
4. Gitchell	3.7	100	0.32±0.09	0.118±0.246	9.7 (8.5-11)	0.37	0.1-1.6 2.4-8.6
HUZ	**3.7-4**	**300**	**0.42±0.05**	**0.023±0.035**	**7.9 (7.4-8.5)**	**0.49**	**0.1-8.7**
5. Horse Mtn.	2??	96	0.42±0.08	0.026±0.050	8.8 (8.0-9.7)	0.56	0.1-6.8 1.8-3.5 (lower left trib)
6. Hardy	0.5	302	0.29±0.04	0.181±0.266	9.6 (9.0-10)	0.38	0.1-10.5 0.1-0.2 (North Fork) 1.2-3.3 (North Fork)
7. Juan	0.5	170	0.46±0.06	0.012±0.020	7.2 (6.4-8.0)	0.60	0.1-13.6 0.1-1.1 (upper left trib)
LUZ	**0.5**	**472**	**0.35±0.03**	**0.072±0.103**	**8.9 (8.4-9.4)**	**0.47**	**0.1-13.6**

* Parenthetical range is the 95% confidence interval on the calculation of the mean width at 1 km^2 from the regression line (Figure 4; Hamilton, 1992).

** Notes on regression ranges (all numbers are drainage areas). All data with A<0.1 km^2 omitted from regressions. Data is from main trunk channel unless otherwise noted. Specific stream notes:

1. Oat Creek, entire stream surveyed.
2. Kinsey Creek, main trunk from 0.9 km^2 to mouth (3.9 km^2) and upper left tributary from 0.3 km^2 to junction with main channel (0.4 km^2) surveyed in 1998; main trunk from 0.1 to 0.4 km^2 surveyed in 1999 (stopped by waterfall).
3. Shipman Creek, main trunk from 3.3 km^2 to mouth (8.7 km^2) surveyed, stopped by waterfall.
4. Gitchell Creek, section between 1.6 and 2.4 km^2 could not be accessed due to waterfalls.
5. Horse Mountain Creek, entire stream surveyed; regressions also include some data from a large left tributary.
6. Hardy Creek, did not survey main trunk from 10.5 km^2 to mouth (13.0 km^2); regressions include some data from the upper (from the divide down) and lower sections (up from junction with main trunk) of the North Fork of Hardy Creek.
7. Juan Creek, did not survey main trunk from 13.6 km^2 to mouth (19.4 km^2), accept a few high-flow width measurements around the junction of Little Juan Creek from 14.4 to 19.1 km^2; regression also includes data from a left tributary near the divide.

Table 4. Schmidt hammer results from study-area stations.

	all stations			bedrock steps ≥0.5 m		no bedrock steps	
creek	**number**	**mean±1σ**	**mode**	**number**	**mean±1σ**	**number**	**mean±1σ**
Oat	30	49.7±10.3	52.5	10	55.3±6.8	20	46.9±10.7
Kinsey	23	48.5±8.9	42.5, 57.5	4	59.1±3.9	19	46.3±8.0
Gitchell	33	44.9±10.5	47.5	5	50.7±12.3	28	43.8±10.1
high-uplift zone	**86**	**47.5±10.1**	**57.5**	**19**	**54.9±8.3**	**67**	**45.4±9.7**
Horse	31	41.8±11.4	52.5	8	51.9±3.2	23	38.2±11.1
Hardy	26	43.1±6.4	42.5	12	46.0±7.0	14	40.6±4.9
Juan	44	45.3±7.5	47.5	8	48.3±5.7	36	44.7±7.8
low-uplift zone	**70**	**44.5±7.2**	**42.5**	**20**	**47.0±6.4**	**50**	**43.5±7.3**

Table 5. Channel bedrock and joint spacing results.

creek	channel bedrock (%) horizontal	vertical	joint spacing (cm)	notes
Oat	29	33	3-26	
Kinsey	78	76	1-31	top survey
	12	17	no data	bottom survey
	20	33		overall
Gitchell	3.6	5.3		top survey
	4.5	4.2	2-21	bottom survey
	4.3	4.8		overall
Horse	5.5	6.6	2-18	
Hardy	5.0	9.5	4-43	
Juan	2.8	2.1	5-48	

Table 6. Parameter values and units

BASIC VARIABLES	
x [m]	streamwise horizontal distance from divide
x_c [m]	distance at $A=10^5$ m^2
z [m]	vertical elevation above sea level
A [m^2]	drainage area
S	channel gradient
S_e	steady-state channel gradient
Q [m^{3}s^{-1}]	stream discharge
w [m]	channel width
E [myr^{-1}]	channel incision rate
U [myr^{-1}]	rock-uplift rate
τ_b [Pa]	bed shear stress
k_w [m$^{(1-3b)}$s^b]	channel width-discharge coefficient
b	channel width-discharge exponent
m	drainage-area exponent (equation 7)
n	slope exponent (equation 7)
m/n	theoretical steady-state channel concavity
θ	actual (empirical) channel concavity
PHYSICAL PARAMETERS	
$\alpha = 3/5$	exponent on (Q/w) quotient
$\beta = 7/10$	exponent on S
$\rho = 1000$ kgm^{-3}	density of water
$g = 9.8$ ms^{-2}	gravitational acceleration
$N = 0.07$ m$^{-1/3}$s	Manning roughness coefficient (estimated; Barnes, 1967)
EMPRICALLY CALIBRATED PARAMETERS	
$c = 1$	discharge-width exponent
$b' = 0.4$	width-area exponent
$k'_w = 0.0215$ m$^{(1-2b')}$	width-area coefficient
REFERENCE SLOPE-AREA DATA (for Figure 12; from Snyder et al, 2000)	
$A_{ref} = 10^6$ m^2	reference drainage area
$U_1 = 0.0005$ myr^{-1}	low-uplift zone rock-uplift rate
$U_2 = 0.004$ myr^{-1}	high-uplift zone rock-uplift rate
$S_1 = 0.14$	low-uplift steady-state slope at A_{ref}
$S_2 = 0.26$	high-uplift steady-state slope at A_{ref}
UNKNOWN PARAMETERS (cannot calculate unique values)	
τ_c [Pa]	threshold/critical shear stress
k_q [ms^{-1}]	discharge-area coefficient (depends on a reference flood recurrence interval)
k_e [myr^{-1}Pa^{-a}]	shear stress-incision rate coefficient
a	shear stress-incision rate exponent
DERIVED PARAMETERS	
k_t [m$^{18/25}$Pa]	shear-stress coefficient (equation 5)
K [m$^{-1/35}$yr^{-1}]	coefficient of erosion (equations 7-8)
$m/n = 0.51$	predicted channel concavity (equations 7-8)

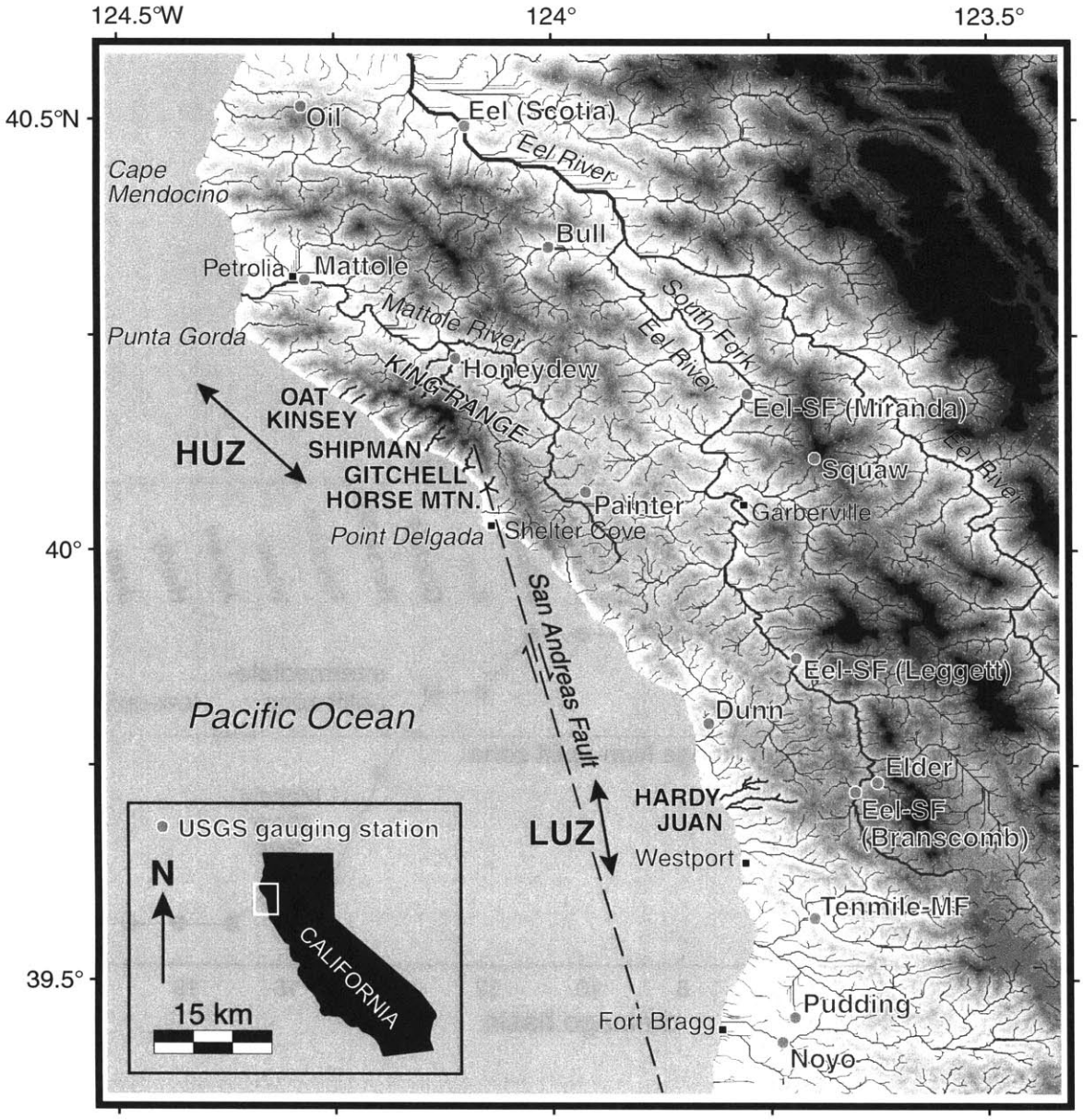

Figure 1. Map of the Mendocino triple junction area, including the drainage network and elevation shading. Drainage network includes all streams with drainage area (A) greater than 1 km^2. Rivers and creeks mentioned in the text are shown with bold lines. The 7 field-studied creeks are marked with capital letters at their mouths, and are separated into high-uplift zone (HUZ) and low-uplift zone (LUZ) channels. Elevation shading ranges from white for 0-100 m to black for all areas over 1000 m. USGS gauging stations used in this study are indicated by dots.

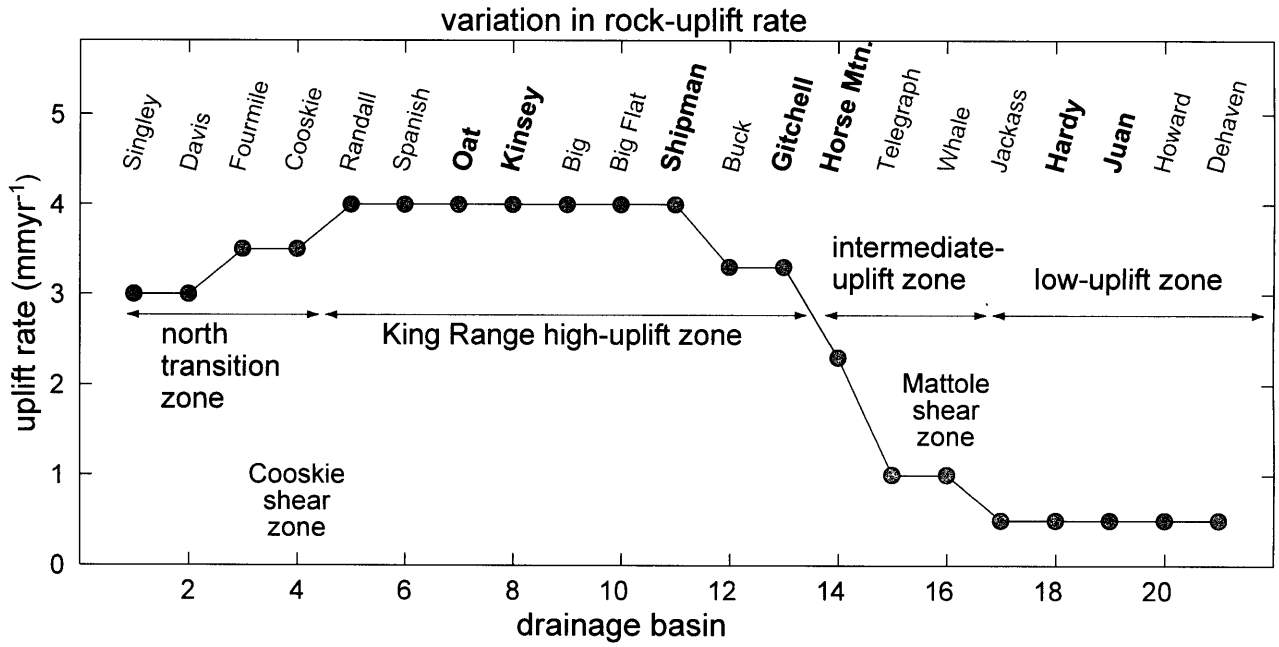

Figure 2. Latest-Pleistocene to Holocene rock-uplift rates for the 21 basins included in this and our previous study (Snyder et al., 2000), from north to south. The 7 field-studied basins are in bold. Data are from Merritts and Bull (1989).

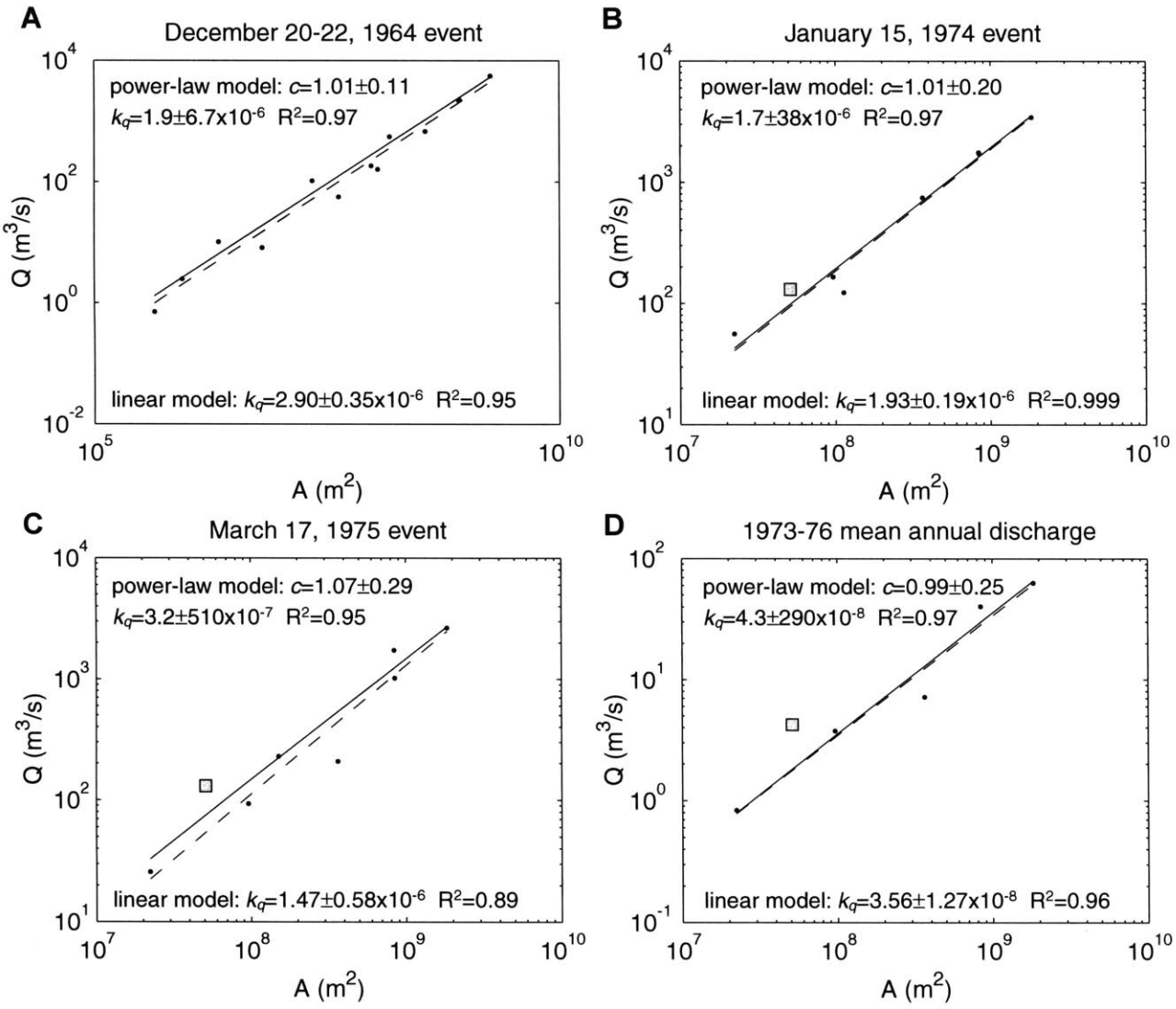

Figure 3. Graphs of discharge vs. drainage area in logrhythmic space. Solid circles are data points from USGS gauging stations. Grey box is the gauging-station data for Honeydew Creek, which is not included in the regressions. Data is in Table 1. Dashed lines are least-squares best-fit regression lines for a power-law model; solid lines are for a linear model. Regression data is in Table 2.

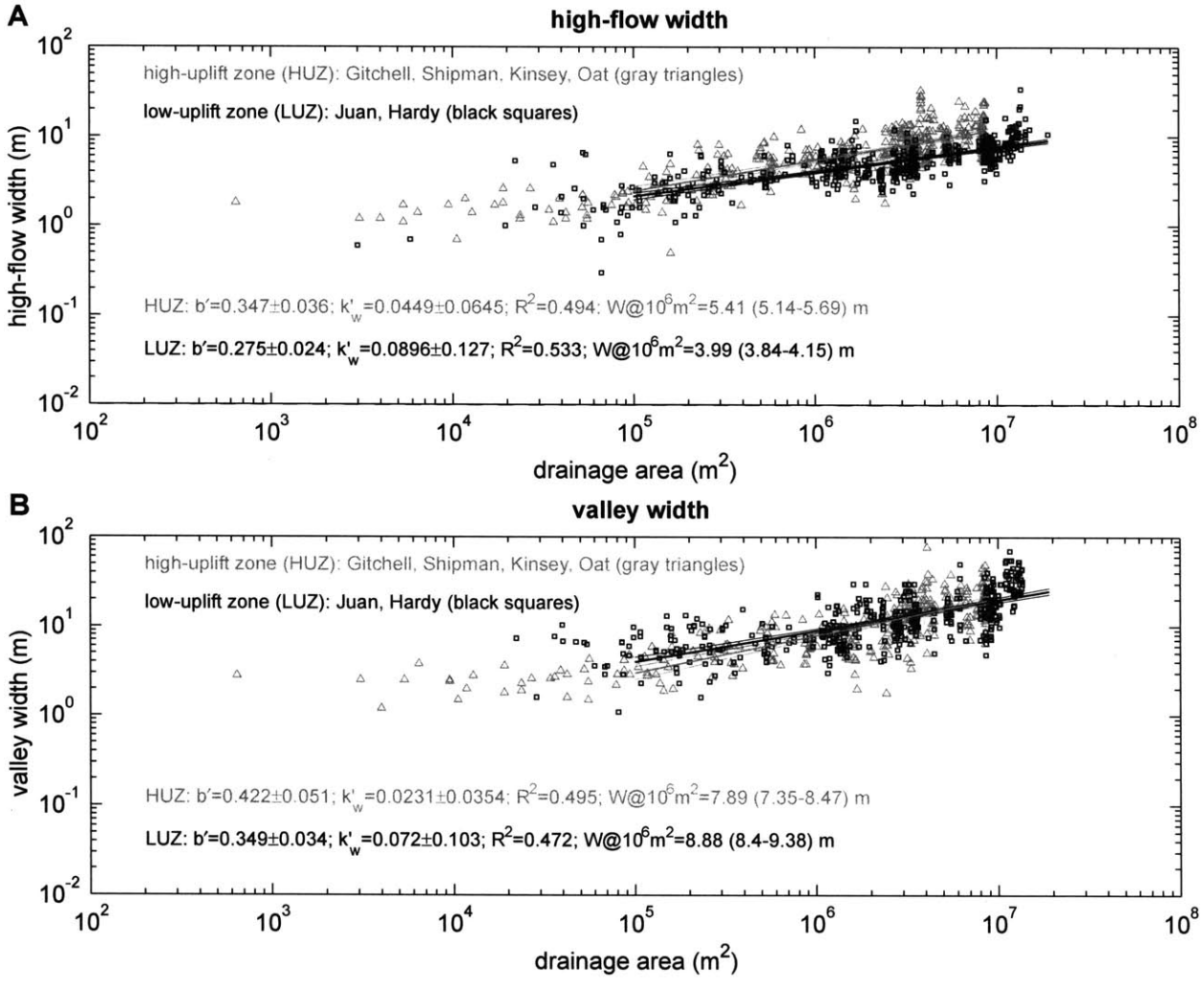

Figure 4. Graphs of width vs. drainage area for (A) high-flow width and (B) valley width. High-uplift zone data are gray triangles, low-uplift zone data are black squares. Lines are least-squares best-fit power-law regressions (heavy lines), with associated 95% confidence hyperbolae (fine lines), for the two datasets, with $A>10^5$ m^2 (Hamilton, 1992). See Table 3 for data for individual streams.

Figure 5. Low-uplift zone land-use pictures. (A) Ruins of train trestles in the channel of Hardy Creek. (B) A partially buried cut tree stump in a 1.5 m-high river-right fill terrace in Juan Creek.

Figure 6. Massive, abraded sandstone boulders armoring the bed of Gitchell Creek.

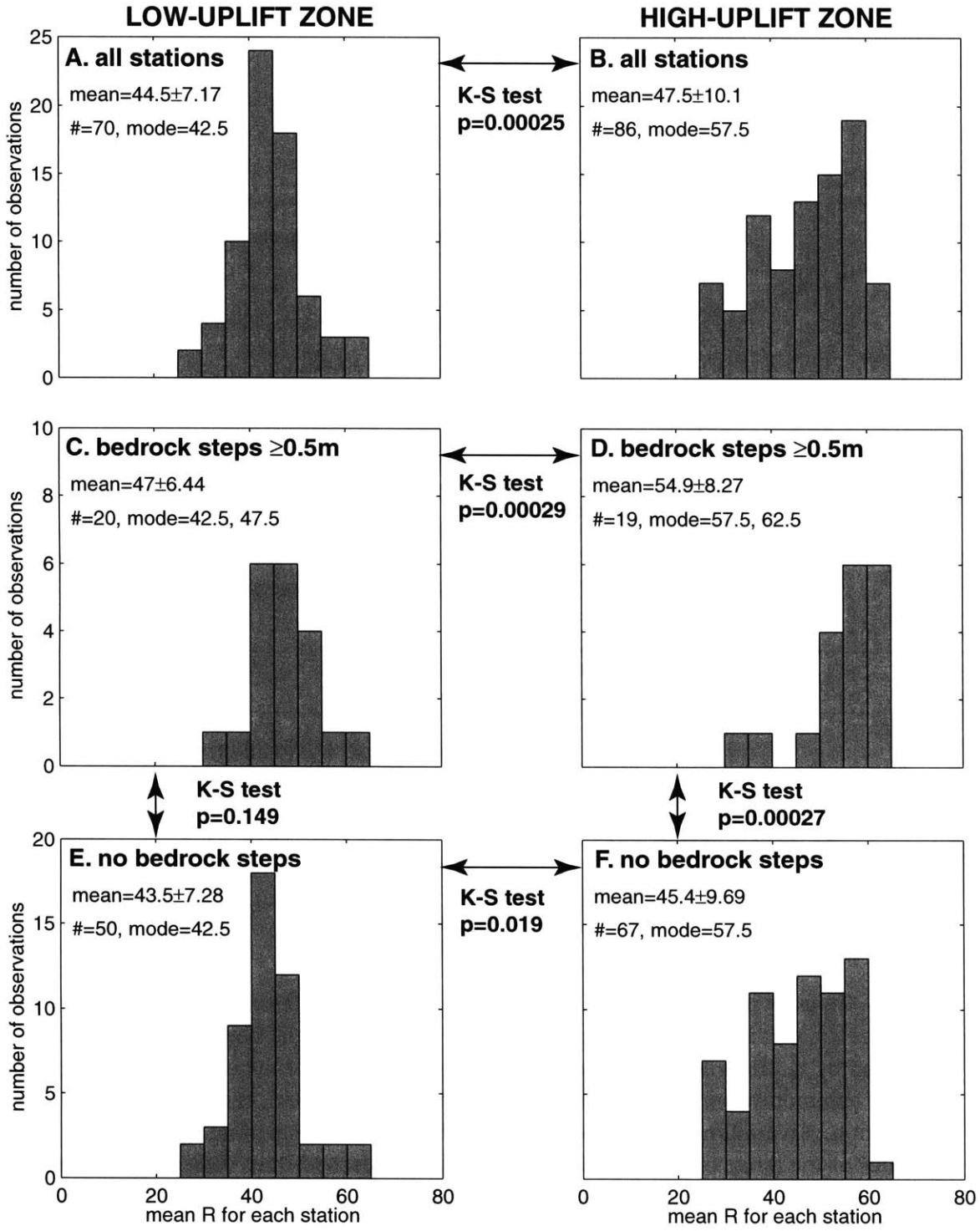

Figure 7. Histograms of Schmidt Hammer data for mean values of each station in the low-uplift zone (left column) and high-uplift zone (right column). Also shown are: sample mean values, with associated 1s error bounds; number of measurements in each sample; and sample modes. Arrows indicate the probability that adjacent pairs of samples are from the same distribution, based on a Kolmogorov-Smirnov (K-S) test. (A-B) All data. (C-D) Data for stations at bedrock steps in the channel greater than 0.5 m high. (E-F) Data for stations not at bedrock steps. See Table 4 for data from individual streams.

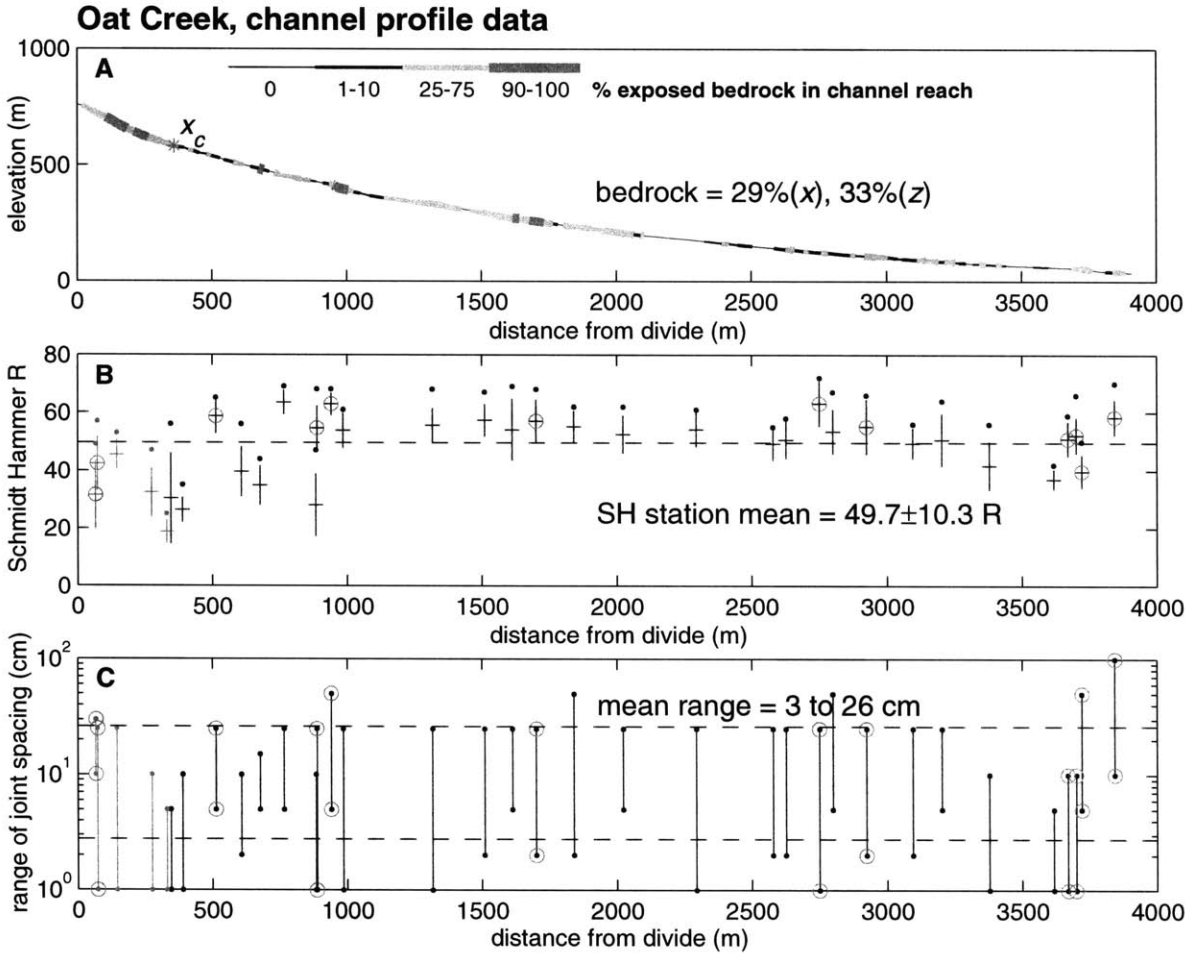

Figure 8. Channel profile data for Oat Creek, in the high-uplift zone. (A) Percent of each channel reach that is exposed bedrock outcrop. The place in the channel where A=10^5 m^2 is denoted by x_c. Bedrock percentage includes only the part of the channel below x_c. (B) Schmidt hammer mean values (crosses), 1σ error bounds (lines), and maxima (dots) for each station. Overall mean value is marked by horizontal dashed line. (C) Visual estimates of the range of joint spacing at each station, dashed lines indicate mean range. Y-axis has a logarithmic scale. (B-C) Circles indicate stations at bedrock steps greater than 0.5 m. Grey data are those in the channel above x_c.

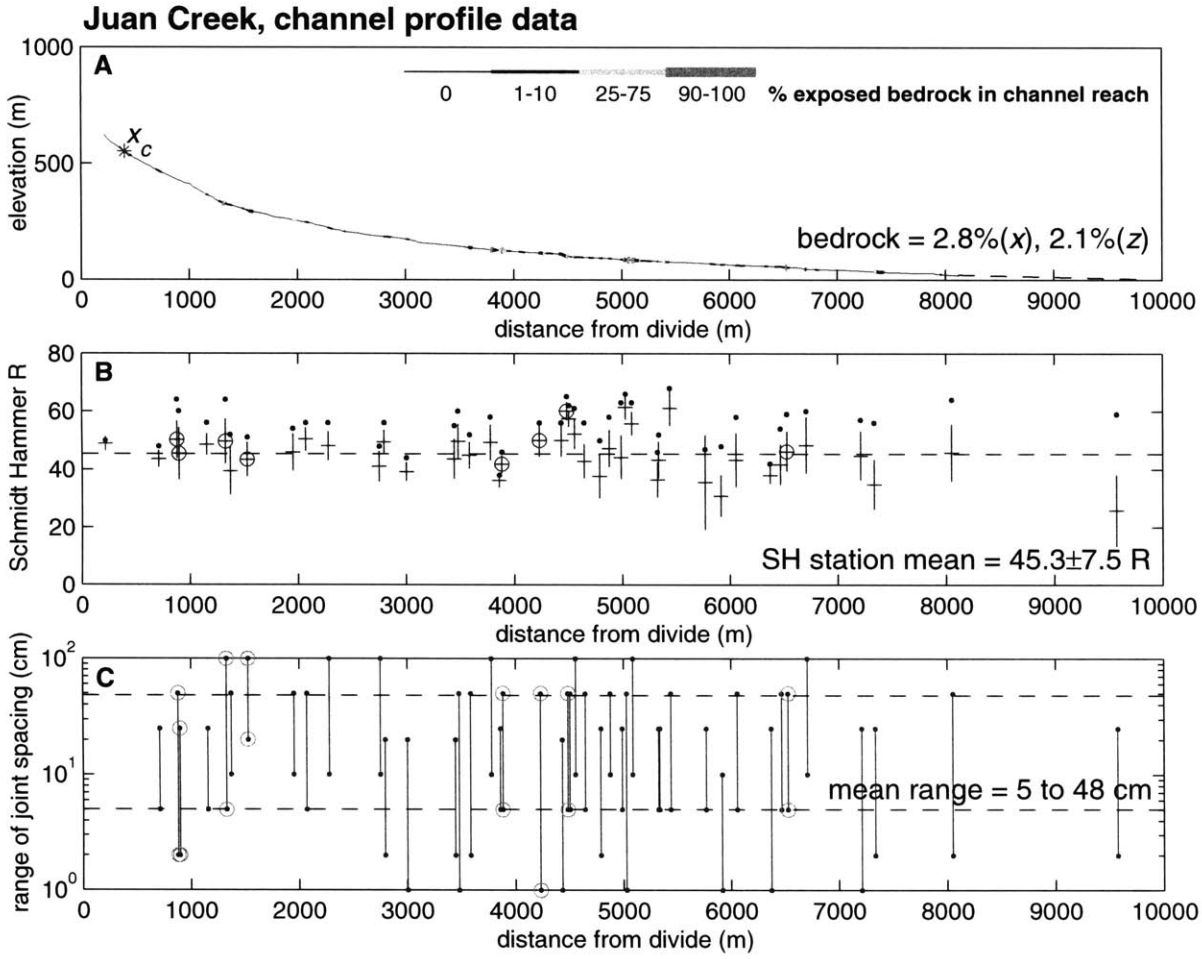

Figure 9. Channel profile data for Juan Creek, in the low-uplift zone. See Figure 8 for description. (A) Area not included in the field survey marked by dashed line.

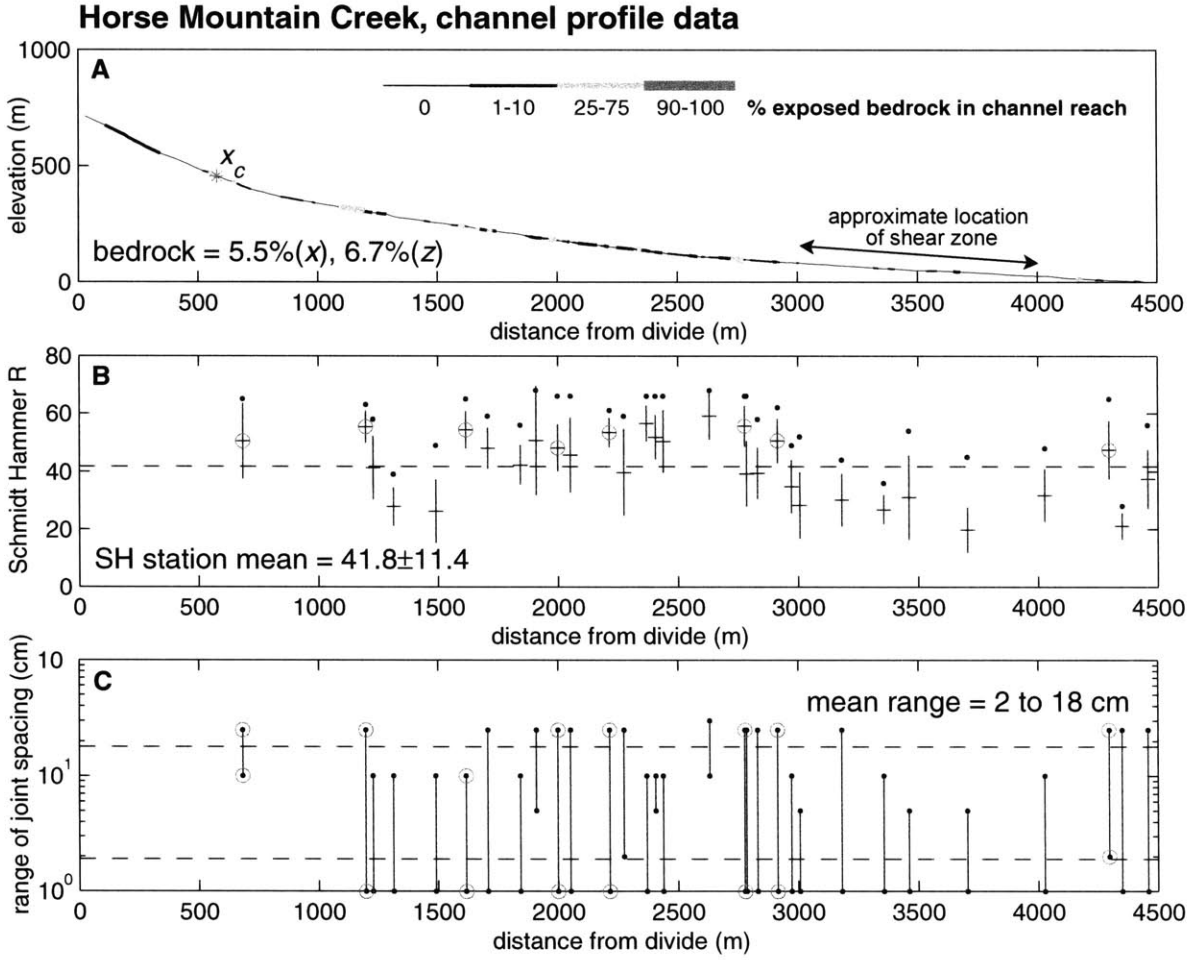

Figure 10. Channel profile data for Horse Mountain Creek, in the intermediate-uplift zone. See Figure 8 for description. (A) Arrow indicates the section of the channel oriented along a major shear zone.

Figure 11. Downstream process transitions in Kinsey Creek (high-uplift zone). (A) Narrow (~2 m wide), ephemeral colluvial gully, approximately 300 m from the divide. (B) Bedrock channel plunge pool at the base of a 2 m-high waterfall, approximately 1400 m from the divide.

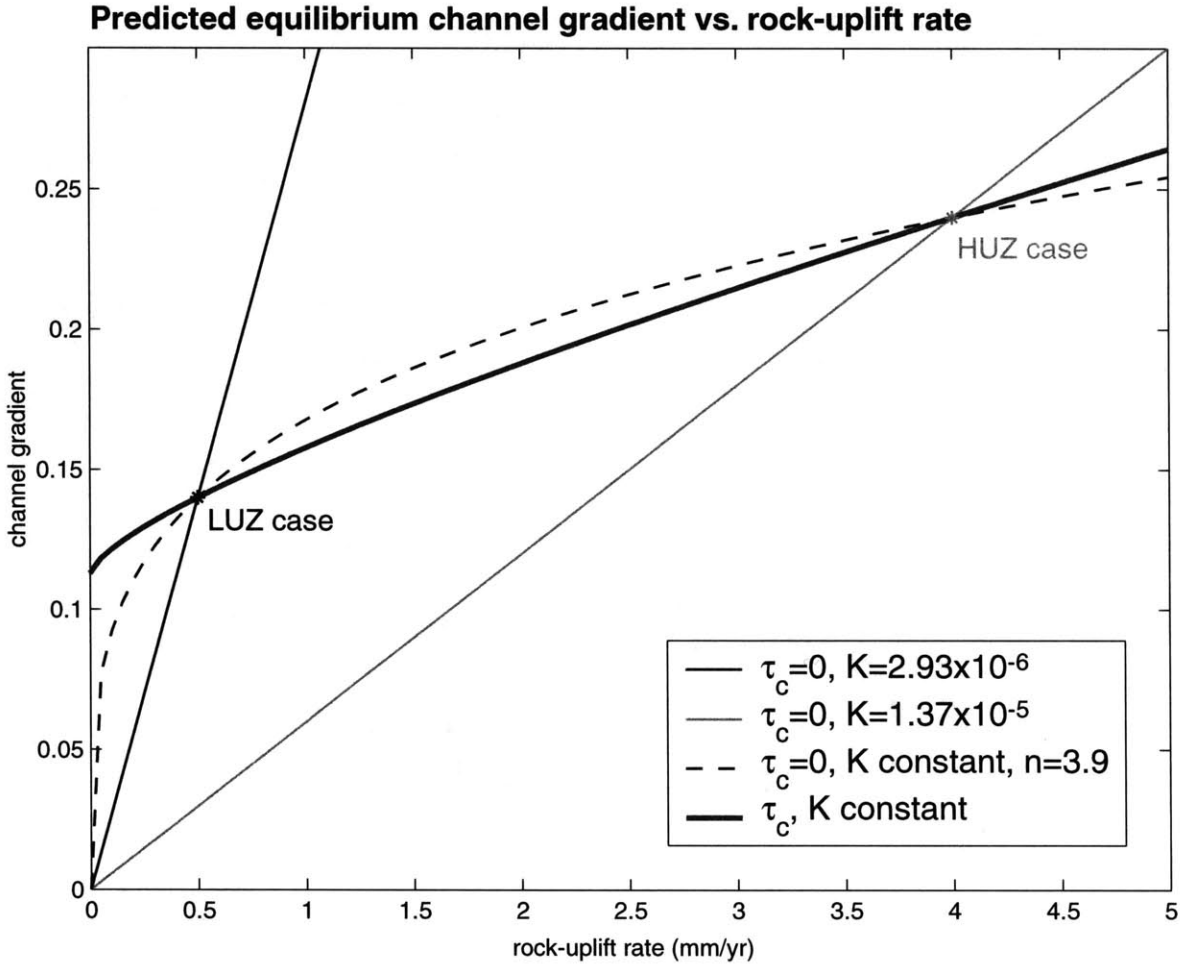

Figure 12. Predicted equilibrium slope at $A=A_{ref}=10^6$ m^2 vs. rock-uplift rate for several models. Stars denote mean values for the HUZ and LUZ based on longitudinal profile data from Snyder et al. (2000). Fine, solid black line is the equation 10 case with n=1 for a LUZ channel; fine, gray line is for a HUZ case. Dashed, black line is the solution to equation 10 to match both data points with a constant value of K. Thick, black line is a solution to equation 9 to match both data points with a constant value of K and τ_c. See Table 6 for parameter values used in these plots.

4. Stochastic floods and erosion thresholds in bedrock rivers: Implications for landscape relief

Noah P. Snyder*, Kelin X Whipple*, Gregory E. Tucker†, and Dorothy J. Merritts‡

* *Department of Earth, Atmospheric and Planetary Sciences, Massachusetts Institute of Technology, Cambridge, MA 02139-4307, USA*

† *School of Geography and the Environment, University of Oxford, Oxford OX1 3TB, UK*

‡ *Geosciences Department, Franklin and Marshall College, Lancaster, PA 17604-3003, USA*

Abstract

Fluvial erosion of bedrock occurs during stochastic flood events when boundary shear stress exceeds a critical threshold to initiate incision. Therefore, efforts to model the evolution of topography over long time scales should include a threshold term and should be driven by a stochastic distribution of erosive events. Climate is poorly represented in most landscape evolution models, so the quantitative relationship between erosion rate and measurable climatic variables has been elusive. Here we make a direct calculation of critical shear stress during a flood event in New York. Second, we apply a stochastic, threshold, bedrock-incision model to a well-studied series of streams in California, with known tectonic and climatic forcing. The results show that even low erosion thresholds, which are exceeded in steep channels during high-frequency flood events, fundamentally limit relief in tectonically active mountain ranges. Field applications of geomorphic models, including physically meaningful thresholds and stochastic climate distributions, are necessary to further our knowledge of interactions among surficial, climatic and crustal processes.

Introduction

Numerous recent field, laboratory, and modeling efforts have been devoted to understanding rates and processes of bedrock-river incision[1-7], with the goal of understanding the evolution of topography in response to tectonic and climatic forcings. Models based on shear stress[1,2,5,6] typically have made the simplifying assumption (either explicitly or implicitly) that bedrock

erosion occurs during major flood events[8] when boundary shear stress is far greater than the threshold value necessary to initiate incision, and therefore the threshold term can be neglected. However, a recent analysis using stochastic, threshold erosion theory[9,10] reveals that this assumption leads to physically unrealistic behavior, with the least variable climate producing the highest erosion rates. This runs counter to the assumption used to justify ignoring the threshold term, and counter to the hypothesis that erosion is more efficient in stormier climates[11,12]. Motivated by this observation, here we (1) make a direct estimate of the critical shear stress required to initiate incision by joint-block plucking on the bed of a river in New York, and (2) apply the Tucker and Bras model[9,10] to a well-constrained field setting in northern California[6,13-15]. The latter yields an indirect field estimate of critical shear stress (in a different geomorphic and tectonic setting). The northern California results also highlight the importance of including nonzero values for critical shear stress in efforts to model bedrock channels and for parameterizing climate using a stochastic rainfall model, by investigating the predicted relationship between steady-state channel slope (and therefore topographic relief) and rock-uplift rate. Through application of surface-process models to well-constrained field settings, we can bridge the gap between our understanding of erosion driven by stochastic events[16] and our efforts to model crustal and atmospheric interactions over geologic time scales[17].

Threshold shear stress for plucking

Many workers[1,7] have postulated that bedrock-river incision rate (E) is a power-law function of boundary shear stress (τ_b) above a threshold (or critical) shear stress (τ_c):

$$E = k_e(\tau_b - \tau_c)^a \text{ or} \tag{1a}$$

$$E = k_e(\tau_b{}^a - \tau_c{}^a), \tag{1b}$$

where k_e is a coefficient of erosion dependent on lithologic resistance and erosion process, and a is an exponent dependent on erosion process. Equation 1a is the commonly used "excess shear stress" form. Equation 1b is similar, equally defensible, and more tractable in some applications[10]. In the case where incision rates are set by plucking of intact blocks along joint or

fracture planes, Whipple *et al.*[7] argued that the value of a in equation 1 should be unity, or slightly higher. In their treatment, other hypothesized incision processes (abrasion, cavitation) likely have higher values of a. Here, we consider values of a from 1 to 1.4, consistent with field observations that plucking (in the sense defined by Whipple *et al.*[7]) is the dominant process in the rivers studied. This situation applies to areas with rocks that are sufficiently fractured to allow fluvial transport of exposed blocks, particularly appropriate when bedrock either (1) is highly fractured (joint spacing 0.1 to 1 m), or (2) breaks into blocks with a small height-to-length ratio[7]. One limitation of this approach is that it does not take into account the role that sediment flux and sediment supply (with associated stochastic distributions and transport threshold) might play in driving incision of bedrock[3].

Boundary shear stress (τ_b) can be estimated from field data. Assuming steady, uniform flow, τ_b is approximated by the product of depth (h) and slope (S):

$$\tau_b = \rho g h S , \qquad (2)$$

where ρ is the density of water and g is gravitational acceleration. Combining equation (2) with the Manning friction relationship gives:

$$\tau_b = \rho g N^{3/5} \left(\frac{Q}{w} \right)^{3/5} S^{7/10} , \qquad (3)$$

where Q is discharge, w is channel width, and N is the Manning roughness coefficient. The value of τ_b given by equations 2 and 3 is the total boundary shear stress, including both skin friction and momentum losses due to form drag on bed or bank roughness elements. For the motion of large blocks, this inclusion of form drag components is appropriate as the blocks themselves determine boundary roughness. The parameters in equations 2 and 3 needed to estimate τ_b can be measured from field and hydrologic data.

In contrast to τ_b, threshold shear stress (τ_c) is difficult to evaluate from field or experimental data. We are aware of no previous studies that actually calculate τ_c for bedrock incision, although measurements of τ_b clearly in excess of τ_c have been made for large paleofloods[8]. Numerous

workers[18] have studied the threshold for particle motion in alluvial-bed rivers, but these calculations are only peripherally relevant to this study of bedrock channels. The case of sediment mobilization on a noncohesive bed of similar-sized particles is quite different from the plucking of large joint blocks. Here we present two calculations of τ_c for incision of bedrock. First, we apply field data from a 1981 flood event in New York to equations 2 and 3 to get an estimate of total boundary shear stress during an observed plucking event. Second, we use data from a well-constrained field site in northern California to back-calculate the critical shear stress that best models an observed relationship between channel gradient (and therefore topographic relief) and rock-uplift rate[6,15].

Calculations of flood shear stress at Fall Creek, Ithaca, New York, USA

Setting. Fall Creek is major west-flowing tributary of Cayuga Lake at Ithaca, in the Finger Lakes region of central New York in the United States. The southern lobes of Lake Ontario ice caps covered the region, and scoured out and oversteepened the lake basins[19]. Upper Fall Creek flows through a valley formerly occupied by a Wisconsinan ice tongue. The retreating glacier left the valley filled with at least 35 m of poorly sorted sand and gravel overlain by till. The creek is actively incising through this fill. Near the Cornell University campus, Fall Creek enters a steep gorge and drops about 200 m over several waterfalls before entering the southern end of Cayuga Lake.

The study site (Figure 1), locally known as "Flat Rock," is the farthest upstream section of bedrock channel in Fall Creek, where the river is superposed on a bedrock rib. This rock is much less erodible than the glacial deposits upstream, and the site therefore dictates the base level for the rest of the creek (a drainage area of 326 km^2). During the time since deglaciation (no more than 14 kyr[19]), ~2 vertical meters of bedrock have been eroded at Flat Rock. The 500-m study reach is located immediately downstream from a 1.5-m-high weir that is the water-supply intake point for Cornell University. The weir marks the uppermost exposed bedrock in Fall Creek.

Lithology. The study reach is underlain by the Upper Devonian Ithaca Formation of shale, siltstone and thin-bedded (1-30 cm) sandstone. The rock is cut by multiple sets of vertical joints

spaced 1-4 m apart. Schmidt hammer measurements on exposed joint planes yield a mean rock mass strength of 51.7±6.8 R units (1σ, n=25); and measurements on subhorizontal bedding planes give 46.4±8.5 R (n=70). For information on the Schmidt hammer methodology used here, see Snyder *et al.*[15].

October 28, 1981 flood event. Plucking of large bedrock slabs (up to 4 m long × 2 m wide × 30 cm thick) occurred at Flat Rock during a major flood event on October 28, 1981 (Figure 2). The flood was the result of 2.6 cm of rain on October 27 and 12.9 cm on October 28, a two-day storm total well above the October monthly mean precipitation of 8.3 cm (Cornell University, Ithaca, NY station data from the Northeast Regional Climate Center). The peak discharge (Q_{pk}) measured at the Fall Creek (Ithaca) gauging station ~1 km downstream of the study reach (Figure 1) was 335 m^3/s. This event was the second largest in the 75-year record at this station (Q_{pk}=439 m^3/s on July 8, 1935). The 1981 event was the only flood that caused significant plucking at Flat Rock in at least the past ~40 years, as deduced from visual observations during the period (A.L. Bloom, personal communication). It significantly modified the morphology of Flat Rock, a popular swimming spot, and washed out several bridges upstream.

Methods. We measured channel gradient (S) for the study reach, flow depth (h), and channel width (w) during the 1981 flood (Table 1). The latter two measurements were made at four representative locations along the 0.5 km study reach. We used reference marks on photographs of the event (Figure 2a) to estimate flow conditions during the flood. Depth (h) and width (w) were measured using a stadia rod and hand level (±20 cm), and laser range finder (±1 m), respectively. Because the channel bank on the north side has a series of terraces cut in glacial sediments, we made two estimates of w: high-flow (to edge of the first north-bank terrace) and valley width (the maximum width possible during the flood, based on photographs). Because S was the parameter most difficult to measure with precision, we used three approximations of local water surface slope during the event, all based on the bed slope. The first two (mean slope over the 0.5 km study reach and over the 100 m reach surrounding each width-measurement station) were from a hand level and stadia rod field survey of the channel bed, with 10 m horizontal spacing. The third slope measurement was from the USGS 7.5' Ithaca East quadrangle map. This estimate includes the ~1.5 m drop of the weir, and is therefore a maximum estimate of

the relevant slope over the reach. Finally, Manning's roughness coefficient (N) was estimated by comparison to similar streams[20,21].

Results and interpretation. The calculations of boundary shear stress (τ_b) during the 1981 flood event are presented in Table 1. Mean estimates of τ_b for the 4 stations based on equation 2 range from 92 Pa to 188 Pa, and from 123 Pa to 202 Pa based on equation 3 (Table 1b). These ranges reflect the differing slope and width estimates for each station. Because floods of only slightly lower magnitude than the 1981 event apparently failed to initiate plucking, we infer that the critical shear stress (τ_c) for this site is only slightly less than our estimates of τ_b. We emphasize that the 1981 flood was a rare, extreme event, consistent with the low postglacial incision rate of the site.

Stochastic floods in a bedrock-channel incision model

The 1981 Fall Creek flood highlights the importance of large, infrequent events in river incision[8]. Such events can be incorporated into geomorphic models using a realistic frequency distribution of floods, along with a threshold for initiating erosion. Tucker and Bras[9] developed a means to incorporate a stochastic distribution of rainfall events into a bedrock-channel evolution model based on shear stress, and we follow their approach here. The Poisson rectangular-pulse rainfall model parameterizes the climate state using exponential distributions of rainfall intensity (P), storm duration (T_r) and interstorm period (T_b)[22]. These variables can be derived from time series of precipitation data. Tucker[10] added an analytical solution for the model with a threshold shear stress, based on equation 1b, and a characteristic "bankfull" runoff event. The formulation gives incision rate (E) as a power-law function of slope (S) and drainage area (A, a proxy for discharge), as in the simple form of the shear stress model ($E=KA^mS^n$)[6]. In the Tucker model[10], the prefactor (coefficient of erosion) in the slope—area function is determined by: (1) physical parameters (k_e, a, ρ, g, N, and channel width); (2) stochastic climate parameters (P, T_r, and T_b); and (3) the critical shear stress (τ_c) in the form of a critical runoff that is a function of A and S. The exponent on drainage area, m equals $3/5a(1-b)$ (where b is the exponent relating width to discharge), and the slope exponent, n equals $7/10a$, in the formulation used here (equation 3). Because this model uses rainfall data to parameterize climatic forcing directly, the only

parameters that cannot easily be constrained from field data are those in equation 1: τ_c, k_e and a. Next, we apply the Tucker model[10] to a set of bedrock streams in northern California[6,15], to constrain values of τ_c and k_e for various values of a, by comparing relief in drainage basins with differing rock-uplift and incision rates.

Coastal streams of the Mendocino triple junction region

Setting. In several previous studies, we have analyzed extensively a series of 21 small, coastal streams on the northern California coast near the Mendocino triple junction[6,14,15]. These drainage basins have received much attention because they are all small (3-20 km^2), share similar lithology, and most importantly, have differing uplift histories, allowing for a comparative analysis of channel response to tectonic forcing. Late Quaternary rock-uplift rates (U) exhibit a well-constrained 8× variation along a 120 km coastal transect, with values from ~4 mm/yr in the King Range, just south of the Mendocino triple junction, to ~0.5 mm/yr in the southern part of the study area[13]. In addition, orographic enhancement of precipitation in the King Range causes a maximum ~2× variation in stream discharge in relation to the low-uplift zone[15]. Lithology of the study area is heavily fractured (joint spacing <1 m) Cenozoic mudstone and sandstone. Field Schmidt hammer measurements and joint surveys indicate that the rock resistance does not vary significantly within the study area. Channel width does not appear to respond to the uplift-rate change in this field area[15]. Finally, Snyder *et al.*[6] showed evidence that the streams are close to steady state (U=E), which means that channel slopes are adjusted to rock-uplift rates, allowing for the substitution of U for E in the Tucker erosion model[10]. Our recent work in the region focused on comparison of digital elevation, field, and hydrological datasets for streams in the King Range high-uplift zone (HUZ) to streams in the southern low-uplift zone (LUZ)[6,15]. We found that a simple form of the shear-stress model for bedrock-channel incision ($E=KA^mS^n$) cannot explain the observed relationship between channel gradient (S, at a given drainage area) and rock-uplift rate (U), unless either: (1) the value of a in equation 1 is greater than 2.5, which is significantly higher than we would expect for plucking-dominated bedrock incision[7]; or (2) there are significant, unexplained differences in k_e between the HUZ and LUZ (i.e. over and above

enhanced orographic precipitation), perhaps related to differences in erosion process or sediment flux[15] (Figure 3).

Parameters and methods. To apply the Tucker model[10] to the California field area, we (1) derived climate parameters from rainfall data, (2) compiled physical parameters from our previous studies, and (3) compared mean relief of HUZ and LUZ streams. We followed the methodology of Eagleson and Hawk[22,23] to calculate representative Poisson pulse model parameters from hourly precipitation data, using the criteria of Restrepo-Posada and Eagleson[24] to define independent rainstorms. To represent the low-uplift zone, we used a 40-year (1954-93) record from Eureka, California, just north of the study area. This record had no gaps in data. Unfortunately, no similar record exists for the HUZ. Therefore, we used the only two consecutive years (1985-6) of nearly complete data available for Honeydew, California to represent the climate state of the HUZ. Honeydew is one of the wettest places in California, and is on the east (lee) side of the King Range (unlike the studied streams, which are the west side), but for reasons explained elsewhere[15], we consider it to be a reasonable proxy for the HUZ climate. The years 1985 and 1986 were somewhat drier than normal, with a mean annual precipitation (P_{ma}) of 1.81 m, as opposed to 2.66 m for 1959-72 (from monthly precipitation data). Furthermore, the data for the Eureka station is measured to 0.01 inch, while the Honeydew station is precise only to 0.1 inch. This difference manifests itself predictably in all three of the parameters, increasing P and T_b, and decreasing T_r for Honeydew (Table 2a). Because the criteria for independent storm events are defined for each individual month, the difference in precision is unimportant in our modeling efforts.

The mean annual precipitation (P_{ma}) predicted by the model ($\langle P \rangle$) can be estimated by multiplying P by the fraction of time taken up by storm events (T_r/T_r+T_b). The frequency distributions for rainfall vary seasonally. In the study region, 80-90% of the P_{ma} falls during the half-year period from October to March. To capture this seasonality while retaining a single frequency distribution, we simply average the statistics for the six rainy months and multiply the time fraction by 0.5. This methodology reproduces the true P_{ma} within 6% (Table 2a). The values of $\langle P \rangle$ reflect a roughly 2× increase in precipitation between the LUZ and HUZ, similar to the

observed increase in discharge (for a given drainage area) in Snyder *et al.*[15], suggesting that this parameterization should yield a reasonable approximation of the orographic effect.

Most of the other necessary model parameters for the HUZ and LUZ were presented in our previous studies[6,15] and reviewed in Table 2. We use data from a representative flood event (March 17, 1975[15]) to parameterize conditions of bankfull discharge and width. This event was chosen because it has an ~2 yr recurrence interval and exhibits a typical 2× variation in discharge between the HUZ and LUZ. Because the downstream relationship between channel width and drainage area ($w=k'_w A^{b'}$) did not vary demonstrably between the HUZ and LUZ, we use a single parameterization, using high-flow width data (similar to bankfull) in this study[9,15]. We convert this relationship to width—discharge ($w=k_w Q^b$) using discharge—area data ($Q=k_q A$) from the 1975 flood. At-station width measurements for this study area are unavailable, so we use an empirical value from the literature[25] for the exponent relating width to discharge at a given channel location (s=0.25). Our calculations assume that infiltration is negligible during storm events, which is consistent with the observed linear relationship between discharge and drainage area during storm events in the region[15]. The calculated values of τ_c are not particularly sensitive to this assumption.

The calculations compared steady-state longitudinal profiles from the high-uplift zone and low-uplift zone (Figure 3a). For simplicity, we focus on a reference drainage area (A_{ref}) of 10^6 m^2 (1 km^2), and compare the mean slopes (S_1, LUZ; S_2, HUZ) at this point (Table 2). This gives us two equations (equation 4 for the LUZ and HUZ cases) with which to solve for three unknowns. We find values of τ_c and k_e for two reference cases, E linear in shear stress (a=1, n=0.7), and E linear in slope (a=1.43; n=1). To demonstrate the influence of orographic precipitation, we do each calculation for two situations: (1) the Eureka/LUZ parameters for both the HUZ and LUZ, and (2) the Eureka parameters for the LUZ, and the Honeydew/HUZ parameters for the HUZ (Table 2). The implicit assumption that the present-day climate is representative of the past ~100 kyr does not significantly affect our conclusions, just the absolute value of τ_c and k_e, as discussed below.

Results and interpretations. Figure 3b shows that the addition of a critical shear stress and stochastic storms to the bedrock-incision model can explain the relationship between slope and uplift rate observed in the Mendocino triple junction region well, without the need to appeal to unexplained changes in k_e or highly nonlinear erosion laws (a>2.5). As shown in Table 2b, the value of τ_c that best explains the data falls in a narrow range from 91 to 144 Pa, for the various scenarios. The inclusion of orographic enhancement of precipitation has a secondary effect, reducing the necessary value of τ_c by 30-40%. Given the uncertainties (related to temporal and/or spatial changes in climate, tectonics, stream geometry and bed friction), the estimated values of τ_c are imprecise. The important point is heuristic: reasonable values of τ_c can easily account for the otherwise surprisingly low relief contrast between the low-uplift and high-uplift zones. Thus, τ_c must be included in bedrock-channel modeling efforts to capture the quantitative temporal evolution of landscapes. Moreover, no meaningful value can be assigned to τ_c unless the full stochastic distribution of flood discharges is represented.

Discussion

We have presented two independent estimates of the critical shear stress required to initiate bedrock incision. Both suggest that relatively small thresholds (τ_c~100-200 Pa, one to two orders of magnitude less than the extreme flood events of Baker and Kale[8]) are appropriate and important for these field sites, although the similarity of the two estimates is likely coincidental. Using a typical Shields threshold of incipient motion for well-sorted sediment[18], this range of shear stress should correspond to a particle diameter of 10-20 cm. In the case of the Fall Creek analysis, the small τ_c is expected: because the blocks have a small height-to-length ratio, they should be transported relatively easily[7]. In this situation, plucking is likely a two-stage process. First, joints are expanded, and blocks are loosened and prepared for plucking by weathering processes (wedging of sediment grains and wood, frost action, etc.). Second, a flood event of sufficiently high shear stress must occur to put the blocks into motion. Because the bedrock at Fall Creek is cut pervasively by open, widely spaced joints, we suspect that the second process is rate limiting.

The low, estimated τ_c values for the California streams merit some discussion. Because these streams are much steeper (S>>0.01) than Fall Creek, these shear stresses correspond to high-frequency events. In the high-uplift zone, the range of τ_c values (Table 2b) corresponds to discharges that occur approximately 8-21% of all days (on the order of mean annual discharge), and in the low-uplift zone, 0.4-3% of all days (approximate recurrence interval on the order of the one-year flood). For comparison, discharges equal to or greater than the October 1981 Fall Creek flood have occurred twice in the 75-yr record, corresponding to about 0.007% of the days during the period. The particularly high frequency of erosive events in the HUZ explains the apparent increase in the effectiveness of erosion processes seen in our previous work (i.e. higher K)[6]. As mentioned above, this shear stress should mobilize 10-20 cm particles, which approximate the size of the typical sediment produced from the pervasively fractured bedrock (joint spacing 0.01-1 m) and are observed on the channel beds. This might indicate that the threshold to initiate motion or entrain the bed particles limits incision in the California streams. Because this is the minimum τ_c necessary to erode bedrock[3], and including it adequately explains the observed gradient versus uplift-rate data (Figure 3b), there is no evidence that differences in sediment flux between the uplift-rate zones play an important role[15], although sediment flux may importantly influence incision rates in other settings[3]. Threshold shear stresses are probably much higher in areas with more competent, less fractured rock. Most importantly, the California results indicate that even a threshold small enough to be exceeded annually dramatically changes the predicted relationship between rock-uplift rate and equilibrium slope, significantly limiting drainage-basin relief at high uplift rates, when compared to models without an erosion threshold (Figure 3b).

Our work in northern California shows that efforts to model landscape evolution will be most successful in reproducing the temporal and spatial evolution of topography in active mountain belts if they include both a well-constrained stochastic precipitation distribution and a critical shear stress for incision. The Poisson pulse rainfall model provides a simple means to parameterize climate, and climate differences throughout a region, removing a key unconstrained variable from most modeling efforts. Tucker and Bras[9] showed that without a threshold term, maximum erosion rates (for n<2) occur in the least variable climate conditions—counter to the observation that big storms do most of the erosion (i.e. Fall Creek). Also, in addition to the high-

uplift relief limit discussed above, the stochastic-threshold model has important implications for post-orogenic decay of topography. Inclusion of τ_c but not stochastic storms predicts a nonzero equilibrium slope even in the absence of uplift (U; Figure 3b), or that relief should persist indefinitely. However, the addition of stochastic rainfall means that some small part of the distribution of storms will exceed always τ_c, causing incision, and eventual removal of topography (S=0) when U=0 (Figure 3b). Because these events are rare, the approach to zero slope after tectonic uplift has ceased can be very slow. This model provides a realistic means for the gradual decline of topography over 100 Myr timescales, as discussed by Baldwin *et al.*[26].

Although much progress has been made, bedrock-river modeling efforts are still hampered by the dearth of field and experimental data constraining the unknown parameters (equation 1). Experimental work by Sklar and Dietrich is making important contributions to quantifying rock resistance to erosion in environments dominated by abrasion[27]. Additional studies are needed in laboratories and field settings of known bedrock incision processes and rates, so that we can constrain values of τ_c, k_e and a for different lithologies and erosion processes[28]. Also, tests of the incision models in well-parameterized streams that are actively responding to changes in tectonic or climatic forcings must be done. With more work in well-chosen sites, our ability to model the long-term growth and decay of topography will be greatly improved, allowing for rigorous testing of hypothesized feedbacks among crustal, surficial, and atmospheric processes[11,17,29-31]. For instance, only by incorporating realistic representations of flood magnitudes and frequencies, and the physics of the erosion process, can we begin to make quantitative inferences about the relationship between climatic variability and the efficiency of terrestrial erosion[11,12,32].

Acknowledgments

Arthur L. Bloom called our attention to the Ithaca site and provided guidance in the field. We also wish to thank: Laurie Snyder and John Wood for field work on Fall Creek; Nicole Gasparini for assistance with the Poisson pulse model; William Coon of the USGS in Ithaca for help with estimating roughness coefficients; and Richard Palmer for sharing photographs of the 1981 flood. This paper benefited from reviews by Dr. Bloom, John Southard, and Kip Hodges.

References

1. Howard, A. D. & Kerby, G. Channel changes in badlands. *Geological Society of America Bulletin* **94**, 739-752 (1983).

2. Willgoose, G., Bras, R. L. & Rodriguez-Iturbe, I. A coupled channel network growth and hillslope evolution model,1 theory. *Water Resources Research* **27**, 1671-1684 (1991).

3. Sklar, L. & Dietrich, W. E. River longitudinal profiles and bedrock incision models: stream power and the influence of sediment supply, in *Rivers Over Rock: Fluvial Processes in Bedrock Channels* (eds. Tinkler, K. J. & Wohl, E. E.) 237-260 (American Geophysical Union, Washington, DC, 1998).

4. Tinkler, K. J. & Wohl, E. E. *Rivers over rock: Fluvial processes in bedrock channels* Geophysical Monograph **107**, (American Geophysical Union, Washington, 1998).

5. Stock, J. D. & Montgomery, D. R. Geologic constraints on bedrock river incision using the stream power law. *Journal of Geophysical Research* **104**, 4983-4993 (1999).

6. Snyder, N. P., Whipple, K. X., Tucker, G. E. & Merritts, D. J. Landscape response to tectonic forcing: DEM analysis of stream profiles in the Mendocino triple junction region, northern California. *Geological Society of America Bulletin* **112**, 1250-1263 (2000).

7. Whipple, K. X., Anderson, R. A. & Hancock, G. S. River incision into bedrock: Mechanics and relative efficacy of plucking, abrasion, and cavitation. *Geological Society of America Bulletin* **112**, 490-503 (2000).

8. Baker, V. R. & Kale, V. S. The role of extreme floods in shaping bedrock channels, in *Rivers Over Rock: Fluvial Processes in Bedrock Channels* (eds. Tinkler, K. J. & Wohl, E. E.) 153-165 (American Geophysical Union, Washington, 1998).

9. Tucker, G. E. & Bras, R. L. A stochastic approach to modeling the role of rainfall variability in drainage basin evolution. *Water Resources Research* **36**, 1953-1964 (2000).

10. Tucker, G. E. Long-term average river erosion and transport rates: Analytical solution for finite-threshold cases. *Water Resources Research* **in preparation** (2001).

11. Molnar, P. & England, P. Late Cenozoic uplift of mountain ranges and global climate change: chicken or egg? *Nature* **346**, 29-34 (1990).

12. Peizhen, Z., Molnar, P. & Downs, W. R. Increased sedimentation rates and grain size 2-4 Myr ago due to the influence of climate change on erosion rates. *Nature* **410**, 891-897 (2001).

13. Merritts, D. & Bull, W. B. Interpreting Quaternary uplift rates at the Mendocino triple junction, northern California, from uplifted marine terraces. *Geology* **17**, 1020-1024 (1989).

14. Merritts, D. & Vincent, K. R. Geomorphic response of coastal streams to low, intermediate, and high rates of uplift, Mendocino junction region, northern California. *Geological Society of America Bulletin* **101**, 1373-1388 (1989).

15. Snyder, N. P., Whipple, K. X., Tucker, G. E. & Merritts, D. J. Channel response to tectonic forcing: analysis of stream morphology and hydrology in the Mendocino triple junction region, northern California. *Geomorphology* **in review** (2001).

16. Benda, L. & Dunne, T. Stochastic forcing of sediment supply to channel networks from landsliding and debris flow. *Water Resources Research* **33**, 2849-2863 (1997).

17. Willet, S. D. Orogeny and orography: The effects of erosion on the structure of mountain belts. *Journal of Geophysical Research* **104**, 28957-28981 (1999).

18. Buffington, J. M. & Montgomery, D. R. A systematic analysis of eight decades of incipient motion studies, with special reference to gravel-bedded rivers. *Water Resources Research* **33**, 1993-2029 (1997).

19. Mullins, H. T. et al. Seismic stratigraphy of the Finger Lakes: A continental record of Heinrick event H-1 and Laurentide ice sheet instability, in *Subsurface geologic investigations of New York Finger Lakes: Implications for Late Quaternary deglaciation and environmental change* (eds. Mullins, H. T. & Eyles, N.) 1-35 (Geological Society of America, Boulder, Colorado, 1996).

20. Barnes, H. H. *Roughness characteristics of natural channels* U.S. Geological Survey Water-Supply Paper **1849**, (1967).

21. Coon, W. F. *Estimation of roughness coefficients for natural stream channels with vegetated banks* U.S. Geological Survey Water-Supply Paper **2441**, (1998).

22. Eagleson, P. S. Climate, soil, and vegetation 2. The distribution of annual precipitation derived from observed storm frequencies. *Water Resources Research* **14**, 713-721 (1978).

23. Hawk, K. L. & Eagleson, P. S. *Climatology of station storm rainfall in the continental United States: Parameters of the Bartlett-Lewis and Poisson rectangular pulses models* Ralph M. Parsons Laboratory Hydrology and Water Resources, (Massachusetts Institute of Technology, Cambridge, 1992).

24. Restrepo-Posada, P. J. & Eagleson, P. S. Identification of independent rainstorms. *Journal of Hydrology* **55**, 303-319 (1982).

25. Leopold, L. B. & Maddock, T., Jr. *The hydraulic geometry of stream channels and some physiographic implications* U.S. Geological Survey Professional Paper **252**, (1953).

26. Baldwin, J. A., Whipple, K. X. & Tucker, G. E. Implications of the shear-stress river incision model for the post-orogenic decay of topography. *Journal of Geophysical Research* **in review** (2001).

27. Sklar, L. & Dietrich, W. E. Relating rates of fluvial bedrock erosion to rock strength: an experimental study (abstract). *EOS, Transactions, AGU* **80**, F448 (1999).

28. Whipple, K. X., Snyder, N. P. & Dollenmayer, K. Rates and processes of bedrock incision by the Upper Ukak River since the 1912 Novarupta ash flow in the Valley of Ten Thousand Smokes, Alaska. *Geology* **28**, 835-838 (2000).

29. Raymo, M. E. & Ruddiman, W. F. Tectonic forcing of late Cenozoic climate. *Nature* **359**, 117-122 (1992).

30. Small, E. E. & Anderson, R. S. Geomorphically driven Late Cenozoic rock uplift in the Sierra Nevada, California. *Science* **270**, 277-280 (1995).

31. Whipple, K. X., Kirby, E. & Brocklehurst, S. H. Geomorphic limits to climate-induced increases in topographic relief. *Nature* **401**, 39-43 (1999).

32. Bull, W. B. *Geomorphic Responses to Climatic Change*, (Oxford University Press, Oxford, 1991).

Table 1a. Total boundary shear stress (τ_b) estimates for each measurement station. Ranges in τ_b reflect three slope estimates (100 m local survey, reach survey mean, and topographic map measurement; Table 1b) and two width measurements (w_h, w_v).

station number	distance from weir (m)	local slope, S	high-flow width, w_h (m)	valley width, w_v (m)	flow depth, d (m)	τ_b range (Pa) eqn. 2	τ_b range (Pa) eqn. 3
1	90	0.0059	25	40	2.4	106-186	132-260
2	180	0.0007	36	41	2.7	19-211	35-209
3	330	0.0032	50	52	2.3	72-178	89-172
4	500	0.0062	32	39	2.3	101-178	134-224

Table 1b. Total boundary shear stress (τ_b) estimates for different slope measurements, mean values from each station.

slope measurement	τ_b (Pa) equation 2	τ_b (Pa) equation 3
map, S = 0.0079	188	202
survey mean, S = 0.0045	107	137
100 m survey mean (see above)	92	123

Q = 335 m^3/s; g = 9.8 m/s^2; ρ = 1000 kg/m^3; N = 0.05 $m^{-1/3}s$

Table 2a. Poisson rectangular-pulse rainfall parameters. Hourly precipitation from the National Climatic Data Center.

station	years of data	mean storm precipitation intensity, P (m/yr)	mean storm duration, T_r (hr)	mean interstorm period, T_b (hr)	predicted ann. precipitation, $\langle P \rangle = 0.5(T_r/T_r+T_b)P$ (m/yr)	observed mean annual precipitation, P_{ma} (m/yr)
Eureka (LUZ)	1954-1993	7.9	20.7	69.7	0.907	0.833
Honeydew (HUZ)	1985-1986	25.3	13.2	74.5	1.915	1.808

Table 2b. Results of Mendocino triple junction streams calculations.

case	shear-stress exponent, a	area exponent, $m=3/5a(1-b)$	slope exponent, $n=7/10a$	critical shear stress, τ_c (Pa)*	shear stress coefficient, k_e ($Pa^{-a}myr^{-1}$)
Eureka	1	0.36	0.70	144	1.33×10^{-3}
Eureka (LUZ)-Honeydew (HUZ)	1	0.36	0.70	102	3.26×10^{-4}
Eureka	1.43	0.51	1	142	9.62×10^{-5}
Eureka (LUZ)-Honeydew (HUZ)	1.43	0.51	1	91	2.17×10^{-5}

Parameter values:
ρ=1000 kgm^{-3}; g=9.8 ms^{-2}; N=0.07 $m^{-1/3}s$; $A_{ref}=10^6$ m^2
b=0.4 (downstream width-discharge exponent, from Snyder *et al.*[15])
s=0.25 (at-a-station width-discharge exponent, from Leopold and Maddock[25])
U_1=0.0005 myr^{-1}; S_1=0.14 (LUZ); U_2=0.004 myr^{-1}; S_2=0.26 (HUZ; from Snyder *et al.*[6])
Eureka/LUZ parameters (for 2/17/75 representative bankfull flood event, from Snyder *et al.*[15]):
$k_{q1}=1.47\times10^{-6} ms^{-1}$ (linear discharge-area coefficient, $Q=k_qA$)
$k_{w1}=4.63$ $m^{0.2}s^{0.4}$ (downstream width-discharge coefficient, $w=k_wQ^b$)
Honeydew/HUZ parameters (for 2/17/75 representative bankfull flood event, from Snyder *et al.*[15]):
$k_{q2}=2.73\times10^{-6} ms^{-1}$; $k_{w2}=3.61$ $m^{0.2}s^{0.4}$

* Critical shear stresses (τ_c) of 91-144 Pa correspond to critical discharges (Q_c) of 0.2-0.5 m^3/s in the LUZ at A_{ref}, and 0.06-0.2 m^3/s in the HUZ. Using daily discharge data from the South Fork of the Eel River at Leggett as a proxy for the LUZ, and Honeydew for the HUZ[15], scaled to station drainage area, Q_c is exceeded on 0.4-3% of all days in the LUZ, and 8-21% of all days in the HUZ.

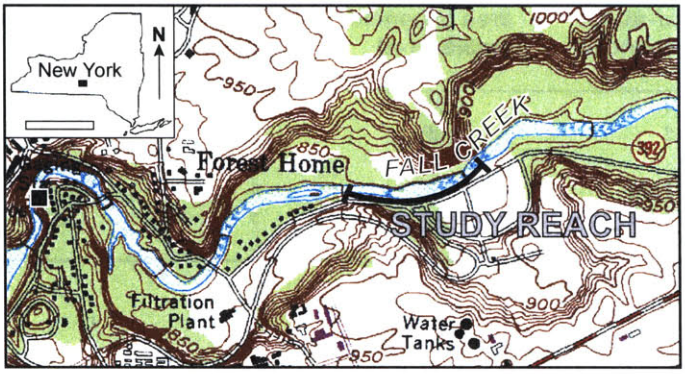

Figure 1. Map of the Flat Rock, Fall Creek field site. Base is the U.S. Geological Survey 7.5' Ithaca East, NY quadrangle, contour interval 10 feet. USGS stream-gauging station used in this study is indicated by the black box on the west side of the map, ~1 km downstream of the study reach. Inset map indicates position within New York state; bar represents 200 m of distance on the study-area map.

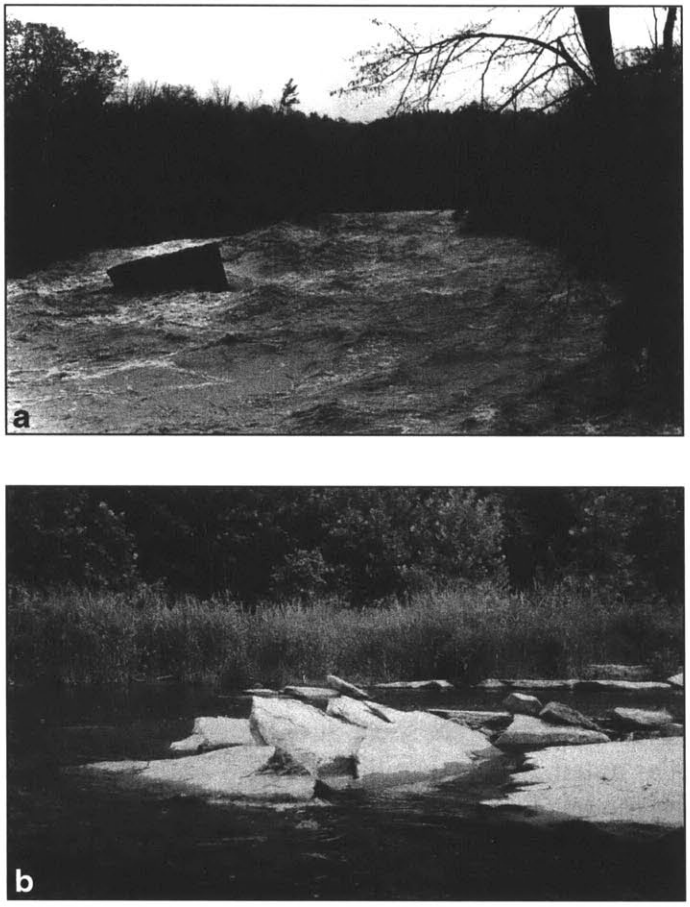

Figure 2. Photographs of the Fall Creek study area. **a**, A view east from the downstream end of the field area of a large plucked block (~4 m in length) actively tumbling downstream at Flat Rock, during the October 28, 1981 flood. Channel width here is 25-52 m (Table 1a). Photograph by Richard Palmer. **b**, Imbricated blocks at Flat Rock during post-flood, low-flow conditions.

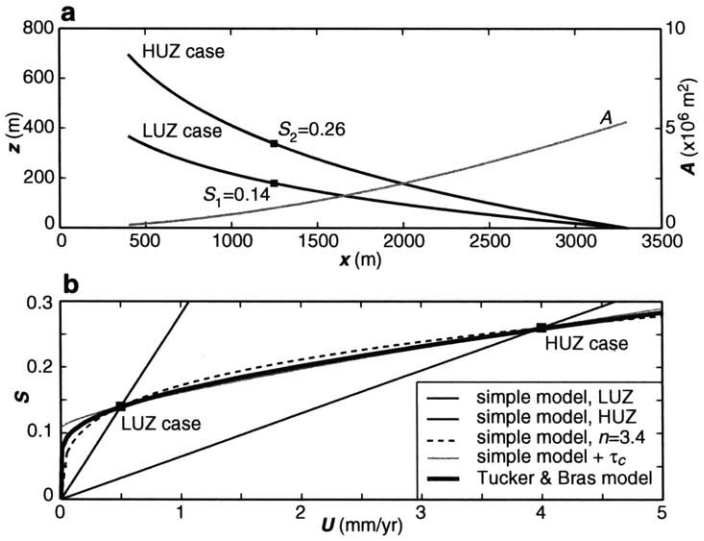

Figure 3. Northern California model setup and results. **a**, Model mean steady-state high-uplift zone (HUZ) and low-uplift zone (LUZ) longitudinal profiles (elevation, z versus distance, x; black lines; left axis), used for calculations. Gray line is the drainage area (A) profile (right axis). Boxes indicate reference slopes (S) at $A=A_{ref}=10^6$ m^2, used in part **b**. **b**, Equilibrium-slope (S) versus uplift-rate (U) curves for different shear-stress-based incision models, all with slope exponent, n=1, except as noted. Slopes calculated at A_{ref}. Thin, solid, dark lines are the simple form of the shear-stress model ($E=KA^mS^n$) with different values of K for the HUZ and LUZ cases[6]. Thin, dashed, dark line is the simple model with constant K, but high slope exponent (n=3.4) to match both cases[6]. Thin, solid, light line is a basic shear stress model including a non-zero τ_c[15]. Note that $S>0$ even when $U=0$, suggesting that topography is never completely erased. Thick, dotted, light line is the Tucker incision model[10] including stochastic storms and τ_c, see Table 2 for parameters used. Note that S approaches zero as U approaches zero. For very low uplift rates, this model approaches steady state very slowly, as only the largest storms in the stochastic distribution are able to initiate incision[26]. Since channel gradient is directly related to drainage basin relief, this plot highlights the predictions different incision models make for the relationship between relief and uplift rate. Note particularly that the addition of a threshold term and stochastic storms in the model yields a limit on relief, because erosion becomes more efficient at higher channel gradient as more frequent events exceed the initiation threshold.

5. Interactions between onshore bedrock-channel incision and nearshore wave-based erosion forced by eustasy and tectonics

Noah P. Snyder and Kelin X Whipple
Department of Earth, Atmospheric and Planetary Sciences, Massachusetts Institute of Technology, Cambridge, MA 02139-4307, USA

Gregory E. Tucker
School of Geography and the Environment, University of Oxford, Oxford OX1 3TB, England

Dorothy J. Merritts
Geosciences Department, Franklin and Marshall College, Lancaster, PA 17604-3003, USA

Abstract

We study the response of bedrock streams to eustatic and tectonic fluctuations in base level. A numerical model coupling onshore fluvial erosion with offshore wave-based erosion is developed. The results of a series of simulations for simple transgressions with constant rate of sea-level change (*SL*) show that response depends on the relative rates of rock uplift (*U*) and wave-based erosion (ε_w). Simple regression runs highlight the importance of nearshore bathymetry. Shoreline position during sea-level fall is set by the relative rate of base-level fall (*U-SL*) and ε_w, and is constant horizontally when these two quantities are equal. The results of models forced by a realistic Late Quaternary sea-level curve are presented. These runs show that a stable shoreline position cannot be obtained if offshore uplift rates exceed ε_w. Only in the presence of a relatively stable shoreline position can fluvial profiles begin to approximate a steady-state condition, with *U* balanced by fluvial erosion rate (ε_f). In the presence of a rapid offshore decrease in uplift rate, short (~5 km) fluvial channels can respond to significant changes in rock-uplift rate in just a few eustatic cycles. The results of the model are compared to real stream-profile data from the Mendocino triple junction region of northern California. The late Holocene sea-level stillstand response exhibited by the simulated channels is similar to the low-gradient mouths seen in the California streams.

Introduction

The response of fluvial systems to eustatic sea-level fluctuations is a classic problem in sedimentology (*e.g.* Wheeler, 1964; Middleton, 1973; Vail *et al.*, 1977; Pitman, 1978; Christie-Blick and Driscoll, 1995). In general, previous analyses focused on transgressions, when sea level rises, shifting the locus of deposition onshore; and regressions, when sea level drops, incising onshore and pushing deposition farther offshore. The geomorphic literature has also given some attention to the development of topography and bathymetry in response to eustatic sea-level change. A number of workers have studied and modeled fluvial profile development of large rivers in coastal alluvial settings (*e.g.* Schumm, 1993; Talling, 1998; Antoine *et al.*, 2000; Tebbens *et al.*, 2000). The creation of fluvial terraces has been used as a template for discussing responses to tectonics, climate and eustasy (*e.g.* Merritts *et al.*, 1994; Pazzaglia *et al.*, 1998; Veldkamp and Van Dijke, 2000). Other workers have studied the development of marine terraces with respect to sea level and tectonics (*e.g.* Bloom *et al.*, 1974; Chappell, 1974; Merritts and Bull, 1989; Cinque *et al.*, 1995). Recently, Anderson *et al.* (1999) used a simple model for wave-based erosion to investigate the cutting and uplift of marine terraces on a tectonically active coastline. Here we build on these research themes by linking a model for onshore, fluvial bedrock incision (*e.g.* Howard and Kerby, 1983; Stock and Montgomery, 1999; Snyder *et al.*, 2000) with the Anderson model for offshore incision, to investigate response of this coupled system to transgressions, regressions, and Late Quaternary sea-level history. The goal is to gain first-order insight into the response of bedrock-floored streams actively incising coastal mountain belts to tectonically and eustatically driven base-level change.

Most recent modeling studies of fluvial response to uplift have treated the case of block uplift relative to a fixed base level (Figure 1A) (*e.g.* Whipple and Tucker, 1999; Snyder *et al.*, 2000). Put another way, these models fix the model lower boundary condition (stream outlet point) at a static elevation. This situation may be acceptable for some specialized tectonic settings, such as uplift of the hanging wall of a normal fault relative to the footwall, or uplift on a high-angle fault relative to a static water level. However, in the case where the fluvial base level migrates in space and time due to eustasy, uplift, and erosion, as with streams on uplifting coastlines, this boundary condition is clearly an oversimplification. Here we present a model with a more realistic treatment for the base-level condition (Figure 1B). Other workers (*e.g.* Willet *et al.*,

2001) have emphasized the role of horizontal advection of topography, as in the case of uplift on the hanging wall of a thrust ramp. This response is also important to the development of fluvial topography, but for simplicity we do not include it in our modeling efforts. However, a horizontal component of rock motion could be easily incorporated into the model presented here (*e.g.* Kirby and Whipple, 2001).

To begin our investigation of bedrock-channel response to uplift and eustasy, we present a simple thought experiment. Figure 2 shows a series of hypothetical situations for onshore and offshore topography, similar to the cases suggested by Summerfield (1985; 1991) and Schumm (1993). The onshore is represented by a concave-up longitudinal stream profile, whereas the offshore is a linear ramp with various gradients. In this experiment, fluvial base level (sea level) is changed from the initial condition (triangle) to the final condition (circle), in the absence of uplift or erosion (except in Figure 2D). The first two panels represent regressions across an offshore that is flatter than the onshore channel (Figure 2A) and steeper than the onshore (Figure 2B). In the first case, we expect a decrease in the ability of the stream to erode and/or transport sediment, so the emergent platform will likely inhibit erosion and induce deposition of a prograding wedge of sediment. In the second case, the newly emergent section of stream is steep, and so a rapidly incising knickpoint will likely propagate upstream. The third and fourth panels show the results of a transgression. In Figure 2C, sea level inundates the lower part of the channel, with little effect on the profile, aside from shortening the stream. This situation is of course unrealistic because in this thought experiment we are ignoring onshore and offshore erosion. Figure 2D is the same as Figure 2C, except that significant wave-based erosion occurs during the transgression, driving a knickpoint up the channel mouth. Previous models of fluvial response to eustatic sea-level fluctuations have typically not included a specific treatment of offshore wave-based erosion (*e.g.* Veldkamp and Van Dijke, 1998). The difference between the two panels (Figure 2C and D) highlights the importance of understanding the interplay of changing base level and erosion patterns. It is this interplay that we will examine in this paper.

The central question of the modeling exercises presented here is: what is the response of the fluvial system to the combined forcings of tectonic rock uplift, eustatic sea-level fluctuations, and offshore wave-based erosion? We approach this question by starting with the simplest cases of transgressions and regressions (constant rate of sea-level rise or fall) on uplifting coastal

rivers. In these experiments, we want to know when the model predicts a knickpoint propagating onshore (*i.e.* Figure 2B, D), or a flat platform (Figure 2A), or no response of the channel (Figure 2C). Once we establish how the model parameters set these responses to a simple sea-level forcing function, we present the second set of experiments, using a realistic Late Quaternary sea-level curve. Because present-day topography and bathymetry represent the integrated effects of the history of forcings, we investigate stream response to the sea-level fluctuations associated with the last few glacial—interglacial cycles. Here the questions turn to the model predictions with respect to the morphology of Late Quaternary tectonic coasts. What channel-mouth morphology is expected at the end of a major transgression? Under what range of parameter space do we expect emergence of a marine terrace and seaward advancement of the shoreline? How do offshore conditions influence the onshore morphology? What does the model predict about steady-state erosion conditions and the development of fluvial relief? In the final part of this paper, model predictions are compared to a well-studied suite of streams in northern California (Merritts and Vincent, 1989; Snyder *et al.*, 2000; Snyder *et al.*, 2001a). We begin with a brief discussion of the model onshore and offshore erosion laws, and a synopsis of the model execution.

Model formulation

We are concerned with the response of a coupled system, with erosion of bedrock by onshore and offshore processes, to tectonic and eustatic forcing. The modeling presented here is meant to apply to uplifting, rocky coastlines, with onshore erosional channels and offshore wave-cut platforms. The model addresses only channel and nearshore longitudinal-profile response, not the evolution of interfluves and headlands, as done by Anderson *et al.* (1999). We make the assumption that for small drainage basins (<50 km^2) undergoing rapid rock-uplift rates (U>0.001 m/yr) both onshore and offshore processes are detachment limited, or that lowering rates are set by the ability to break off pieces of intact bedrock. In these systems, the sediment created by bedrock detachment is transported rapidly away (to the far offshore), with minor, temporary storage in floodplains, fans, terraces, and beaches. Adding sediment transport and deposition to model transport-limited fluvial conditions (*e.g.* Willgoose *et al.*, 1991; Sklar and Dietrich, 1998; Veldkamp and Van Dijke, 1998; Whipple and Tucker, 2001) remains an important next step to

extend the applicability of the model to a wider range of settings. Our initial goal is to capture the first-order response of detachment-limited systems.

Onshore fluvial incision. Incision of bedrock by rivers (ε_f, defined as positive downward) is often modeled as a power-law function of basal shear stress or unit stream power, either of which can be expressed as a function of channel gradient (S) and drainage area (A) (Howard and Kerby, 1983; Whipple and Tucker, 1999):

$$\varepsilon_f = KA^m S^n, \tag{1}$$

where K is a dimensional coefficient dependent on a variety of factors (Stock and Montgomery, 1999; Whipple and Tucker, 1999), and m and n are exponents dependent on erosion process, channel width, and discharge. We use the version of Equation 1 that applies to detachment-limited bedrock incision. Theoretical predictions for the value of n range from 2/3 to 5/3, but the best field estimates are typically 2/3 to 1 (Howard and Kerby, 1983; Stock and Montgomery, 1999; Whipple *et al.*, 2000; Kirby and Whipple, 2001). The ratio of the exponents (m/n) is generally found to be between 0.4 and 0.6 (from theory and observation, *e.g.* Snyder *et al.*, 2000), although exceptions have been reported (Sklar and Dietrich, 1998). For simplicity, we use m=0.5 and n=1. The influence of the plausible range of m and n have been discussed elsewhere (Howard *et al.*, 1994; Whipple and Tucker, 1999; Snyder *et al.*, 2000), and here the emphasis is on the interaction between the onshore and offshore. Although we have shown previously that this model is oversimplified in its omission of a realistic treatment of climate and a threshold shear stress to initiate incision (Snyder *et al.*, 2001a, b), for the purposes of this study Equation 1 is sufficient, because it does capture the first-order form and tectonic response of channel longitudinal profiles with a minimum of free parameters (Snyder *et al.*, 2000).

In the case where channel incision (ε_f) balances rock-uplift rate (U, defined as positive upward, with a steady-state condition: U=ε_f), U can be substituted for ε_f in Equation 1, yielding a solution for steady-state slope (S_e):

$$S_e = \left(\frac{U}{K}\right)^{1/n} A^{-m/n}. \tag{2}$$

This theoretical steady-state power-law relationship between S and A is similar in form to a commonly observed empirical relation:

$$S = k_s A^{-\theta}, \tag{3}$$

where the coefficient k_s is the channel steepness, and θ is the profile concavity. For comparison of empirical parameters from slope—area regressions to theoretical model inputs, we define k_{sl} equal to $(U/K)^{1/n}$, the theoretical steady-state channel steepness. Equations 2 and 3 are equivalent if and only if (1) $U=\varepsilon_f$, and (2) U, K, m and n do not vary downstream, as discussed by Snyder *et al.* (2000). In reality, these criteria are only approximately met in most field settings, because they implicitly require that the channel is uplifted vertically on a block relative to a fixed base level, and that none of the factors that go into K (*e.g.* climate, lithology, and possibly sediment flux relative to carrying capacity) vary downstream. Previously we have studied the role of controls on K, including discharge (and associated climate), lithology, channel width, and sediment flux (Snyder *et al.*, 2001a, b). These factors are intentionally not considered here, because we wish to isolate the effect that a fluctuating base level has on channel form and response.

Offshore wave-based erosion. We are concerned with development of nearshore bathymetry over 10-100 kyr timescales in uplifting, tectonically active coastlines, where shelf sediment deposition and storage is minimal. Compared to the fluvial system, this situation has received relatively little attention in the geomorphic literature, although cliffed, rocky coastlines are common throughout the world (Sunamura, 1992). The most comprehensive treatment of the problem is the numerical modeling work by Anderson *et al.* (1999), which dealt with the two-dimensional evolution of marine terraces. Faced with a similar problem, here we use the Anderson model to describe the erosion of the shelf. The basic postulate of the model is that sea-bed erosion rate (ε_w, defined positive downward) is a linear function of the rate of energy dissipation ($\mathrm{d}E/\mathrm{d}t$), which can be expressed as an exponential function of water depth:

$$\varepsilon_w = \beta(\mathrm{d}E/\mathrm{d}t) = \beta(\mathrm{d}E/\mathrm{d}t)_0 \exp(-4h/h_{wb}) = \beta' \exp(-4h/h_{wb}), \tag{4}$$

where $(\mathrm{d}E/\mathrm{d}t)_0$ is the energy dissipation rate in very shallow water, h is the water depth, h_{wb} is the depth where $\mathrm{d}E/\mathrm{d}t$ is essentially zero (the wave base), and β is a dimensional coefficient that

relates the rate of dissipation of wave energy to erosion rate. Because we have no constraints on the value of either $(dE/dt)_o$ or β, we simply use β' as an adjustable parameter that encompasses both $(dE/dt)_o$ and β ($\beta'=\beta(dE/dt)_o$). For the problem of offshore bedrock platform erosion, the effective wave base (h_{wb}) is also essentially unknown, and this parameter sets the width of the shelf affected by erosion.

Anderson *et al.* (1999) were concerned with the development of coastal cliffs, which form the inner edges of marine terraces. They modeled sea-cliff retreat by integrating the wave energy dissipated on the shelf and assuming that the rest of the energy is expended in horizontal cliff retreat. In this way, they simulated the effect of increased or decreased wave dissipation across a wide or narrow shelf, respectively. Although this model may be appropriate for interfluvial areas where cliff erosion is driven by undercutting by waves and subsequent mass wasting, it is not appropriate for the mouths of channels where cliffs are not present and erosion is driven by a combination of wave and fluvial processes. We do not include the cliff-retreat component of the Anderson model in our efforts, because it simply acts to impart an additional lowering on the model node just upstream of sea level. This simplification has one obvious advantage and one disadvantage. Equation 4 indicates that wave-based erosion rate (ε_w) is a maximum when the water depth (h) is zero—consistent with the idea that breaking waves are the most powerful in driving erosion. This means that the maximum and most important value of ε_w is described by only one unknown parameter (β'), making the application to modeling quite simple. However, because dissipation rate (dE/dt) is purely a function of h, and not the change in amount incoming wave energy due to interaction with shelf bathymetry (dE/dx), the width and slope of the shelf have no effect on ε_w, making this model a clear oversimplification: we expect that erosion due to waves breaking on the shoreline should be less for a wide, flat shelf than for a narrow, steep shelf (Adams *et al.*, 2000). This limitation means that the model cannot predict the long-term development of nearshore bathymetry. Therefore, we limit application to single transgressions and regressions, and a few glacial—interglacial cycles. Lacking a more sophisticated model for wave-based erosion (which would necessarily involve more unknown parameters), we proceed with this simple approach, which is sufficient to capture the first-order interaction between onshore and offshore erosion processes over short timescales (<1 Myr).

Model setup: all cases

In this section, we outline the application of model, including initial profile conditions, uplift-rate boundary conditions, and the coupling of the two erosion models. In the first modeling exercise we look at the response of uplifting coastlines in general to simple transgressions and regressions, and in the second part we take the specific example of the last few glacial—interglacial cycles (120-782 kyr). In the latter experiments, the resulting landforms are compared to the topography and bathymetry of a series of previously studied channels in northern California (Merritts and Vincent, 1989; Snyder *et al.*, 2000; Snyder *et al.*, 2001a, b). For both cases we use some parameter values derived from the California field area, but we emphasize that the results are generally applicable to uplifting coastlines and that the conclusions reached are independent of the particular parameter values used.

Initial conditions. The model profiles consist of evenly spaced (50 m) horizontal nodes (x), with elevations (z) decreasing from the top of the fluvial system (about 300-400 m downstream from the divide; Snyder *et al.*, 2000) to the end of offshore profile. For the onshore, fluvial part of the profile, the initial condition is simply a model steady-state channel, for block uplift relative to a fixed base level, generated using an integrated form of Equation 2, and an empirical power-law relationship (Hack, 1973) between drainage area (A) and distance downstream (x) (Figure 3). Different profiles are generated for both low (0.5 mm/yr) and high (4 mm/yr) uplift-rate conditions, using average parameters from Snyder *et al.* (2000) (Table 1). For the offshore part of the profile, a linear ramp of constant gradient (S_{ramp}=0.01-0.1) was used, with the range of S_{ramp} chosen on the basis of northern California nearshore bathymetry, to yield cases where the offshore is flatter or steeper than the onshore (Figure 3). Only the relative gradients are important, not the absolute values. The onshore drainage area function is assumed to extend offshore but is used only when subaerially exposed, a simplification not expected to significantly affect model results.

Uplift-rate boundary conditions. As mentioned above, the profiles are subjected to rock uplift rates of 0.5 mm/yr and 4 mm/yr (Figure 3). This is the range seen in the northern California study area (Merritts and Bull, 1989), and it is representative of tectonically active coastlines in general. The model has constant uplift rate for the entire onshore portion of the initial profile,

and part of the offshore portion, in some model configurations. At some distance offshore, the uplift rate makes a rapid, linear decrease (over 5 km in x) to zero at the seaward (right) boundary (Figure 3C). This gradient is arbitrarily chosen, and it is simply meant to represent a decrease in uplift rate distributed over a narrow zone, such as might occur at a fault zone. We used two different positions for boundary of the uplifting block: (1) far enough offshore so that the erosive part of the model does not interact with the uplift ramp during the entire model run (typically at least 15 km from the initial shoreline), termed the constant-uplift-rate boundary condition, and (2) at the initial shoreline, termed the uplift-rate-gradient boundary condition (Figure 3C). In the first boundary condition, the uplift-rate drop is unimportant to the model, whereas in the second the spatially variable uplift rates are directly important to the system response. These two cases allow us to isolate the role of the uplift-rate boundary condition.

Coupling of erosion laws. The model response depends fundamentally on the relative magnitudes of four rates: rock uplift (U), onshore incision (ε_f, initially set equal to U), sea-level change (SL), and offshore erosion (ε_w, set by β'), and we focus on these values in the presentation of model results. The bottom panels on Figure 3 show the initial values of each of these rates, for the various initial profile conditions. Once the model is running, ε_f and ε_w vary based on the topography and bathymetry, and apply to a domain of nodes defined by the location of the shoreline (x_{sl}). In practice, each model time step involves the following sequence of four steps:

1. A new sea level (z_{sl}) is calculated, based on an input function. The model node with elevation closest to this value is assigned to be the sea-level node (x_{sl}).

2. Fluvial erosion rate (ε_f) is calculated based on Equation 1 for all nodes landward of x_{sl}, using the downstream slope.

3. Wave-based erosion rate (ε_w) is calculated based on Equation 4 for all nodes from x_{sl} to the offshore boundary.

4. All nodes are uplifted and eroded an amount equal to the sum of U and the applicable erosion rate (ε_f or ε_w) multiplied by the time step (dt).

Model results and interpretation 1: general cases

Approach. For the general cases we used simple, constant-rate, sea-level functions that roughly approximate the last glacial regression (100 m fall in 100 kyr) and transgression (100 m rise in 20 kyr). We ran the model for a vast part of parameter space, systematically varying the offshore erosion rate coefficient (β'), wave base (h_{wb}), uplift rate (U), uplift boundary condition, and offshore bathymetry (S_{ramp}). We use two uplift-rate cases, with corresponding initial onshore erosion rates (set equal to U), and two sea-level cases, as well as two S_{ramp} values and two positions of the U boundary condition (Figure 3C). For simplicity, we used only one value of wave base (h_{wb}=100 m) for all of the model results shown here, because h_{wb} affects only the width of the shelf affected by wave-based erosion, and therefore it plays a secondary role in channel response. Because ε_w reaches a maximum at sea level ($\varepsilon_{w,sl}$) that sets the response, in the discussion of the results we focus on this value (not β'). We have done model runs varying $\varepsilon_{w,sl}$ from zero to values greater than the relative rate of base-level change (U-SL). We present a sampling of plots that are representative of parameter space, chosen to highlight key aspects of channel response to eustatic forcing. The central question with each run is the how the morphology of the previously steady-state river mouth is affected by the combined forcings of eustasy and uplift (*i.e.* generation of a knickpoint or flat platform). We include some interpretation of the results of the transgression and regression cases in their respective subsections, and a brief discussion of the overall implications of the general modeling in the last part of this section.

Transgressions. The initial-profile conditions for the transgression cases are simply a steady-state stream onshore, and a steep ramp (S_{ramp}=0.1) offshore (Figure 4). Because the rate of sea-level rise (SL=5 mm/yr) is faster than uplift rate, the offshore conditions are unimportant. The entire onshore profile is uplifted at a constant rate.

The response of channels to transgression is straightforward. Because SL is always greater than U, the streams shorten as the ocean inundates the channel. The response of the mouth and nearshore is set by the relative difference between U and $\varepsilon_{w,sl}$. If uplift rate equals or is on the same order as offshore erosion rate ($U \approx \varepsilon_{w,sl}$) then there is no effect on the onshore part of the profile, and the nearshore flattens slightly as the inundated channel approaches h_{wb} (Figure 4A).

If uplift rate greatly exceeds offshore erosion rate ($U>\varepsilon_{w,sl}$), then the mouth of the channel flattens, as does the nearshore (Figure 4B). Finally, if wave-based erosion rate exceeds uplift rate ($U<\varepsilon_{w,sl}$), then a knickpoint at the channel mouth is driven upstream with the rising sea level, and a flat platform is created in the nearshore (Figure 4C-D).

Regressions. Modeling channel response to regressions is more complicated than the transgression case, because the offshore profile and uplift boundary conditions are important. To explore the range of possibilities, we use two different offshore ramp gradients (S_{ramp}) and two different uplift boundary conditions. In the regression case, the rate of sea-level decline (SL=-1 mm/yr) is in the opposite direction from uplift rate (U), making the channel experience an increased rate of relative base-level change (U-SL). For this reason, the channel grows seaward at a maximum rate (for small ε_w) of (U-SL)/ S_{ramp}. Here, we consider the regression modeling in three parts: (1) gradual S_{ramp}, (2) steep S_{ramp} (both with the constant uplift-rate boundary condition outside of the erosive domain), and (3) a steep S_{ramp} with the uplift-rate gradient boundary condition (Figure 3). Note that a gradual S_{ramp} and a proximal boundary to the uplifting block are mutually inconsistent, so only the steep S_{ramp} condition is considered in this case.

Figure 5 shows four model results for regression over a gradual ramp (S_{ramp}=0.01), with the uplift-rate boundary condition seaward of the domain of erosion. This value of S_{ramp} is less than the slope of the channel mouth. In the case where the wave-based erosion rate is less than the rate of base-level fall ($\varepsilon_{w,sl}<U$-SL) a wide, gradual platform emerges as the position of the channel mouth (x_{sl}) regresses over the gradual ramp (Figure 5A, B, D). The emergent, low-gradient channel is not only flatter than the steady-state initial condition, but it also has a different concavity (θ), because of the regression of x_{sl}. Below, we investigate this further. If offshore erosion balances the relative position of sea level ($\varepsilon_{w,sl}$ =U-SL), then x_{sl} remains fixed, lowering at rate SL, and the channel mouth steepens as a knickpoint is developed (Figure 5C). This occurs because wave-based erosion (ε_w) removes the uplifting seabed instead of regressing along the ramp. The high ε_w also causes the offshore to be bladed off at an extremely low slope. Of course, if ε_w is even faster than U-SL ($\varepsilon_{w,sl}>U$-SL), then x_{sl} actually transgresses and drives a knickpoint inland (a case not shown in Figure 5).

Figure 6 illustrates the same model runs as Figure 5 but with a value of S_{ramp} greater than the slope of the channel mouth (for both low-uplift and high-uplift cases). The key difference is seen in Figure 6A, where the low-uplift-rate channel mouth gets steeper as it regresses onto the ramp. Conversely, Figure 6B and 6D show that for high U, the channel mouth is actually less steep—a gradual platform is created, in spite of the initially steep offshore ramp. Figure 6C, where the x_{sl} is fixed, is little different than Figure 5C.

The new channel-profile segments created during a regression exhibit a lower concavity (θ) than the fixed-base-level steady-state initial channel (Figures 5 and 6), because the base level is both dropping and extending seaward. This new concavity is set by S_{ramp}, U, SL and $\varepsilon_{w,sl}$, and exists because the relationship between onshore distance and drainage area ($A=k_a x^h$) continues into the newly emergent channel (Figure 3). The channel does exhibit a steady-state form (slope unchanging with time), but it is not strictly speaking a "steady-state channel" because the mouth is constantly migrating seaward, extending its length, and the whole channel is experiencing net uplift at a constant rate. If the model is allowed to run indefinitely, with an infinitely long ramp, the channel eventually achieves this new steady form from mouth to divide.

When uplifting a ramp, instead of uplift relative to a fixed base level, the maximum onshore slope at the outlet (and therefore maximum ε_f) is set by the gradient of the offshore ramp. In the high-uplift cases (U=4 mm/yr), this situation causes the newly created stream to be less steep than the initial condition for all but the steepest ramps (S_{ramp}>>0.5). In the low-uplift cases (U=0.5 mm/yr) the mouth is steeper than the initial condition for S_{ramp} greater than about 0.05. This observation highlights the importance of understanding the controls on the development of bathymetry to adequately predict channel response to eustatic regressions. A proper erosion law for offshore bedrock platforms is needed (including the effects of sediment deposition, shelf width, distribution of storms, cutting of offshore canyons, etc.) to be able to model long-term (~1 Myr) evolution of nearshore bathymetry.

When the shoreline position (x_{sl}) regresses through variable rock-uplift rates (uplift-rate-gradient boundary condition), results are much more complicated, particularly in the high-uplift cases because of the steep gradient in U immediately offshore from the initial condition (Figure 7). These cases have U linearly decreasing over 5 km in the offshore from a maximum of the

onshore uplift rate at the initial location of x_{sl} (Figure 3). The steep bathymetric ramp is used (S_{ramp}=0.1, as in Figure 6). Figure 7D shows that as x_{sl} regresses into the zone experiencing lower uplift rates, the rate of horizontal seaward migration slows and eventually halts at the point where $\varepsilon_{w,sl}$ equals *U-SL*, continuously lowering the outlet at rate *SL*, as in the Figure 5C and 6C examples. This yields significant changes in the width (narrower) and slope (steeper) of the emergent channel segment that is created during regression in high-*U* conditions (compare with Figure 6D). The low-*U* cases are not particularly different from the cases where the uplift rate is constant throughout the entire erosive part of the system, because the *U* gradient is less dramatic. However, the long-term evolution of the profiles would be quite different, because the location of x_{sl} would eventually regress to the point where $\varepsilon_{w,sl}$=*U-SL* (as seen in Figure 7D). Comparison with runs with the uplift-rate gradient over shorter and longer horizontal distances (not shown) indicates that the presence of an offshore uplift-rate gradient is much more important to the model results than the magnitude of the gradient. These uplift-rate gradient boundary condition examples simply serve to show that uplift-rate boundary condition is critical for setting the topographic response of streams to eustatic sea-level changes and rock uplift.

In summary, the results of the general modeling of regressions indicate that the initial bathymetry is critical in setting the response of the onshore stream channel. Within a range of plausible values of the offshore slope (S_{ramp}=0.01-0.1), the *U*=0.5 mm/yr cases exhibit steeper emergent channel segments for greater values of S_{ramp}. The *U*=4 mm/yr cases persistently exhibit flat emergent platforms, unless the regression occurs across a significant uplift-rate gradient boundary. These results are modified by high wave-based erosion rates ($\varepsilon_{w,sl}$>*U-SL*). In all regression cases, channel response is quite different than that predicted by the simple case of uplift relative to a fixed base level (*i.e.* S_{ramp}=∞).

Interpretation of general model results. The simple models of transgressions and regressions presented above show that the development of nearshore bathymetry is critical to setting the response of uplifting rivers to eustatic sea-level fluctuations. Bathymetry has direct implications during regressions, as we have shown. During transgressions, bathymetry has only an indirect influence, presumably modulating wave-based erosion rates, although this effect is not treated here. However, the simple cases presented so far capture only the influence of a single transgression or regression, starting with a known, simple initial condition. The situation

becomes more complicated when a realistic sea-level curve is used to drive the model, as we do in the following section. To highlight this point, consider the transgression case (Figure 4). Although the bathymetry is not important to stream profile during the sea-level rise, as soon as SL is less than U (for low ε_w), the nearshore platform will begin to emerge, and the channel response to this relative regression will depend critically on the offshore profile. If this emergent platform is flat, then deposition will likely occur at the channel mouth, because the slope of the river would be insufficient to transport the sediment load (*e.g.* Figure 4B). Conversely, a knickpoint—flat platform pair may emerge, and this may have a more complicated response (*e.g.* Figure 4D). In any case, this response will be set by the offshore topography developed during the transgression, which is set by wave-based erosion, a process that lacks a sophisticated geomorphic model at present. In the late Holocene (past ~6 kyr), global sea level is in a post-transgression stillstand situation as described above, so this is directly relevant to the study of modern river profiles. In the next section, we run the model forced by a realistic Late Quaternary sea-level curve and compare the onshore and offshore topography predicted by the model to that of the Mendocino triple junction area of northern California.

Model results and interpretation 2: Late Quaternary sea-level function

Approach. We now move beyond a constant rate of sea-level change, to explore the response of the model to realistic eustatic fluctuations. In the second set of experiments, the model is forced by a realistic Late Quaternary sea-level curve. The deep-sea oxygen isotope record is a reasonable proxy for glacial ice volume and therefore sea level (*e.g.* Chappell *et al.*, 1996). We use the stacked, normalized SPECMAP $\delta^{18}O$ record of Imbrie *et al.* (1984), transformed via a second-order polynomial (Anderson *et al.*, 1999) to produce a reasonable representation of Quaternary sea level (Figure 8). This record begins at a negative $\delta^{18}O$ excursion (highstand) at 782 ka. Our purpose with this modeling is not to attempt to reproduce exactly present-day topography but to investigate model response to a realistic sea-level history. Therefore, although the transformation from $\delta^{18}O$ is imperfect, and the timing of the $\delta^{18}O$ record is approximate, the sea-level curve shown in Figure 8 is certainly adequate for our purpose, inasmuch as it is a reasonable representation of the rate and magnitude of eustatic sea-level fluctuations over the Late Quaternary (Anderson *et al.*, 1999).

For this experiment, we investigated both the response to a single glacial—interglacial cycle and the model prediction for how fluvial topography evolves over time. Therefore, for each set of initial conditions, the model was run from the previous interglacial highstand (120 ka) to the present highstand, and for three or more highstands (330-782 ka) to the present (Figure 8). These longer runs de-emphasize the importance of initial conditions. All of the runs start at a highstand and end at the present.

For the initial stream longitudinal profile, we used a 5-km channel, developed in the same way as the first experiment (for parameters see Table 1). This shorter channel has the advantage that the model profile responds rapidly, reaching a constant form in less time than a channel 10 km long. As before, we used values of rock uplift rate (U) and two positions for the edge of the uplifting block. We also investigated the response to a change from a low-uplift-rate to a high-uplift-rate scenario. To further de-emphasize the importance of initial conditions, the model runs presented here use offshore ramp gradients (S_{ramp}) chosen to match the outlet slopes for the various uplift conditions (S_{ramp}=0.05 for U=0.0005 m/yr; S_{ramp} =0.1 for U=0.004 m/yr). For simplicity, we also do not vary offshore erosion rates (ε_w=0.0005 m/yr) and wave base (h_{wb}=100 m). We have already investigated how all of these parameters influence the response, and we discuss these results both in the previous sections and below.

The second set of experiments has two interrelated purposes, with associated questions. First, as in the first experiment, we investigate how sea-level forcing affects the channel mouth. Do we expect knickpoints or flat platforms? Is the coastline advancing or retreating through time? In the discussion section, the model results are compared to present day coastal morphology in northern California.

The second purpose of this suite of experiments is to analyze the stream longitudinal profiles as a whole, using models run for several glacial—interglacial cycles. In a previous study (Snyder *et al.*, 2000), we used regressions of data on channel gradient (S) versus drainage area (A; Equation 3) to estimate model parameters (Equation 2). This analysis was based on the hypothesis that the channels were adjusted to block uplift relative to a fixed base level (Figure 1). Here we can test the range of parameter space where the steady-state hypothesis is valid for a variable base level. This is done by comparing empirical channel steepness (k_s) and concavity (θ) from S—A

regressions of model profiles (Equation 3) to input model parameters that correspond to steady-state steepness ($(U/K)^{1/n}=k_{sl}$) and concavity (m/n, Equations 1 and 2). As we have previously discussed extensively (Snyder *et al.*, 2000), θ and k_s covary strongly, so for comparison purposes we calculate a value of steepness (k_{s2}) for a fixed concavity (θ=0.5=m/n), a technique directly analogous to the representative slope method of Sklar and Dietrich (1998). We also calculate slopes at 10-m contour intervals, to minimize regression bias and be consistent with our prior methodology (Snyder *et al.*, 2000). Finally, we further consider the question of steady state by investigating the response of channels to an acceleration in U, again comparing model profiles to those of our previous study (Snyder *et al.*, 2000).

Constant-uplift-rate boundary condition. Figure 9 illustrates the results of model runs for constant low and high rock-uplift rates, forced by 120 and 782 kyr of the Quaternary sea-level curves (Figure 8). For a single glacial—interglacial cycle (120 kyr), the response depends largely on the initial offshore conditions. In the two cases shown (Figure 9A and B), S_{ramp} is slightly steeper than the fluvial outlet slope. However, as seen in the previous regression experiments, the resulting emergent channel is on average slightly flatter than the original onshore channel gradient. For the low-uplift rate example (U=0.0005 m/yr, Figure 9A), the response is quite subtle, with only a slight emergent platform forming. Because the rock-uplift rate equals the wave-based erosion rate at sea level ($U=\varepsilon_{w,sl}$) and the initial and final sea levels are the same in the model run, the shoreline position (x_{sl}, z_{sl}) has not changed. Moreover, the regression of onshore S—A data indicates that the overall profile has changed only a minor amount ($\theta=m/n$=0.5, $k_s \approx k_{s2} \approx k_{sl}$=125), reflecting a small deviation from the initial steady-state condition. Conversely, in the high-uplift case (U=0.004 m/yr, Figure 9B), the channel has several breaks in slope reflecting the complex history of sea-level rises and falls during the 120-kyr model period. The shoreline position has prograded seaward more than 3 km, lengthening the channel significantly. The channel mouth is an emergent flat platform, resulting from post-transgression uplift of the wave-cut platform during the late Holocene stillstand. The S—A data are not linear in log space, and the regression yields a high concavity (θ=0.56) and low steepness (k_{s2}=166). In both cases, the upper parts of the channel do not deviate from the initial condition, indicating that the base-level perturbations have not yet affected the entire channel.

The 782 kyr model runs (Figures 9C and D) have profiles that reflect the integrated effect of 7-8 glacial—interglacial cycles. In both cases, the channel has lengthened because of net uplift. Associated with the lengthening is a net decrease in channel gradient. The perturbations propagate slowly through the low-uplift channel (Figure 9C), and the uppermost part has yet to respond. In the high-uplift case (Figure 9D), the entire channel has responded and is uplifting as the channel lengthens. Given even more time, the low-uplift channel will also begin to experience net uplift throughout. Because the channel is lengthening and overall relief (total elevation drop on the fluvial system) is increasing, a true steady state is impossible to attain in a situation with constant uplift rate throughout the model domain. However, as discussed previously, the channels are approaching an steady-state form, with an average concavity (θ) near the model input value (m/n), and a low steepness (k_{s2}), as suggested by Figure 9D.

Uplift-rate-gradient boundary condition. The results of four model runs with a steep gradient in uplift rate in the initial 5 km offshore are shown in Figure 10. As before, the entire channels have not fully responded in one glacial—interglacial cycle (Figure 10A and B). The affect on the low-uplift case is minor. The high-uplift case shows a set of migrating knickpoints and flats traveling up the channel, as well as the emergent wave-cut platform at the channel mouth.

In the 330-kyr model runs (Figures 10C and D), both channels have responded to the fluctuating base level from their mouths to their divides. Experience with longer runs (up to 782 kyr) indicates that further changes to the profiles are extremely minor. Both channels have achieved a quasi-steady-state condition—the position of the channel does not change significantly in x or z over time. As in the simple regressions, the maximum seaward shoreline position is set by the place where the relative rate of base-level fall, set by the uplift rate (which is decreasing with increasing x) and the rate of sea-level fall during regressions, balances the wave-based erosion rate ($\varepsilon_{w,sl}$). Because the magnitude and frequency of the regressions is reasonably constant, this position changes little once it is established. Therefore, the channels cease to lengthen significantly, even in high-uplift cases, and the profile achieves a quasi-steady-state position. In both cases, the S—A regressions indicate that the overall channel form (as indicated by θ and k_{s2}) is very similar to the input values (m/n=0.5 and k_{si}=125 or 200).

Discussion

Steady-state channel profiles. A central goal of this modeling exercise is to establish what can be learned from analysis of channel longitudinal profiles that experience complex base-level forcing. To use regressions of channel gradient against drainage area (S—A) to constrain model parameters (*e.g.* Snyder *et al.*, 2000), channels must be in a steady state, with fluvial erosion rates balancing rock-uplift rates ($\varepsilon_f = U$). The model results indicate that in absence of an offshore decrease in uplift rates, steady state is impossible (Figure 9). During the transient seaward advance of the shoreline (at a horizontal rate set by S_{ramp}), the channel should be less steep than the model prediction for a fixed base level, although concavity may be fairly close to the model prediction. The history of the advance should be recorded in an emergent flight of very wide (>1 km per eustatic cycle) marine terraces (*i.e.* Figure 9D). In practice, such a situation (unrestricted advance of x_{sl} due to high U offshore) may be short lived (in geologic terms), because the shoreline position will rapidly transgress until it reaches a point where wave-based erosion balances uplift rates during regressions (Figure 10). Slope—area regressions of data from quasi-steady-state channels with fixed x_{sl} by an offshore decrease in U should yield reasonable matches to theoretical parameters, provided that the channels have had sufficient time to equilibrate fully.

The integrated history of sea-level fluctuations introduces significant, systematic scatter to the S data (Figure 10). The knickpoints and flats become less pronounced as they migrate upstream. This attenuation of eustatic effects is probably partially a real feature of slope variations in detachment-limited channels, as is the case for the response of transport-limited channels (Schumm, 1993; Whipple and Tucker, 2001). However, part of this attenuation is undoubtedly the result of numerical diffusion due to the coarse model node spacing (50 m), as discussed by Baldwin *et al.* (2001). Slope datasets from real channels also exhibit scatter, particularly when derived from coarse (pixel size ≥10m) digital elevation models (*e.g.* Snyder *et al.*, 2000) (see also Figure 12, below). Inaccuracies in data collection aside, gradients in steep, bedrock streams vary locally over ~50-m reaches because of variations in lithologic resistance, input of colluvium from adjacent hillslopes, and many other factors (Snyder *et al.*, 2000). These sorts of disruptions introduce non-systematic scatter into S data, unlike the regular variations of Figure 10. However, the modeling presented here suggests that some amount of the scatter seen in local channel

gradients of coastal bedrock channels may be a result of fluctuating base level, particularly if these fluctuations were of higher frequency than those of Figure 8.

We have seen that short (5 km) channels adjust from the initial, artificial condition to a new quasi-steady-state form in just three eustatic cycles, given a steep drop off in uplift rates offshore. What about response to an acceleration in uplift rate? How can channels be expected to behave as they pass from low to high uplift conditions? The simulations presented in Figure 11 illustrate such an acceleration. The initial condition is a 5-km channel adjusted to a low-uplift rate (U=0.0005 m/yr), with a steep offshore ramp (implicitly with an offshore decrease in uplift rate). The model runs with U=0.004 m/yr and the uplift-rate-gradient boundary condition. To keep pace with high uplift rates, the channel steepens from the mouth up. In 120 kyr, this wave of steepening has reached about half way up the length of the channel, and the shoreline position has regressed about 1 km (Figure 11A). By 330 kyr, the channel has steepened to the divide, indicating nearly complete response (Figure 11B). During the extra 210 kyr of the longer model run, the shoreline transgressed only another ~0.5 km. Given even more time, the shoreline position remains nearly static. Of course, longer channels would take longer to respond to uplift-rate changes (Whipple and Tucker, 1999).

Comparison to Mendocino triple junction channels. We have studied extensively a set of 21 small, coastal streams near the Mendocino triple junction in northern California (Snyder *et al.*, 2000; Snyder *et al.*, 2001a, b). Rock uplift rates vary along a 120-km-long coast-parallel transect from 0.0005 m/yr in the south to 0.004 m/yr in the north (Merritts and Bull, 1989). In our previous studies we have compared channel characteristics (gradient, lithology, width, discharge) from streams in the low-uplift zone to streams in the high-uplift zone (Figure 12). In our initial analysis of watershed-scale topography from digital elevation models, we found that all the stream profiles were smooth and concave up, suggesting that they may be approximately in a steady state with uplift rates (Snyder *et al.*, 2000). Our analysis of S—A data from the streams depended on the steady-state hypothesis, with the assumption that eustatic sea-level changes did not significantly affect the channel form. One of the goals of this modeling exercise is to find the range of conditions where this assumption may be valid. A further goal is to compare the channel morphology predicted by the model to present-day channels.

As shown above, the steady-state hypothesis is compatible with channels experiencing complex base-level forcing if there is an offshore decrease in rock-uplift rates. At some distance offshore in the Mendocino triple junction region uplift rates must decrease, but little is known about the offshore tectonics. Because the uplift-rate data come from studies of emergent marine terraces, we have no information about how far the shoreline uplift rates extend into the Pacific Ocean. Therefore, we can only conclude that the steady-state hypothesis is consistent with an offshore decrease in rock-uplift rates in the Mendocino triple junction region.

A surprising finding of longitudinal-profile analyses of the California streams (Merritts and Vincent, 1989; Snyder *et al.*, 2000) was that the high-uplift rate channels have steepened (and therefore responded; Figure 12) during the short, 100-kyr period since the onset of high-uplift rates (Merritts and Bull, 1989). A theoretical calculation of response time, based on an assumed fixed base level, found that the channels should reach a new steady state in 50-200 kyr. The case modeled in Figure 11 is essentially the situation for the high-uplift channels, with full response of a 5-km channel in about 330 kyr. Because the modeled scenario is highly simplified, this difference in response time is certainly within uncertainty. The case simply shows that with a reasonable uplift-rate boundary condition, we might expect that the channels are in an approximate steady state, and therefore *S—A* regressions do yield reasonable estimates of Equation 1 model parameters.

The northern California streams typically exhibit a drop in gradient near their mouths (Figure 12). This is particularly true in the case of larger streams (drainage area $\geq$10 km^2) and rivers of the region that have significant alluvial deposits at their mouths (Merritts *et al.*, 1994; Snyder *et al.*, 2000). For this reason we limited our profile analysis to drainage areas less than 5 km^2, a value conservatively chosen to avoid process transitions from erosive bedrock channels to depositional alluvial channels (Snyder *et al.*, 2000). Smaller channels, such as Kinsey Creek, also have a package of alluvium at the mouth, although any slight reduction in slope does not extend far enough upstream to affect the *S—A* analysis significantly (Figure 12B). As discussed by Merritts *et al.* (1994), alluviation of uplifting river mouths is expected during the post-transgression stillstand (last 6 kyr), when offshore wave-cut platforms begin to emerge as channel mouths. We see this situation in the model runs, particularly for the high-uplift cases, where U is significantly greater than that of the latest Holocene rate of sea-level rise. This is also

the case in U=0.0005 m/yr model runs when S_{ramp} is less than 0.05. Of course, the model is not tracking sediment deposition, and the large drop in slope of the high-uplift channel mouths (*i.e.* Figures 10B and D) would undoubtedly be attenuated by sediment deposition in a more sophisticated fluvial model.

As discussed and modeled elsewhere (*e.g.* Bloom *et al.*, 1974; Merritts and Bull, 1989; Cinque *et al.*, 1995; Anderson *et al.*, 1999), uplifting coastlines are commonly identified by emergent marine terraces, as is the case in the Mendocino triple junction region. The only point we wish to add about marine terrace relates to the uplift-rate boundary condition. The narrow (<100 m, Merritts *et al.*, 1992), young (<100 kyr, since an acceleration in uplift rates, Merritts and Bull, 1989), emergent marine terraces around Cape Mendocino, abandoned after minor Late Pleistocene highstands (Figure 8), are consistent with the modest shoreline advance predicted with a steep uplift-rate gradient (*i.e.* Figure 11). If high uplift rates extend very far offshore, then we might expect to see a wider zone of newly emergent (post—100 ka) marine terraces as the shoreline transgresses rapidly (*i.e.* Figures 9B and D). Much of the northern California coast (including the older, higher terraces of the Cape Mendocino area) exhibits a flight of wide (~1 km) marine terraces (*e.g.* Merritts *et al.*, 1992; Anderson *et al.*, 1999), which may be consistent with little offshore gradient in uplift rates. The modeling presented here suggests that the development and evolution of marine-terraced coastlines should depend critically on the offshore uplift-rate conditions.

The bathymetry of the Mendocino triple junction area shares some similarities to the model bathymetry. In the high-uplift zone, the nearshore (3-5 km) seabed gradient is quite low (S≈0.02), whereas farther offshore the gradient is much steeper (S≈0.1; Figure 12B). Of course, the models reflect this, with flat wave-cut platforms in the nearshore and steeper conditions offshore (set by S_{ramp}). However, the seabed offshore from Juan Creek has a fairly constant gradient around 0.01 (Figure 12A), a situation not represented particularly well by the model profiles. This real difference in shelf morphology may reflect differing tectonic settings or differing wave climates. Moreover, the shelf of northern California coast is cut in many places by vast canyons (similar to those discussed by Talling, 1998), which are also totally ignored by the model. Further advances in our ability to model channel response to eustatic fluctuations will depend on the development of more sophisticated wave-based bedrock erosion models.

Conclusions: channel response to eustatic forcings

Our modeling efforts show that the response of uplifting bedrock streams to fluctuations in base level caused by eustasy depends fundamentally on three factors: (1) nearshore bathymetry; (2) the relationship between the relative rate of base-level change and wave-based erosion; and (3) offshore rock-uplift conditions. Here we review some of our findings and suggest avenues for further field research and modeling.

The details of channel response to any given regression are set by the nearshore bathymetry. At core, the development of bathymetry depends on eustatic sea-level changes, rock-uplift rate and wave-based erosion. The model presented here treats the latter in the simplest possible manner, ignoring many important controls on the evolution of shelf morphology, including wave dissipation as a function of width, stochastic influences on wave energy and direction, sediment deposition, and erosion of offshore canyons. Further advances in the modeling of channel response to fluctuating sea-level will depend on development of a proper wave-based bedrock erosion law. Although much is known about sediment transport in coastal environments, relatively little has been done on erosion of bedrock. Measurements by Adams *et al.* (2000) of delivery of wave energy to coastlines represent an exciting new research direction to achieve the goal of understanding the evolution of shelf bathymetry on uplifting coastlines.

Channels lengthen over time when rock-uplift rates exceed wave-based erosion rates. This simple fact is not generally included in river-incision modeling efforts, which treat the case of block uplift relative to a fixed base level. However, the model presented here shows that channel lengthening changes the response to uplift quite remarkably. If onshore rock-uplift rates extend far into the offshore, then channels will generally grow seaward. Along with the increase in length comes an increase in divide-to-mouth relief, and changes in stream-profile concavity and steepness. The regression persists until the shoreline reaches a zone where rock-uplift rates decrease. A stable maximum regression shoreline position is attained at the point where the relative rate of base-level fall (uplift rate plus regressing sea level) balances wave-based erosion. Once the channel reaches this position, it ceases to lengthen significantly, and relief ceases to increase. Only at this point can the channel approximate a steady-state condition, with fluvial incision rates balancing uplift rates. This condition will persist until a key forcing changes, such

as tectonic regime, climate, or magnitude of sea-level oscillations. The offshore uplift-rate conditions are the most important control on the overall development of drainage basins and fluvial relief when eustatic forcing is considered.

Acknowledgments

This paper benefited from discussions and correspondence with Robert Anderson, Neal Driscoll, Bill Lyons, and Matt Reuer; and reviews by Kip Hodges and John Southard.

References Cited

Adams, P.N., Anderson, R.S., and Revenaugh, J.S., 2000, Seismic measurements of the shaking of seacliffs: Determining the relative effects of oceanographic variables: EOS, Transactions, AGU, p. F508.

Anderson, R.S., Densmore, A.L., and Ellis, M.A., 1999, The generation and degradation of marine terraces: Basin Research, v. 11, p. 7-19.

Antoine, P., Lautridou, J.P., and Laurent, M., 2000, Long-term fluvial archives in NW France: response of the Seine and Somme rivers to tectonic movements, climatic variations and sea-level changes: Geomorphology, v. 33, p. 183-207.

Baldwin, J.A., Whipple, K.X., and Tucker, G.E., 2001, Implications of the shear-stress river incision model for the post-orogenic decay of topography: Journal of Geophysical Research, v. in review.

Bloom, A.L., Broecker, W.W., Chappell, J.M.A., Mathews, R.K., and Mesolella, K.J., 1974, Quaternary sea level fluctuations on a tectonic coast: New $^{230}Th/^{234}U$ dates from the Huon Penninsula, New Guinea: Quaternary Research, v. 4, p. 185-205.

Chappell, J., 1974, The geomorphology and evolution of small valleys in dated coral reef terraces, New Guinea: Journal of Geology, v. 82, p. 795-812.

Chappell, J., Omura, A., Esat, T., McCulloch, M., Pandolfi, J., Ota, Y., and Pillans, B., 1996, Reconciliation of late Quaternary sea levels derived from coral terraces at Huon Peninsula with deep sea oxygen isotope records: Earth and Planetary Science Letters, v. 14, p. 227-236.

Christie-Blick, N., and Driscoll, N.W., 1995, Sequence stratigraphy: Annual Reviews of Earth and Planetary Science, v. 23, p. 451-478.

Cinque, A., De Pippo, T., and Pomano, P., 1995, Coastal slope terracing and relative sea-level changes: deductions based on computer simulations: Earth Surface Processes and Landforms, v. 20, p. 87-103.

Hack, J.T., 1973, Stream profile analysis and stream-gradient index: J. Res. U.S. Geological Survey, v. 1, p. 421-429.

Howard, A.D., and Kerby, G., 1983, Channel changes in badlands: Geological Society of America Bulletin, v. 94, p. 739-752.

Howard, A.D., Seidl, M.A., and Dietrich, W.E., 1994, Modeling fluvial erosion on regional to continental scales: Journal of Geophysical Research, v. 99, p. 13,971-13,986.

Imbrie, J., Hays, J.D., Martinson, D.G., McIntyre, A., Mix, A.C., Morley, J.J., Pisias, N.G., Prell, W.L., and Shackleton, N.J., 1984, The orbital theory of Pleistocene climate: Support from a revised chronology of the marine $\delta^{18}0$ record, *in* Berger, A.L., Imbrie, J., Hays, J., Kukla, G., and Saltzman, B., eds., Milankovitch and Climate: Dordrecht, Netherlands, D. Reidel, p. 269-305.

Kirby, E., and Whipple, K.X., 2001, Quantifying differential rock-uplift rates via stream profile analysis: Geology, v. 29, p. 415-418.

Merritts, D., and Bull, W.B., 1989, Interpreting Quaternary uplift rates at the Mendocino triple junction, northern California, from uplifted marine terraces: Geology, v. 17, p. 1020-1024.

Merritts, D., and Vincent, K.R., 1989, Geomorphic response of coastal streams to low, intermediate, and high rates of uplift, Mendocino junction region, northern California: Geological Society of America Bulletin, v. 101, p. 1373-1388.

Merritts, D.J., Chadwick, O.A., Hendricks, D.M., Brimhall, G.H., and Lewis, C.J., 1992, The mass balance of soil evolution on late Quaternary marine terraces, northern California: GSA Bulletin, v. 104, p. 1456-1470.

Merritts, D.J., Vincent, K.R., and Wohl, E.E., 1994, Long river profiles, tectonism, and eustasy: A guide to interpreting fluvial terraces: Journal of Geophysical Research, v. 99, p. 14031-14050.

Middleton, G.V., 1973, Johannes Walther's law of correlation of facies: Geological Society of America Bulletin, v. 84, p. 979-988.

Pazzaglia, F.J., Gardner, T.W., and Merritts, D.J., 1998, Bedrock fluvial incision and longitudinal profile development over geologic timescales determined by fluvial terraces, *in* Tinkler, K.J., and Wohl, E.E., eds., Rivers Over Rock: Fluvial Processes in Bedrock Channels: Geophysical Monograph 107: Washington, American Geophysical Union, p. 207-236.

Pitman, W.C., 1978, Relationship between eustacy and stratigraphic sequences of passive margins: Geological Society of America Bulletin, v. 89, p. 1389-1403.

Schumm, S.A., 1993, River response to baselevel change: Implications for sequence stratigraphy: Journal of Geology, v. 101, p. 279-294.

Sklar, L., and Dietrich, W.E., 1998, River longitudinal profiles and bedrock incision models: stream power and the influence of sediment supply, *in* Tinkler, K.J., and Wohl, E.E., eds., Rivers Over Rock: Fluvial Processes in Bedrock Channels: Geophysical Monograph 107: Washington, DC, American Geophysical Union, p. 237-260.

Snyder, N.P., Whipple, K.X., Tucker, G.E., and Merritts, D.J., 2000, Landscape response to tectonic forcing: DEM analysis of stream profiles in the Mendocino triple junction region, northern California: Geological Society of America Bulletin, v. 112, p. 1250-1263.

—, 2001a, Channel response to tectonic forcing: analysis of stream morphology and hydrology in the Mendocino triple junction region, northern California: Geomorphology, v. in review.

—, 2001b, Stochastic floods and erosion thresholds in bedrock rivers: implications for landscape relief: in preparation.

Stock, J.D., and Montgomery, D.R., 1999, Geologic constraints on bedrock river incision using the stream power law: Journal of Geophysical Research, v. 104, p. 4983-4993.

Summerfield, M.A., 1985, Plate tectonics and landscape development on the African continent, *in* Morisawa, M., and Hack, J.T., eds., Tectonic Geomorphology: Boston, Allen & Unwin, p. 27-51.

—, 1991, Global Geomorphology, Harlow, England, Longman Group, Ltd.

Sunamura, T., 1992, Geomorphology of Rocky Coasts, New York, John Wiley & Sons.

Talling, P.J., 1998, How and where do incised valleys form if sea level remains above the shelf edge?: Geology, v. 26, p. 87-90.

Tebbens, L.A., Veldkamp, A., and Van Dijke, J.J., 2000, Modeling longitudinal-profile development in response to Late Quaternary tectonics, climate and sea-level changes: the River Meuse: Global and Planetary Change, v. 27, p. 165-186.

Vail, P.R., Mitchum, R.M., Todd, R.G., Widmier, J.M., Thompson, S., Sangree, J.B., Bubb, J.N., and Hatlelid, W.G., 1977, Seismic stratigraphy and global changes of sea level, *in* Payton, C.E., ed., Seismic stratigraphy- applications to hydrocarbon exploration: Memoir: Tulsa, OK, The American Association of Petroleum Geologists, p. 49-212.

Veldkamp, A., and Van Dijke, J.J., 1998, Modelling long-term erosion and sedimentation processes in fluvial systems: A case study for the Allier/Loire system, *in* Benito, G., Baker, V.R., and Gregory, K.J., eds., Paleohydrology and Environmental Change: New York, John Wiley and Sons.

—, 2000, Simulating internal and external controls on fluvial terrace stratigraphy: a qualitative comparison with the Maas record: Geomorphology, v. 33, p. 225-236.

Wheeler, H.E., 1964, Baselevel, lithosphere surface, and time-stratigraphy: Geological Society of America Bulletin, v. 75, p. 599-610.

Whipple, K.X., and Tucker, G.E., 1999, Dynamics of the stream-power river incision model: Implications for the height limits of mountain ranges, landscape response timescales, and research needs: Journal of Geophysical Research, v. 104, p. 17661-17674.

Whipple, K.X., Anderson, R.A., and Hancock, G.S., 2000, River incision into bedrock: Mechanics and relative efficacy of plucking, abrasion, and cavitation: Geological Society of America Bulletin, v. 112, p. 490-503.

Whipple, K.X., and Tucker, G.E., 2001, Transitions between detachment-limited and transport-limited river incision: Implications for the form, occurrence, and dynamics of "mixed-bedrock-alluvial" channel systems: Journal of Geophysical Research, v. in review.

Willet, S.D., Slingerland, R., and Hovius, N., 2001, Uplift, shortening, and steady state topography in active mountain belts: American Journal of Science, v. in press.

Willgoose, G., Bras, R.L., and Rodriguez-Iturbe, I., 1991, A coupled channel network growth and hillslope evolution model,1 theory: Water Resources Research, v. 27, p. 1671-1684.

Table 1. Model parameters

General

U	rock-uplift rate, positive upward (m/yr)
SL	rate of sea-level rise or fall (m/yr)
A	drainage area (m^2)
S	topographic gradient (m/m)
SL	rate of sea-level change (m/yr)
t	model time (yr)
z	elevation, relative to sea level at t=0 (m)
z_{sl}	elevation of sea level at time t (m)
x	horizontal distance downstream from divide (m)
x_{sl}	horizontal position of the sea-level node (m)
S_{ramp}	gradient of the model offshore ramp
h	water depth (m)

Onshore fluvial incision (Equations 1-2)

ε_f	vertical fluvial incision rate, positive downward (m/yr)
m	drainage-area exponent
	m=0.5
n	slope exponent
	n=1
K	coefficient of fluvial incision (m^{1-2m}/yr)
	$K=4\times10^{-6}$ yr^{-1} for U=0.0005 m/yr and m=0.5
	$K=2\times10^{-5}$ yr^{-1} for U=0.004 m/yr and m=0.5
	(values chosen to match basin relief in Snyder *et al.*, 2000)
S_e	theoretical steady-state channel gradient
k_{sl}	theoretical steady-state channel steepness ($m^{2m\,n}$, from $k_{sl}=(U/K)^{1/n}$)
	k_{sl}=125 m for $K=4\times10^{-6}$ yr^{-1}
	k_{sl}=200 m for $K=2\times10^{-5}$ yr^{-1}
m/n	theoretical steady-state channel concavity
	m/n=0.5

Empirical fluvial parameters

k_s	channel steepness ($m^{2\theta}$, from Equation 3)
θ	channel concavity
k_{s2}	channel steepness, from regression with θ=0.5
k_a	coefficient ($m^{2-\alpha}$, from $A=k_a x^{\alpha}$)
	k_a=15.6 $m^{0.46}$ (for 10-km model streams, from Juan Creek; Snyder *et al.*, 2000)
	k_a=4.72 $m^{0.28}$ (for 5-km model streams, from Kinsey Creek; Snyder *et al.*, 2000)
α	exponent
	α=1.54 (for 10-km model streams, from Juan Creek; Snyder *et al.*, 2000)
	α=1.72 (for 5-km model streams, from Kinsey Creek; Snyder *et al.*, 2000)

Offshore wave-based erosion (Equation 4)

ε_w	vertical wave-based erosion rate, positive downward (m/yr)
$\varepsilon_{w,sl}$	vertical wave-based erosion rate at sea level (h=0) (m/yr)
E	wave energy (J)
dE/dt	wave energy dissipation rate (J/yr)
dE/dx	horizontal spatial derivative of wave energy (J/m)
β	wave-energy coefficient (m/J)
$(dE/dt)_o$	wave-energy dissipation rate in very shallow water (J/yr)
β'	adjustable parameter, $\beta'=\beta(dE/dt)_o$ (m/yr)
h_{wb}	depth of wave base (m)
	h_{wb}=100 m for all model runs presented here

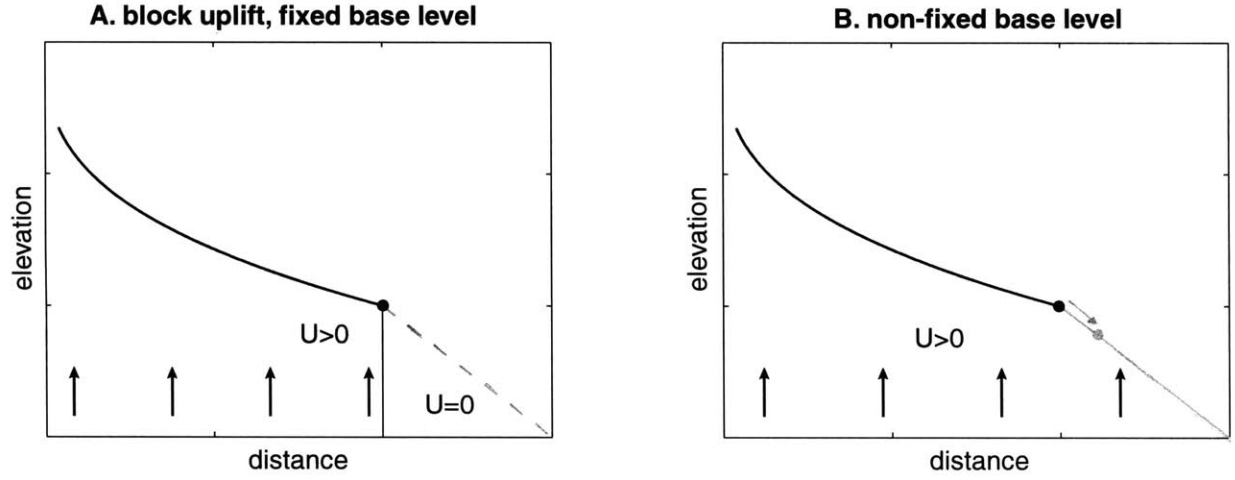

Figure 1. Block uplift and fluvial base level demonstration. (A) An example of a typical fluvial channel model. A concave-up stream longitudinal profile (solid line) is uplifted vertically at a constant rate, relative to a fixed base level outlet point (marked by the black dot). Physically, this base level must mark a significant discontinuity in deformation, for instance a fault. To the right of the of the dot, the rock-uplift rate (U) drops as a step function to zero. This part of the profile (dashed line) is unimportant to models with this boundary condition. (B) Similar to (A) but here the entire profile uplifts at the same rate. In this case, fluvial base level (black dot) simply represents the change from subaerial (black line) to subaqueous conditions (gray line). If this base level drops (*i.e.* regression, gray dot) then the fluvial system will respond according to the gradient of the newly emergent channel (between the black dot and gray dot).

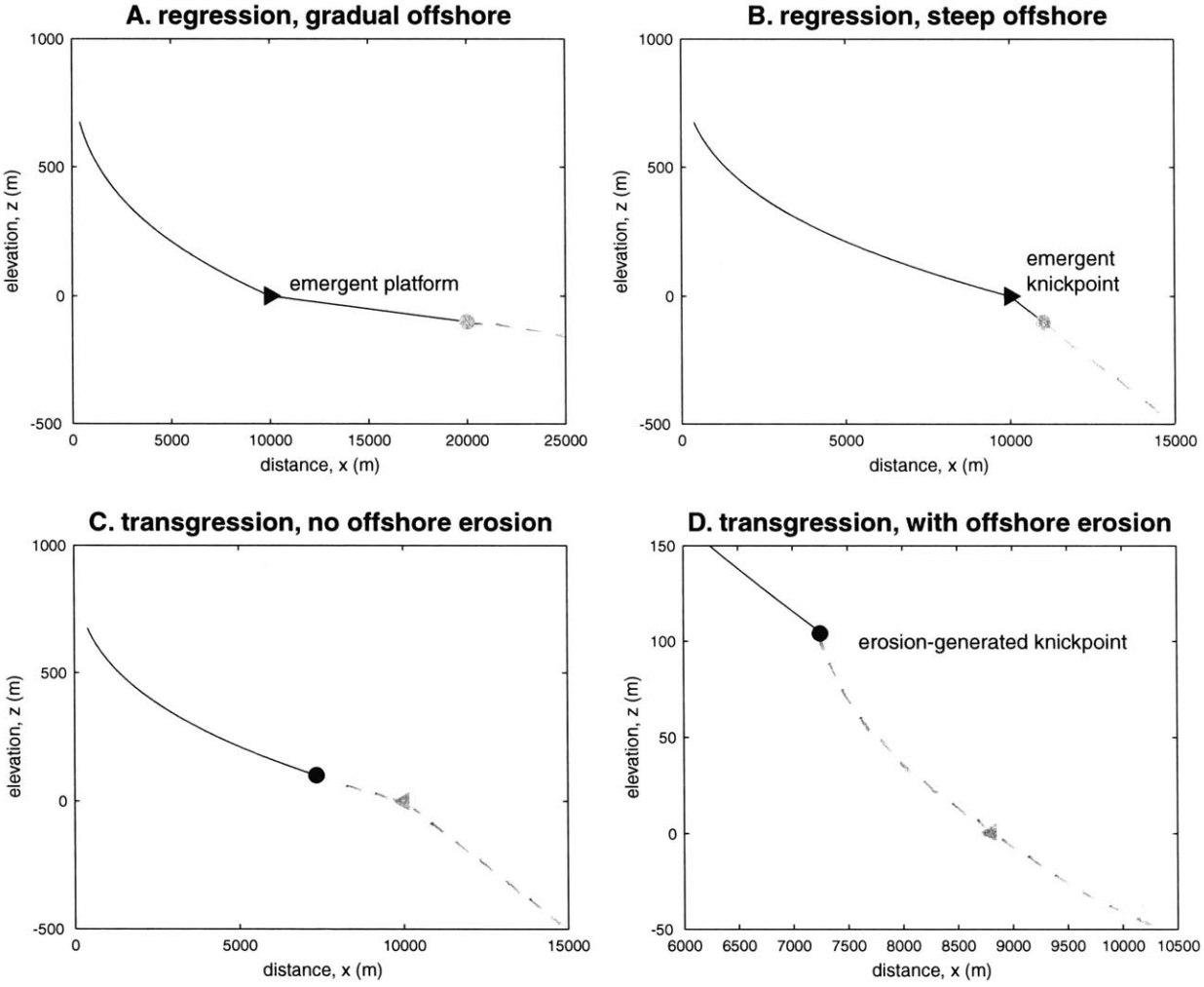

Figure 2. Cartoon examples of model regressions and transgressions, without uplift or erosion (in A-C). In each panel, the initial location of sea level is marked by the triangle (pointing in the direction of motion of the coastline), and the final location is marked by the dot. To the left of the triangle is a concave-up stream longitudinal profile, to the right is a bathymetric ramp of constant gradient. Note that the scale is different in each figure. (A) Regression over a gradual offshore. The emergent stream segment is relatively flat, and will therefore likely be a zone of deposition. (B) Regression over a steep offshore. The emergent channel is a knickpoint, responding with high incision rates. (C) Transgression without offshore erosion. The location of the fluvial base level moves up the channel without any significant response. (D) Transgression with offshore erosion. If offshore, wave-based erosion rates are high, then the seabed at the transgressing shoreline will be steep, pushing a knickpoint onshore.

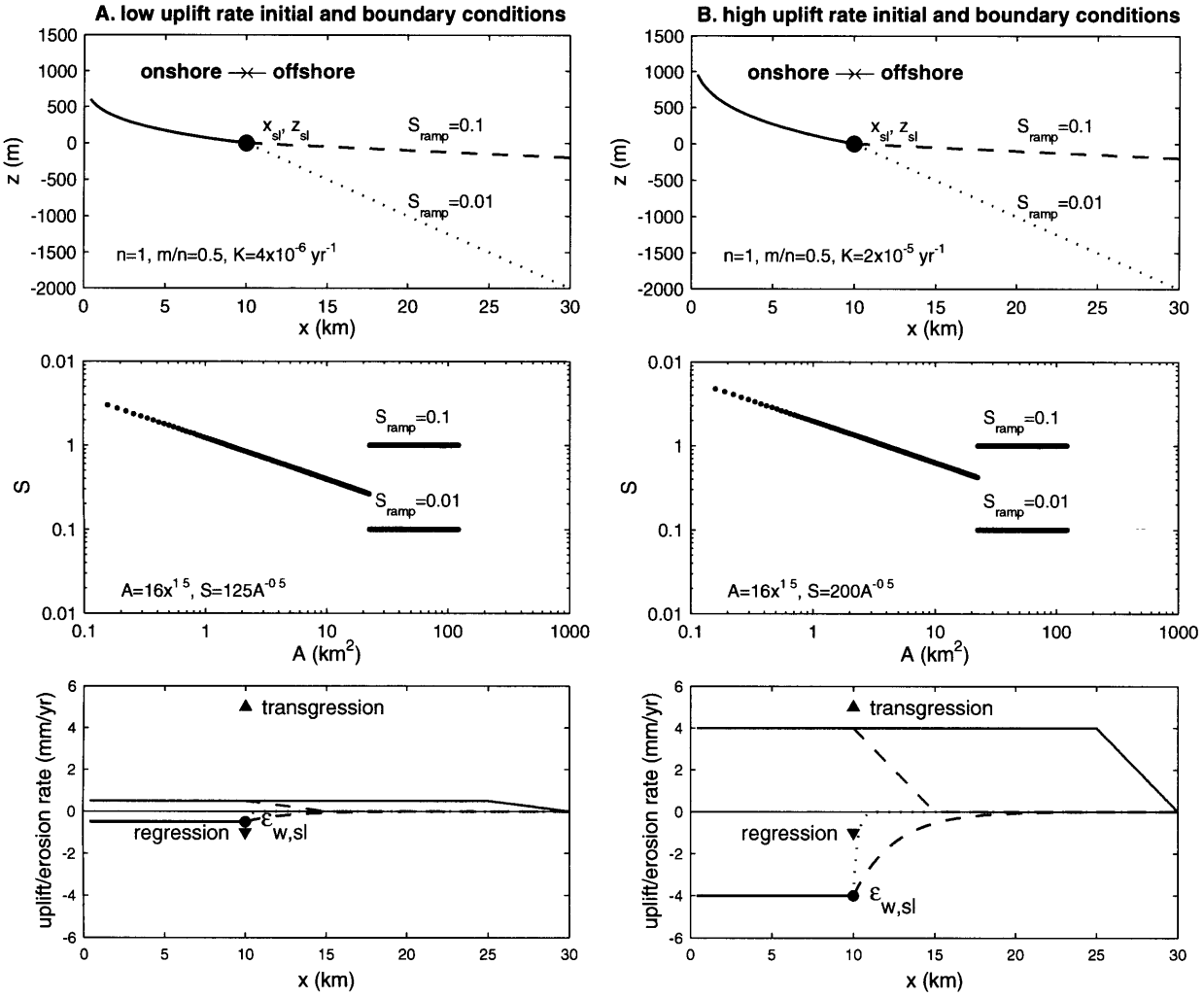

Figure 3. Model initial and boundary conditions. Top panels are initial longitudinal profiles: a concave-up stream channel (solid line), adjusted to the uplift rate for a fixed base-level boundary condition (*i.e.* Figure 1A); and two offshore conditions, gradual (S_{ramp}=0.01, dashed line) and steep (S_{ramp}=0.1, dotted line). The black dot marks the initial shoreline position. Parameter values for the onshore stream profiles are shown in the lower left corner. Middle panels are log-space slope (S) vs. drainage area (A) plots, for the longitudinal profiles in the top panels. Bottom panels compare the four rates relevant to stream response. Positive lines are rock-uplift rates (U), which are constant for the length of initial stream profile, and drop rapidly (over 5 km) to zero at some position in the offshore. In the constant uplift-rate boundary condition (solid gray line) the rate is constant until a point far enough offshore that it will not be part of the model erosion domain during regressions, so that the offshore boundary does not influence the model results. In the uplift-rate gradient boundary condition (dashed gray line), the steep gradient in U begins at the initial shoreline. Triangles represent the rates of sea level rise (transgression) and fall (regression) used for the simple model runs. Lines below zero represent initial erosion rates, plotted as negative values for clarity. Onshore fluvial incision rate (ε_f, from equation 2, solid line) is set in magnitude to equal U. Offshore wave-based erosion rate (ε_w, from equation 4, dashed line for S_{ramp}=0.1, dotted line for S_{ramp}=0.01) is varied in the model runs. The maximum value occurs at sea level ($\varepsilon_{w,sl}$). (A) The left panels are for low-uplift conditions (U=0.0005 m/yr). (B) The right panels are for high-uplift conditions (U=0.004 m/yr).

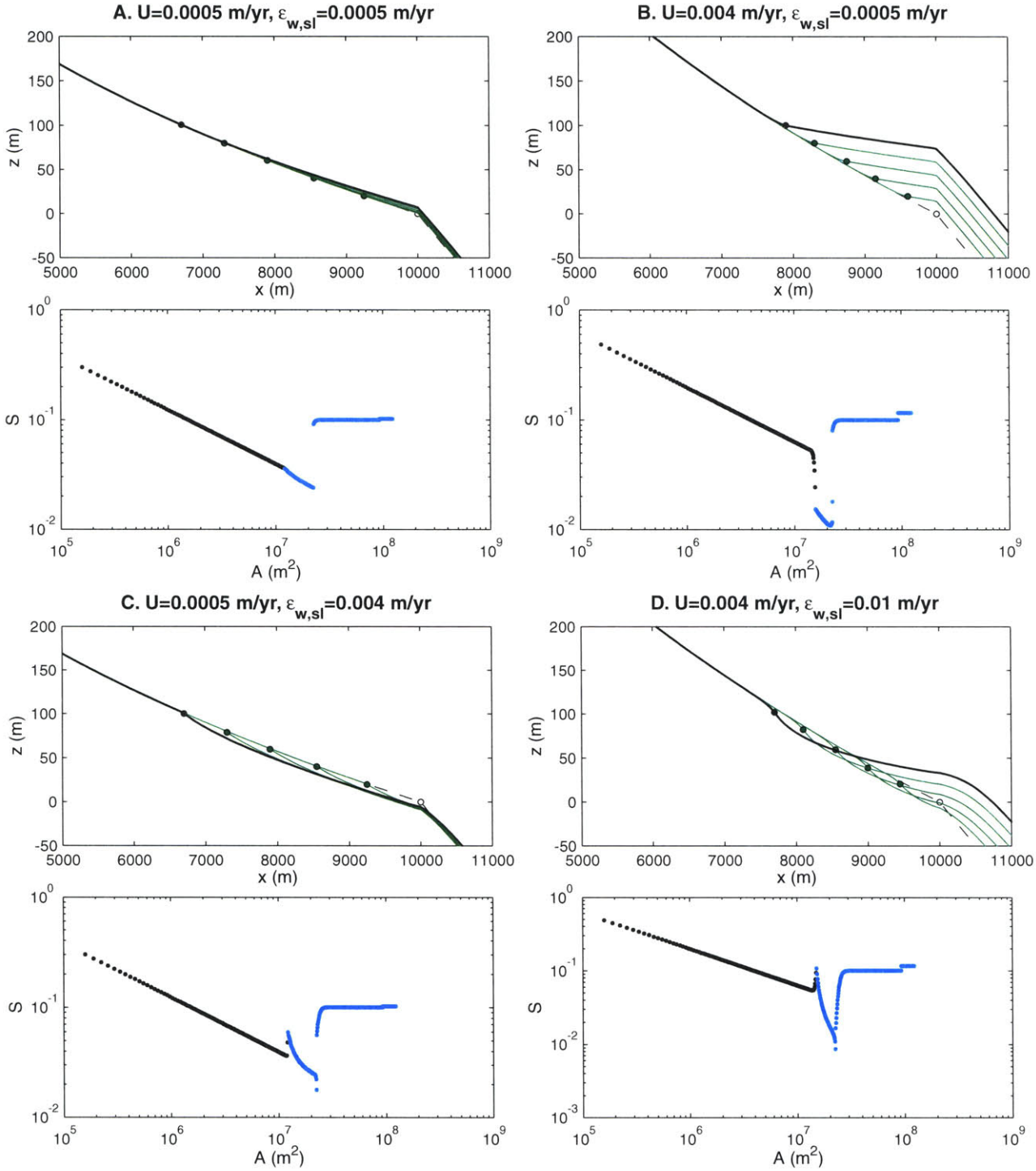

Figure 4. Model runs for simple transgressions (SL=0.005 m/yr for 20 kyr). Top panels show detail views of the longitudinal profiles, with initial conditions (dashed lines), 4 evenly spaced (in model time) intermediate conditions (green/gray lines), and final condition (black lines). Location of sea level for each profile is marked by the circles (open for initial, green/gray for intermediate, black for final). Bottom panels are slope (S) vs. drainage area (A) plots for the final profiles. Onshore points are shown in black, offshore points are shown in blue/gray. Note that the drainage area values used for the offshore points are only applicable if they become onshore points, and are only used here for clarity in plotting. See Table 1 for parameter values used in all model runs. (A) Low uplift rate, low wave-based erosion rate case. (B) High uplift rate, low wave-based erosion rate case. (C) Low uplift rate, high wave-based erosion rate case. (D) High uplift rate, high wave-based erosion rate case.

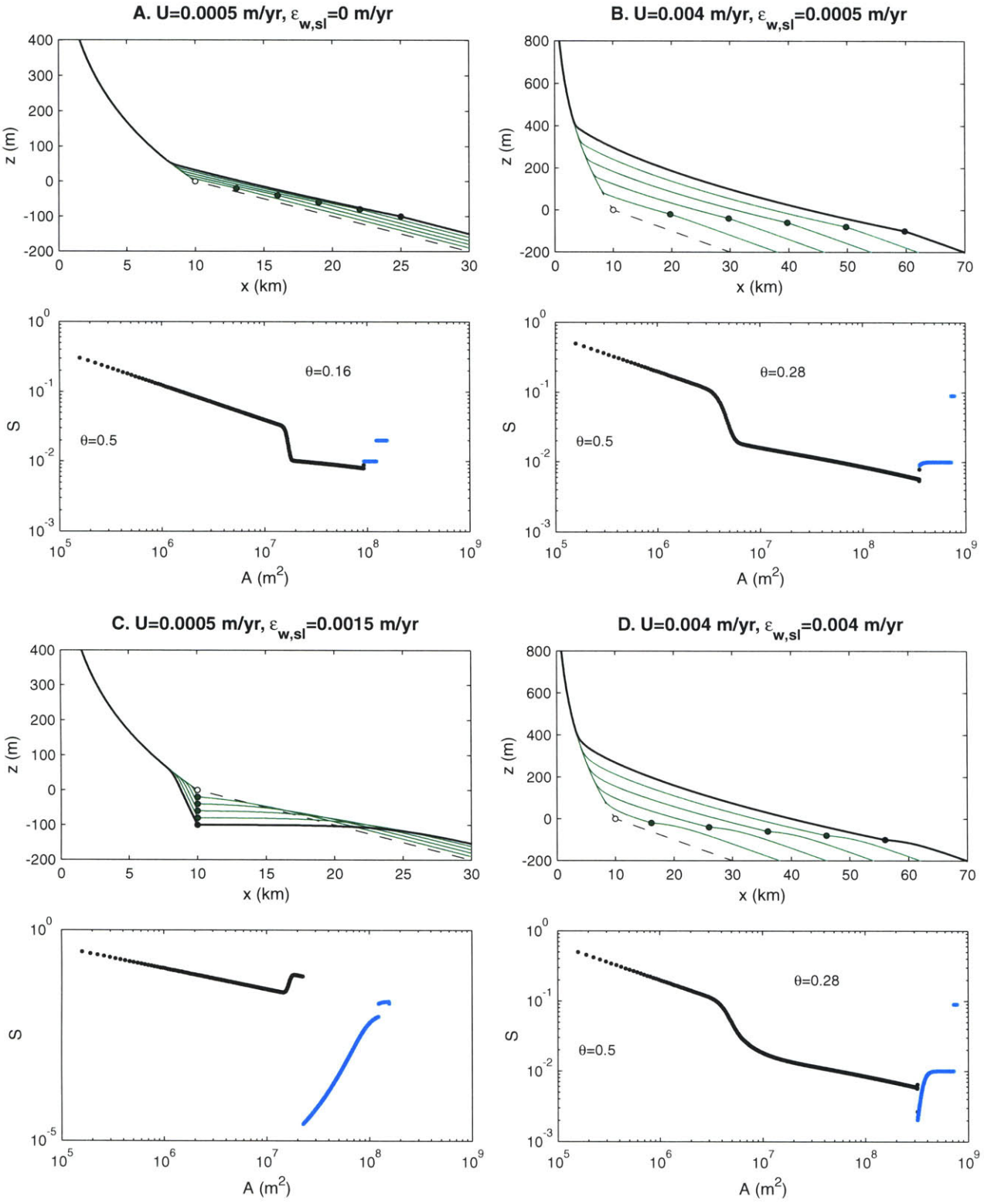

Figure 5. Model runs for simple regressions (SL=-0.001 m/yr for 100 kyr), with a gradual offshore ramp (S_{ramp}=0.01), and constant uplift rate throughout the modeled erosion domain. Note that the scale is different in the top panels. See figure 4 for description. (A) Low uplift rate, no wave-based erosion case. (B) High uplift rate, low wave-based erosion case. (C) Low uplift rate case, with wave-based erosion set to balance relative rate of base level fall ($\varepsilon_{w,sl}$=U-SL). (D) High uplift rate, moderate-high wave-based erosion rate case.

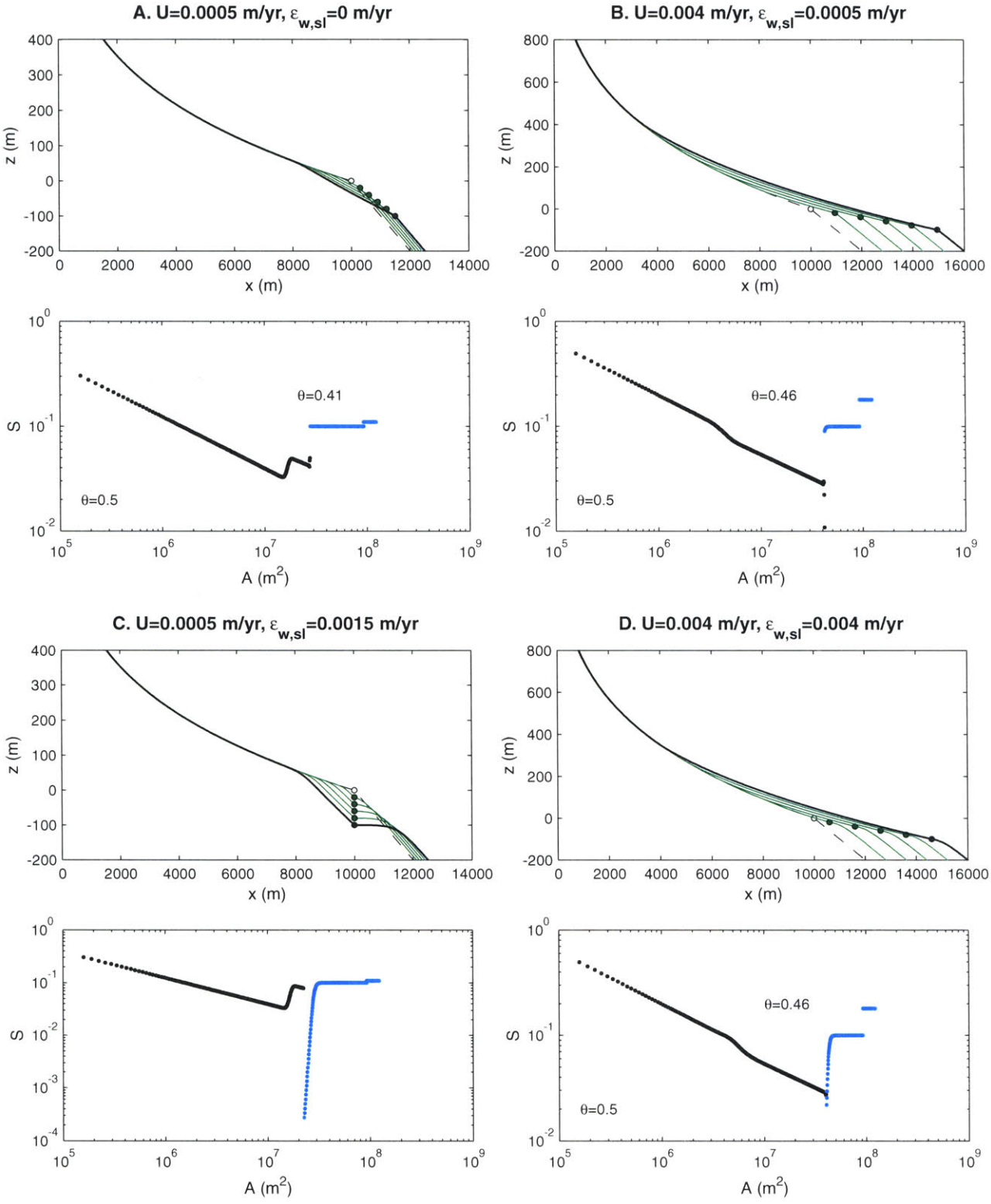

Figure 6. Model runs for simple regressions (SL=-0.001 m/yr for 100 kyr), with a steep offshore ramp (S_{ramp}=0.1), and constant uplift rate throughout the modeled erosion domain. All cases are the same as figure 5. See figure 4 for general description.

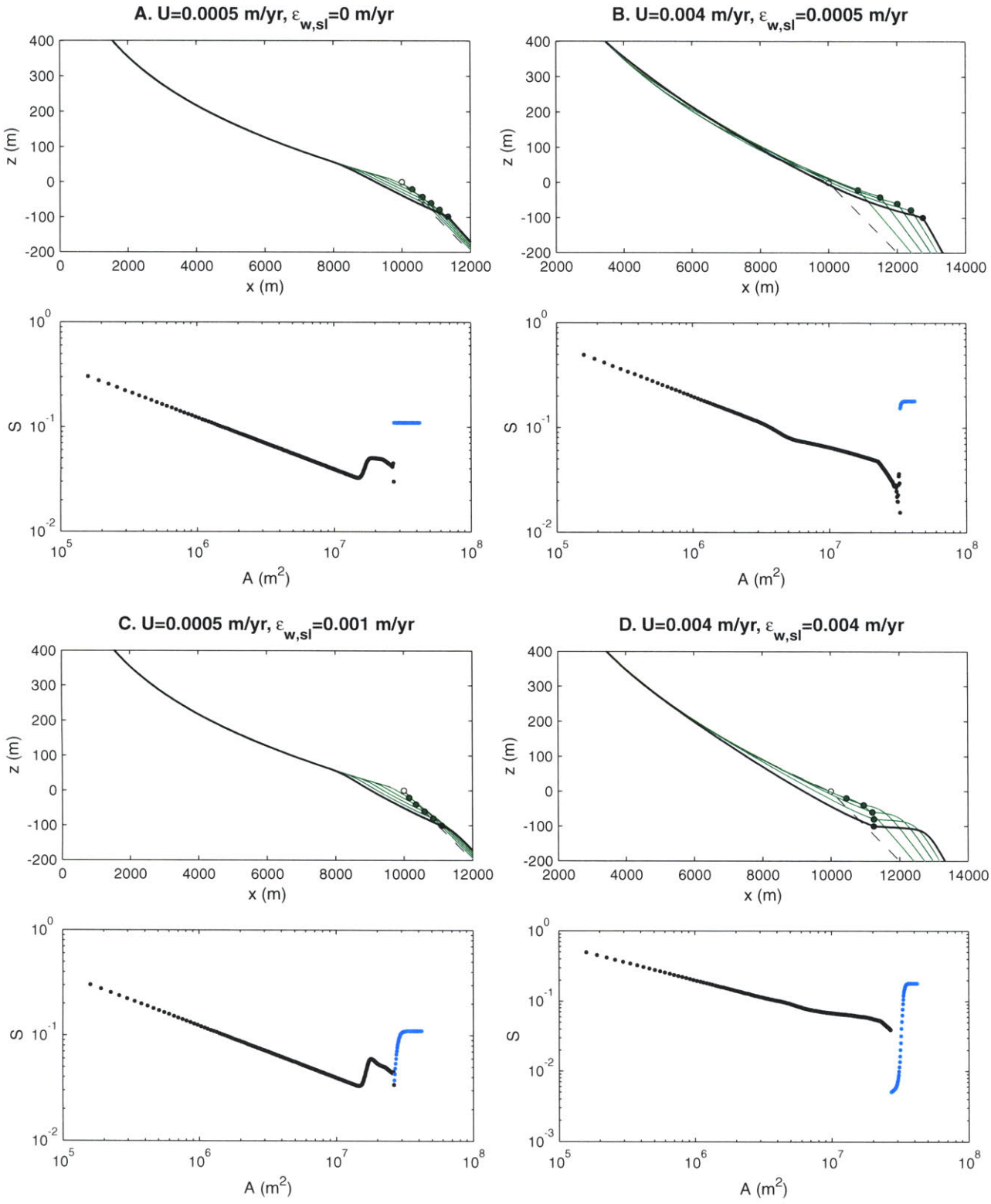

Figure 7. Model runs for simple regressions (SL=-0.001 m/yr for 100 kyr), with a steep offshore ramp (S_{ramp}=0.1), and the uplift-rate gradient boundary condition (steep drop at the location of the initial shoreline). (A) Low uplift rate, no wave-based erosion case. (B) High uplift rate, low wave-based erosion case. (C) Low uplift-rate case, moderate wave-based erosion case. (D) High uplift rate, moderate-high wave-based erosion rate case.

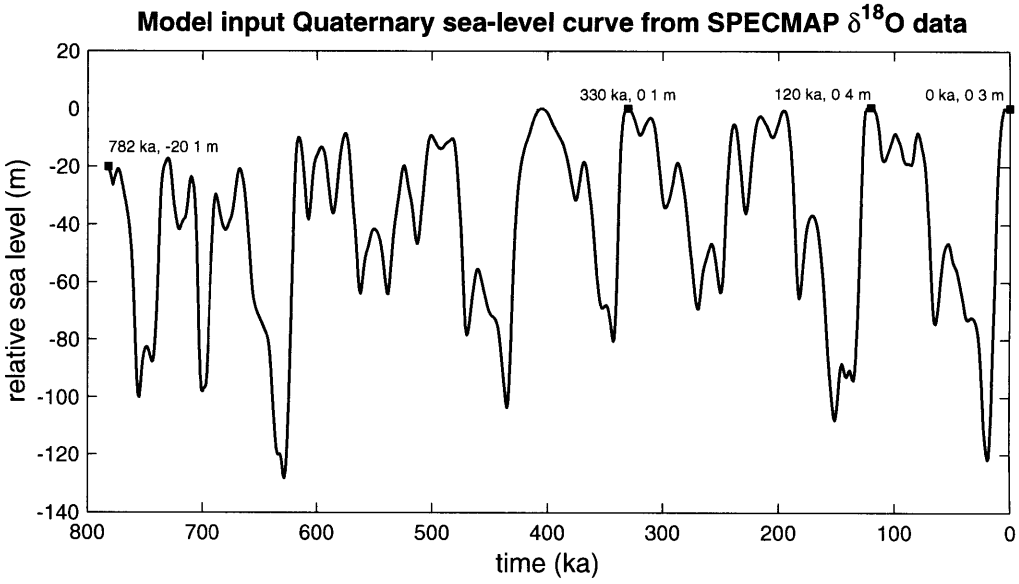

Figure 8. Approximate Late Quaternary sea-level curve used as model input. Original data is the Imbrie *et al.* (1984) stacked, normalized SPECMAP $\delta^{18}O$ curve. This is transformed to sea level via an empirical polynomial (relative sea level = $-32.841-(33.747\delta^{18}O)-(8.5605(\delta^{18}O)^2)$, Anderson *et al.* 1999). Various highstand times and sea levels, used as model initial times, are indicated by labeled boxes.

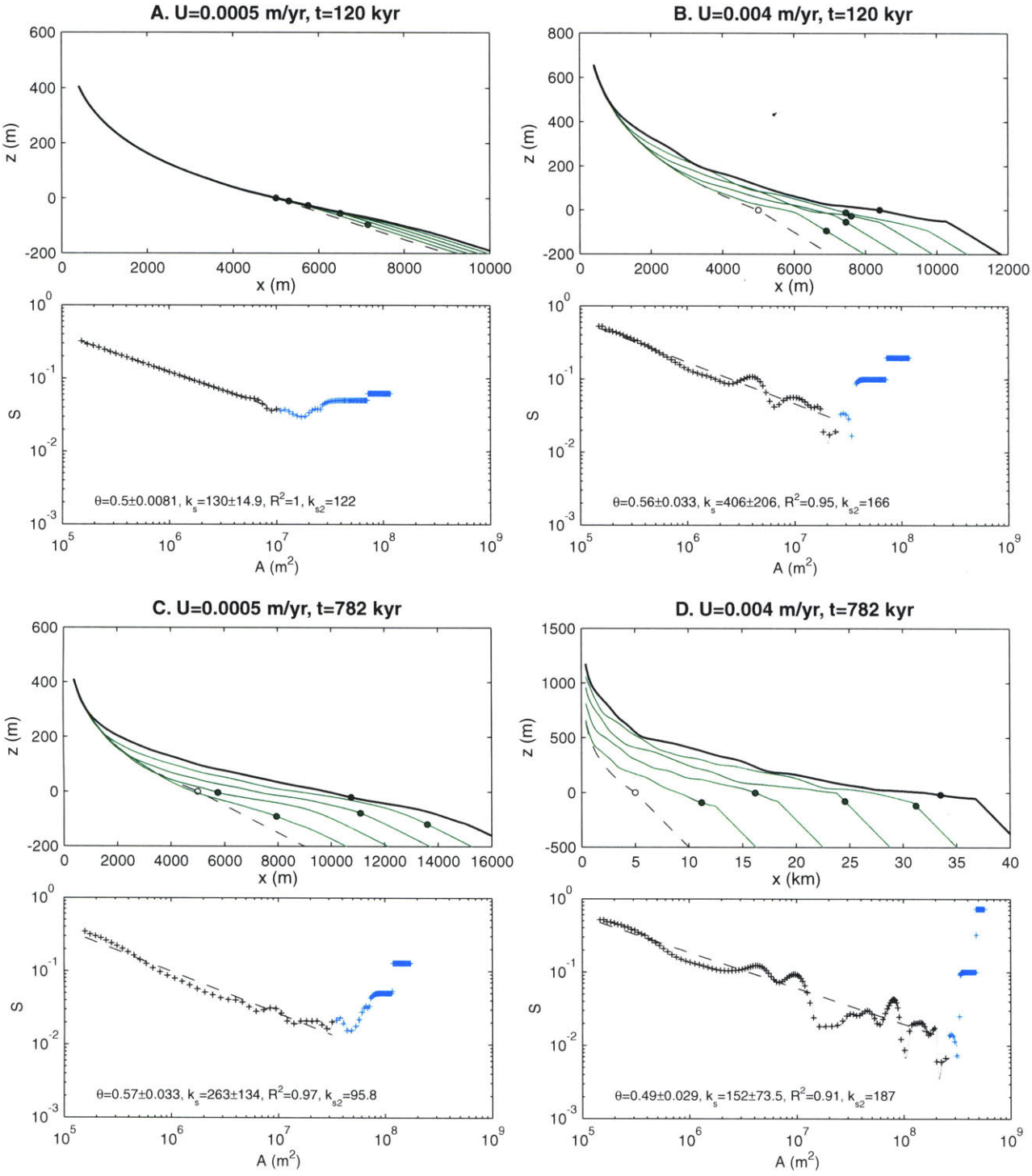

Figure 9. Model results with Quaternary sea-level curve, and constant uplift rates throughout the erosive part of the offshore. General description of plots is the same as Figure 4. Bottom panel (slope-area data) has crosses for channel gradient calculated on 10-m elevation contours, and small dots (often obscured) for slopes of individual data points. Dashed regression lines and regression values are calculated based on the contoured slope data. Offshore data points are shown in blue/gray, and are not included in regressions. See text, Figure 12 caption and Snyder *et al.* (2000) for further information about regression techniques. $\varepsilon_{w,sl}$=0.0005 m/yr for all model runs in Figures 9-11. (A) Single glacial-interglacial cycle (120 kyr), low uplift rate. (B) Single glacial-interglacial cycle (120 kyr), high uplift rate. (C) Multiple cycles (782 kyr), low uplift rate. (D) Multiple cycles (782 kyr), high uplift rate.

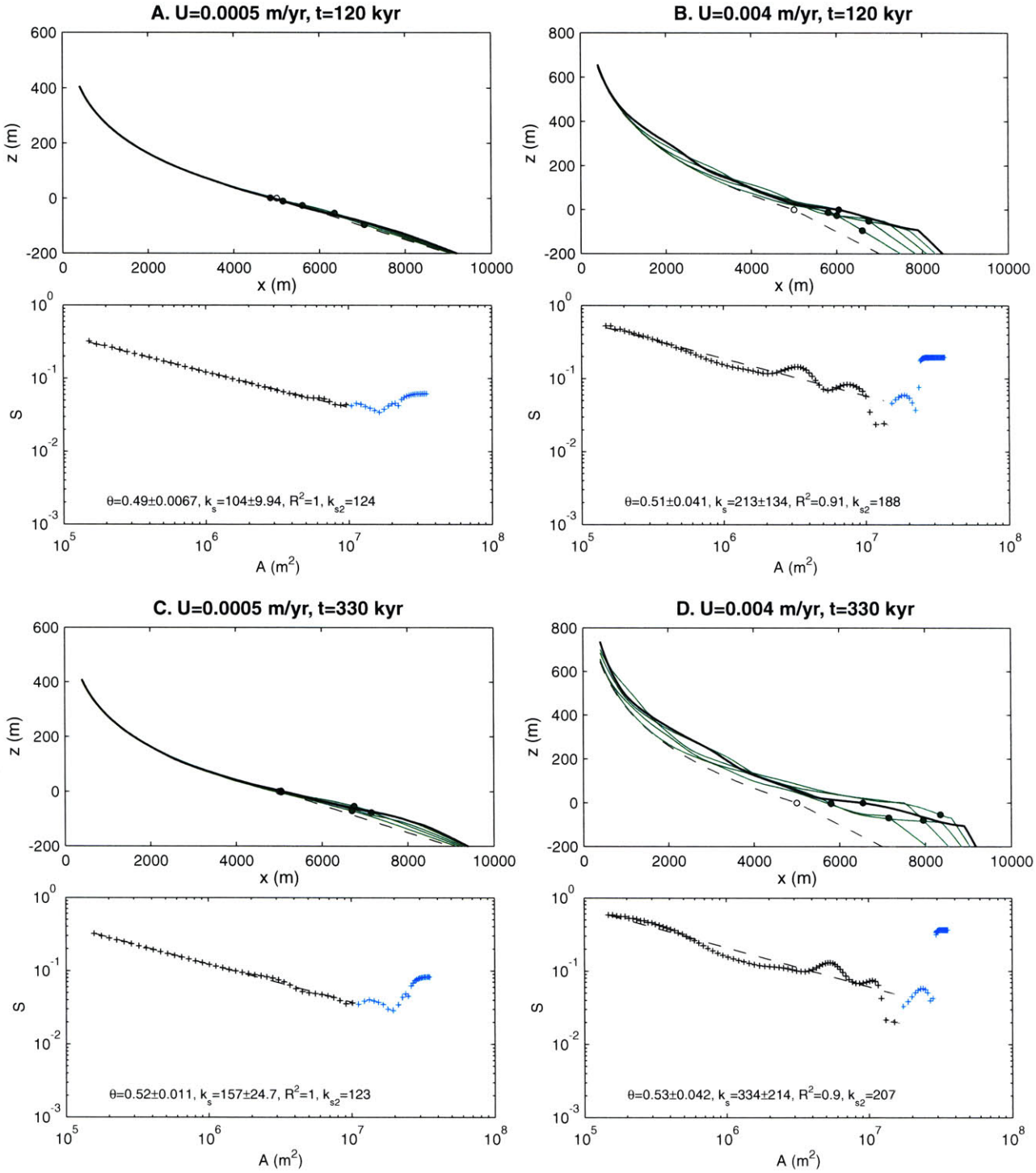

Figure 10. Model results with Quaternary sea-level curve, and rapid drop in rock-uplift rate between x=5 km and x=10 km (uplift-gradient boundary condition). See figures 4 and 9 for description. (A) Single glacial-interglacial cycle (120 kyr), low uplift rate. (B) Single glacial-interglacial cycle (120 kyr), high uplift rate. (C) Multiple cycles (330 kyr), low uplift rate. (D) Multiple cycles (330 kyr), high uplift rate.

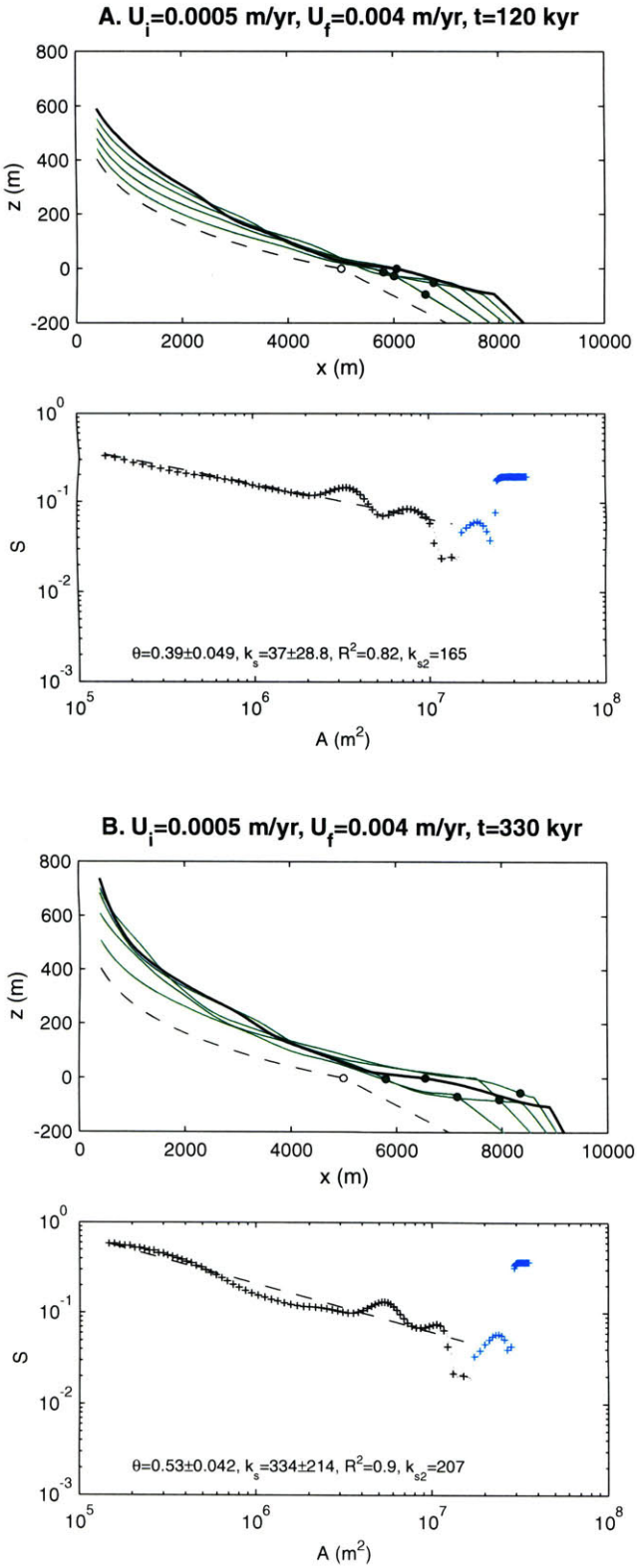

Figure 11. Model results with Quaternary sea-level curve, transition from low- to high-uplift rate conditions, and uplift-gradient boundary condition. See figures 4 and 9 for description. (A) Single glacial-interglacial cycle (120 kyr). (B) Multiple cycles (330 kyr).

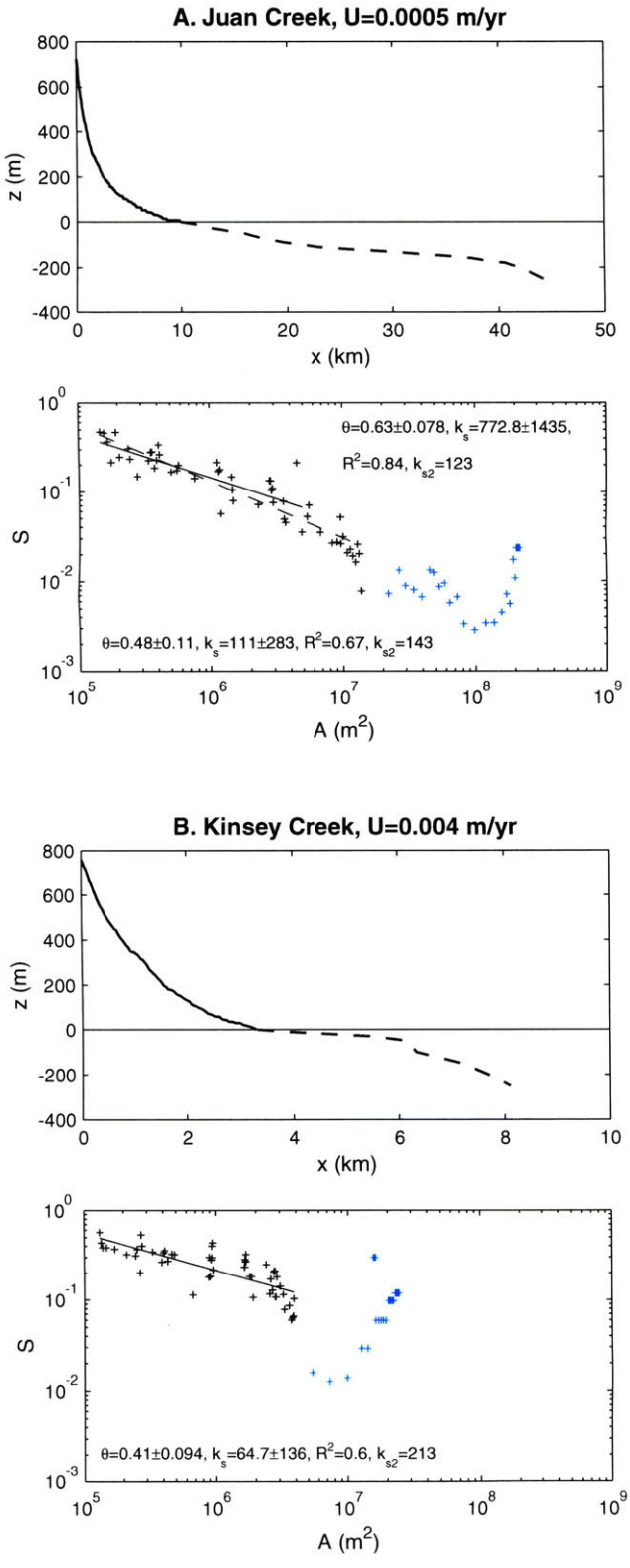

Figure 12. Longitudinal-profile data for two streams in the Mendocino triple junction study area. Top panels are longitudinal profiles. Thick, solid line is the onshore fluvial channel, derived from USGS 30 m digital elevation models. Dashed line is the offshore bathymetry, extending perpendicular to contours from the channel mouth, digitized from 1:250,000 topographic-bathymetric maps. Bottom panels are plots of channel gradient (S) against drainage area (A). Dark crosses are onshore data points, blue/gray crosses are offshore. Slopes are calculated on 10-m contour intervals, as done in our previous analysis of these streams (Snyder *et al.* 2000). Regression lines are least-squares best fits to subsets of the onshore data, beginning at the top of the fluvial system (A=10^5 m^2). Slight discrepancies between the regression fits on these plots and those in Snyder *et al.* (2000) reflect different regression domains. See Snyder *et al.* (2000) for full details on regression methodology. A. Juan Creek (low-uplift zone). Solid regression line is for the subset of data chosen to exclude the alluvial section at the mouth (A<5×10^6 m^2), best-fit parameters are shown in the lower left. Dashed regression line is the entire subset of onshore data, parameters are in upper right. B. Kinsey Creek (high-uplift zone). Regression line is for the entire onshore channel.

4230 – 15